FRACTURE AND FATIGUE CHARACTERIZATION OF STABILIZED SOILS AND SULFUR-EXTENDED ASPHALT USING MONOTONIC AND CYCLIC SEMI-CIRCULAR BENDING TESTS

A Dissertation

by

JUN ZHANG

Submitted to the Office of Graduate and Professional Studies of
Texas A&M University
in partial fulfillment of the requirements for the degree of

DOCTOR OF PHILOSOPHY

Chair of Committee,	Maryam Sakhaeifar
Co-Chair of Committee,	Dallas N. Little
Committee Members,	Robert Lytton
	Anastasia H. Muliana
Head of Department,	Robin Autenrieth

December 2017

Major Subject: Civil Engineering

ABSTRACT

The primary goal of this research is to develop test methodologies to characterize fracture and fatigue performances of chemically stabilized soils and asphalt mixtures. The fracture resistance of a chemically stabilized base or subbase layer is important for durability and sustainability of the pavement structure. Thus, an appropriate test protocol to characterize the fracture resistance of the stabilized bases, subbases and subgrade soils is essential for design of pavement materials and structures. This research proposed a protocol based on the semi-circular bending (SCB) test to measure fracture resistance (i.e., fracture energy and fracture toughness) of the chemically stabilized material (CSM). The effects of three test variables including specimen thickness, notch length and loading rate on fracture properties were investigated, and appropriate values for these test variables were selected for the SCB test protocol. The proposed SCB test method was successful in characterizing the fracture resistance of three different CSMs. In order to more definitively address fracture properties of the CSM three-dimensional cohesive zone modeling was used and the simulations agreed very well with the experimental results. Both of the fracture properties obtained from the experiment and the cohesive zone modeling indicated that polymer-stabilized limestone exhibited a much higher fracture resistance than cement-stabilized limestone and cement-stabilized sand. In order to characterize crack growth of CSMs, a compliance method based on the cyclic SCB test was proposed, which was successfully used to characterize crack growth rate of cement stabilized

materials. This method is promising as it shows much higher coefficients of correlation when fitting the data to the Paris' law equation.

Characterizing fracture behavior and crack propagation of asphalt mixtures is helpful for optimizing mixture design and predicting cracking performance of asphalt pavements. This research used a digital image correlation (DIC) system to measure the horizontal strain field of a crack tip, which is consistent with the SCB fracture test results. It is observed that the horizontal strain field is more localized at a lower testing temperature and a higher peak load. In addition, this research proposed a new method based on the cyclic semi-circular bending test to characterize crack growth rate of asphalt mixtures. To accurately capture crack length for determining crack growth rate, a DIC is used, and crack mouth opening displacement (CMOD) is measured by linear variable differential transformers. Correlations between crack length and CMOD are established, which are used to determine crack lengths corresponding to loading cycles over the testing process. The proposed cyclic semi-circular bending test successfully characterizes the Paris's law coefficients of sulfur-extended asphalt mixtures. The cyclic semi-circular bending test provides substantially lower coefficients of variance in terms of cycles to fatigue failure compared with other traditional fatigue tests. Test results were used to determine the impact of sulfur content on fatigue life with the conclusion that a low level of sulfur added in the case of 15% change the rheology (softener) of the asphalt to the degree that more damage is caused in a controlled-stress mode loading. However, an increase in sulfur content (30% and 45%) apparently produces a stiffer mixture that is more resistant to damage and is comparable to the control mixture.

DEDICATION

To my beloved wife and son, and to my family for their love and support.

ACKNOWLEDGEMENTS

CONTRIBUTORS AND FUNDING SOURCES

Contributors

This work was supported by a dissertation committee consisting of Dr. Maryam Sakhaeifar as advisor, Dr. Dallas N. Little as co-advisor and Dr. Robert Lytton of the Department of Civil Engineering, Dr. Anastasia H. Muliana of the Department of Mechanical Engineering at Texas A&M University and Dr. Yong-Rak Kim of the Department of Civil Engineering at University of Nebraska-Lincoln.

The numerical simulation in Chapter 4 was guided by Dr. Yong-Rak Kim and Dr. Taesun You of the Department of Civil Engineering at University of Nebraska-Lincoln. All other work conducted for the dissertation was completed by the student independently.

Funding Sources

TABLE OF CONTENTS

LIST OF FIGURES

LIST OF TABLES

1. INTRODUCTION

1.1 Problems

Paved road system is one of major transportation systems in the United States. Due to its important role in transportation, billions of dollars are annually spent in pavement projects for reconstruction, rehabilitation and maintenance by transportation agencies. Despite such spending, 28% of nation's major roadways are in need of total reconstruction, due to the severe level of distresses according to a report in the Washington Post (Ingraham 2015). Cracking is one of major distresses occurring in the pavement system, which is a consequence of accumulation of damage under repeated traffic loading. Under repeated loading applications, the cracks initiate and continue to propagate, and finally connect. According to a report by California Department of Transportation (Caltrans) (Caltrans 2013), for the pavement condition, both fair and poor conditions have minor or significant cracking observed in the pavements. These cracks can allow the infiltration of moisture into the asphalt pavement systems, which further deteriorate the life of pavement service.

Besides the upper layers of asphalt pavement, stability of materials comprising pavement sublayers has a significant impact on the long-term pavement performance. A typical pavement structure is composed of a surface layer, base layer and subgrade. Portland cement, lime or polymers are used to treat underlying materials (aggregates and soils) to provide a stabilized base course with a better support for the surface layer. However, the rigid matrix often developed with cementitious and pozzolanic stabilizers often produces chemically stabilized materials (CSMs) that are susceptible to fracture and

fatigue. Fracture-susceptible paving materials compromise the life and sustainability of the pavement structure. Thus, a better understanding of the fracture behavior and cracking mechanisms in pavement materials is essential to designing pavements with better resistance to cracking and longer service life, which will further reduce the expensive costs for rehabilitation and maintenance.

Therefore, characterization of fracture and fatigue performances of pavement materials in the laboratory is an important step for material design. Chemically stabilized soils have the advantages of providing a strong support for the upper layers and exhibiting higher fracture and fatigue resistance than the un-stabilized soils. Due to such advantages, they have gained increasing attention, and various chemical stabilizers are developed for soil stabilization. One of the promising stabilizers is polymer, which shows equivalent compressive strength and stiffness but superior fracture toughness compared with cement-stabilized soils. However, the traditional laboratory test methods lack efficiency or accuracy. The traditional tests are Disk-shaped Compact Tension (DCT) test and indirect tension (IDT) test. The sample preparation for the DCT is complex because two small loading holes are needed to be drilled in the specimen, which is not easy, especially for the weaker stabilized materials. The IDT test has high concentration of loads at two loading points, complex stress distribution and multiple cracks occurring in the specimen, which increase test variability and compromise the accuracy of test results. The monotonic Semi-circular Bending (SCB) test is a simple three-point bending test, which was firstly used for rocks and has been widely used for fracture characterization of asphalt concrete by many researchers and agencies (Molenaar et al. 2002; Li et al. 2004; Van et al. 2008;

Kim et al. 2012; Im et al. 2014). Compared with the traditional tests, the SCB test has several advantages: (1) a simple test procedure; (2) simple and efficient sample preparation; (3) a sensitive fracture test due to bending mode. It should be emphasized that the sample preparation for the SCB test is simple and efficient. One cylindrical compacted sample can produce two SCB specimens, which also reduce the test variability since the two specimens are from one compacted sample. The SCB specimen also requires less materials compared to other traditional tests. Therefore, this research is to develop test methodologies using the monotonic and cyclic SCB test serve as the surrogates to the traditional tests for characterizing fracture and fatigue performances of the CSM, respectively.

For asphalt mixtures, the monotonic SCB test has been widely used due to its advantages. However, the cyclic SCB fatigue test has not been well established. The current popular fatigue tests include Bend Beam Fatigue (BBF) test, Simplified Viscoelastic Continuum Damage (S-VECD) test, Texas Overlay Test (OT), repeated direct tension test. The BBF test is a strain-controlled test to determine the fatigue life of a beam specimen subjected to repeated flexural bending until failure (Tayebali et al. 1996; Ghuzlan et al. 2000; Wagoner et al. 2005; Shu et al. 2008). The S-VECD test is to determine the damage characteristics curve of asphalt mixtures from direct tension cyclic fatigue test, and the damage parameters is used with MEPDG or more advanced models to simulate pavement fatigue performance (Park et al. 1996; Daniel et al. 2002; Underwood et al. 2012). The OT test is a strain controlled test to determine the failure cycles of a specimen glued onto two metallic plates-one mobile and the other fixed during

3

the testing process (Lytton et al. 1989; Zhou et al. 2007). The repeated direct tension test is a strain controlled test to obtain Paris' law or failure cycles of a cylindrical specimen subjected to repeated tension (Luo et al. 2013). These fatigue tests have been developed and used for characterization of fatigue resistance of asphalt mixtures, but all these tests require highly trained technicians due to complex sample preparation or testing. Similarly with the monotonic SCB test, the cyclic SCB fatigue test has the advantages of simple sample preparation and test setup. Thus, exploring the feasibility of the cyclic SCB test for asphalt mixtures is meaningful.

From the linear elastic fracture mechanics (LEFM), the presence of a crack in a specimen leads to an increase in the compliance of the specimen. Measurement of the compliance of a cracked specimen is a simple and accurate method for determine the crack opening and closure (Marsh et al. 1991). Roque et al. (1999) proposed to determine crack growth rate parameters of asphalt mixtures using the Indirect Tension (IDT) test which is a compliance-based approach that the horizontal displacement of two gauge points was correlated to the vertical cracking length. The IDT test is a simple test, but there are several drawbacks. Firstly, the IDT specimen has complex stress distribution due to the indirect tension mode and high concentration of loads at two loading points. Secondly, there are multiple cracks occurring along the centerline of the specimen instead of a single crack (Birgisson et al. 2008). In addition, the correlation of the horizontal displacement to the vertical cracking length was simulated using the finite element method, which was not validated by the experiment. On the contrary, the cyclic SCB test can overcome the drawbacks, and a digital image correlation (DIC) system can be used to validate the

displacement-based approach for the cyclic SCB test. In this research, sulfur-extended asphalt (SEA) is used for asphalt mixture, which is to use sulfur as a binder extender to substitute for part of asphalt. An abundance of low-cost elemental sulfur as the by-product of the oil and gas refinery process has driven the increasing interest in the use of SEA for asphalt pavement. The SEA can improve the rutting resistance of asphalt pavement, but the major concern is fracture and fatigue resistance. Thus, the proposed cyclic SCB test is used to optimize the sulfur dosage in terms of fatigue resistance of SEA mixtures.

1.2 Objectives

The goal of this research is to characterize fracture and fatigue performances of chemically stabilized soils and asphalt mixtures using monotonic and cyclic SCB tests. The primary objectives of this research are as follows:

1) to develop a methodology based on the monotonic SCB test to characterize fracture resistance of chemically stabilized mateirals (CSM).

2) to develop a methodology based on the cyclic SCB test to characterize fatigue performance of chemically stabilized materials.

3) to investigate the fracture process zone of a crack tip for fine aggregates matrix (FAM) mixture.

4) to develop a methodology based on the cyclic SCB test to characterize fatigue performance of asphalt mixtures.

5) to characterize fracture and fatigue performances of sulfur-extended asphalt (SEA) mixtures using the proposed methodologies.

To accomplish these objectives, the specific tasks include:

- Propose a fracture test methodology based on the monotonic SCB test for CSMs including methods of sample preparation and data analysis,

- Investigate effects of test variables on the monotonic SCB test results,

- Simulate the SCB fracture tests performed on CSMs using cohesive zone model,

- Propose a SCB fatigue test methodology based on the compliance-calibration and displacement-calibration methods for CSMs,

- Evaluate the rheological properties of SEA,

- Perform the monotonic SCB test on FAM specimens and investigate the fracture process zone using the digital image correlation (DIC) system.

- Propose a fatigue test methodology based on displacement-calibration method with use of a DIC system for asphalt mixture.

2. THEORETICAL BACKGROUND

Brittle fracture has been concerned for a long time. In the ancient time, many structures were designed to be in compression instead of tension for preventing fracture failure. At the beginning, attention was paid to the tensile strength of materials. A major shift from emphasis in the theory of strength of materials to discussion of the role of slow crack growth in fatigue failure occurred in the 19th century with the introduction of malleable iron (Sanford 2003). By the end of the 19th century, Inglis (1913) made a milestone work, in which he solved a elasticity problem of an elliptical hole in an uniformly loaded plate, and deduced some important observations about the stress state around the tip of a crack-like defect (Sanford 2003). Based on the work by Inglis (1913), Griffith (1921) developed a theory of brittle fracture based on energy concepts. The theories based on both the stress analysis and energy concepts have been introduced and are important foundations for the discipline of Linear Elastic Fracture Mechanics (LEFM). Stress intensity factor (i.e., K) is a very important concept in LEFM, which is widely used in fracture and fatigue characterization of various materials. The concept of stress intensity factor is also used in this research for fracture and fatigue characterization. This chapter will present the derivation of the concept of stress intensity factor.

2.1 Field Equations of Elasticity

The attention is restricted to be focused on the two-dimensional formulation since the solution of elasticity problems in three dimensions is extremely difficult (Sanford 2003). In two special cases of plane strain and plane stress, antiplane behavior

is restricted and the equations of elasticity can be formulated in two dimensions. Thus, the two conditions of plane strain and plane stress are used for the derivation of the concept of stress intensity factor.

In a state of plane strain,

$$\varepsilon_z = 0, \gamma_{xz} = 0, \gamma_{yz} = 0 \ , \tag{2.1}$$

The plane-strain form of Hook's law:

$$\varepsilon_x = \frac{1+v}{E}[(1-v)\sigma_x - v\sigma_y] \tag{2.2a}$$

$$\varepsilon_y = \frac{1+v}{E}[(1-v)\sigma_y - v\sigma_x] \tag{2.2b}$$

$$\sigma_x = \frac{E}{(1+v)(1-2v)}[(1-v)\varepsilon_x + v\varepsilon_y] \tag{2.2c}$$

$$\sigma_x = \frac{E}{(1+v)(1-2v)}[(1-v)\varepsilon_y + v\varepsilon_x] \tag{2.2d}$$

$$\tau_{xy} = G\gamma_{xy} \tag{2.2e}$$

In a state of plane stress,

$$\sigma_z = 0, \tau_{xz} = 0, \tau_{yz} = 0 \tag{2.3}$$

The plane-stress form of Hook's law:

$$\varepsilon_x = \frac{1}{E}(\sigma_x - v\sigma_y) \tag{2.4a}$$

$$\varepsilon_y = \frac{1}{E}(\sigma_y - v\sigma_x) \tag{2.4b}$$

$$\sigma_x = \frac{E}{1-v^2}(\varepsilon_x + v\varepsilon_y) \qquad (2.4c)$$

$$\sigma_y = \frac{E}{1-v^2}(\varepsilon_y + v\varepsilon_x) \qquad (2.4d)$$

$$\tau_{xy} = G\gamma_{xy} \qquad (2.4e)$$

The general problem of linear elasticity in the X-Y plane has eight unkowns σ_x , σ_y , τ_{xy} , ε_x , ε_y , γ_{xy} , u ,and v . In order to solve these eight unkowns, eight equations are needed (Sanford 2003). The Hook's law provides three equations either in the case of plane strain or plane stress. The kinematic equations provide three more equations:

$$\varepsilon_x = \frac{\partial u}{\partial x} \;,\; \varepsilon_y = \frac{\partial v}{\partial y} \;,\; \text{and } \gamma_{xy} = \frac{\partial v}{\partial x} + \frac{\partial u}{\partial y} \qquad (2.5)$$

The static equilibrium provides the remaining two equations:

$$\frac{\partial \sigma_x}{\partial x} + \frac{\partial \tau_{xy}}{\partial y} = 0 \;, \qquad (2.6a)$$

$$\frac{\partial \tau_{xy}}{\partial x} + \frac{\partial \sigma_y}{\partial y} = 0 \;. \qquad (2.6b)$$

For Equation 2.5, if the strains are prescribed, there are three equations and two unknowns (i.e., u and v), and no unique solution could be found. Thus, there is some relationship between the three strains to ensure the unique solution (Sanford 2003). Differentiate the last equation of Equation 2.5 and substitute the first two equations of Equation 2.5 to obtain the compatibility equation:

9

$$\frac{\partial^2 \gamma_{xy}}{\partial x \partial y} = \frac{\partial^2 \varepsilon_x}{\partial y^2} + \frac{\partial^2 \varepsilon_y}{\partial x^2} \tag{2.7}$$

The compatibility equation gives the necessary constraint to ensure that the body is continuous under the applied load.

The best way to solve these eight equations is to solve the reduced set of equations. Airy (1863) developed a method. He defined a function $F(x, y)$:

$$\sigma_x = \frac{\partial^2 F}{\partial y^2} \ , \ \sigma_y = \frac{\partial^2 F}{\partial x^2} \ , \text{ and } \tau_{xy} = -\frac{\partial^2 F}{\partial x \partial y} \tag{2.8}$$

It is found that the Airy function F satisfies the equilibrium equations when substituting them into Equation 2.6. The kinematic equations are used to derive the compatibility equation. When substituting the Hook's law equations in the compatibility equation, solving the eight equations can be reduced to solving one equation (Sanford 2003):

$$(1-v)\left[\frac{\partial^2 \sigma_y}{\partial x^2} + \frac{\partial^2 \sigma_x}{\partial y^2}\right] - v\left[\frac{\partial^2 \sigma_x}{\partial x^2} + \frac{\partial^2 \sigma_y}{\partial y^2}\right] = 2\frac{\partial \tau_{xy}}{\partial x \partial y} \tag{2.9}$$

When substituting Equation 2.8 into Equation 2.9, the compatibility equation can be:

$$\frac{\partial^4 F}{\partial x^4} + 2\frac{\partial^4 F}{\partial x^2 \partial y^2} + \frac{\partial^4 F}{\partial y^4} = 0 \text{ or } \nabla^4 F = 0 \tag{2.10}$$

Where ∇^2 is the harmonic operator.

With use of the Airy stress function, solving the elasticity problem in the plane becomes finding a suitable Airy stress function F which satisfies Equation 2.10 and the

boundary condition (Sanford 2003). It should be noted that the compatibility equation leads to Equation 2.10 when substituting the Hook's law for either plane strain or plane stress.

2.2 The Generalized Westergaard Method

The generalized Westergaard method introduces the complex variables into the mathematical formulation of the elasticity problem in two dimensions (Westergaard 1939 and Sanford 1979). The complex analytic functions satisfies the biharmonic equation (i.e., Equation 2.10), and it offers great convenience for solving the elasticity problem.

$Z(z)$ is a defined complex function with one complex variable z (Sanford 2003).

$$Z(z) = \text{Re}\, Z(z) + i\, \text{Im}\, Z(z) \text{ or } Z(x+iy) = \phi(x, y) + i\varphi(x, y) \tag{2.11}$$

Where $\phi(x, y)$ and $\varphi(x, y)$ are real functions and they are not necessarily independent. When the value of Z has a unique derivative at every point in the domain, the function $Z(z)$ is analytic. The complex analytic function $Z(z)$ has unique properties, which will be derived as follows:

$$\frac{\partial Z(z)}{\partial x} = \frac{\partial Z(z)}{\partial z} \cdot \frac{\partial z}{\partial x} = \frac{\partial Z(z)}{\partial z} \cdot 1 = Z' \tag{2.12a}$$

$$\frac{\partial Z(z)}{\partial y} = \frac{\partial Z(z)}{\partial z} \cdot \frac{\partial z}{\partial y} = \frac{\partial Z(z)}{\partial z} \cdot i = iZ' \tag{2.12b}$$

Alternatively,

$$\frac{\partial Z(z)}{\partial x} = \frac{\partial \operatorname{Re} Z(z)}{\partial x} + i\frac{\partial \operatorname{Im} Z(z)}{\partial x} \tag{2.13a}$$

$$\frac{\partial Z(z)}{\partial y} = \frac{\partial \operatorname{Re} Z(z)}{\partial y} + i\frac{\partial \operatorname{Im} Z(z)}{\partial y} \tag{2.13b}$$

From Equation 2.12, obtain:

$$i\frac{\partial Z(z)}{\partial x} = \frac{\partial Z(z)}{\partial y} \tag{2.14}$$

Substituting Equation 2.14 into Equation 2.13 gives:

$$\frac{\partial \operatorname{Re} Z(z)}{\partial y} = -\frac{\partial \operatorname{Im} Z(z)}{\partial x} \tag{2.15a}$$

$$\frac{\partial \operatorname{Im} Z(z)}{\partial y} = \frac{\partial \operatorname{Re} Z(z)}{\partial x} \tag{2.15b}$$

Equations 2.15 is called Cauchy-Riemann conditions. When a complex function meets the conditions, the complex function is analytic because the Cauchy-Riemann conditions provide the necessary and sufficient conditions for the complex function being analytic (Sanford 2003). The analytic complex function has a unique property which will be presented below. Differentiating Equation 2.15a with respect to y and Equation 2.15b with respect to x and adding the two equations give:

$$\left(\frac{\partial^2}{\partial x^2} + \frac{\partial^2}{\partial y^2}\right)\operatorname{Re} Z(z) = \nabla^2 \operatorname{Re} Z = 0 \tag{2.16}$$

Similarly, we have

$$\left(\frac{\partial^2}{\partial x^2}+\frac{\partial^2}{\partial y^2}\right)\mathrm{Im}\,Z(z)=\nabla^2\,\mathrm{Im}\,Z=0 \qquad (2.17)$$

Thus, the real and imaginary parts of any complex analytic function are harmonic functions, which have:

$$\nabla^4\,\mathrm{Re}\,Z=0 \text{ and } \nabla^4\,\mathrm{Im}\,Z=0 \;. \qquad (2.18)$$

Equation 2.18 is the unique property of the complex analytical function.

An Airy stress function is defined as follows (Sanford 1979):

$$F(z)=\mathrm{Re}\,\tilde{\tilde{Z}}(z)+y[\mathrm{Im}\,\tilde{Z}(z)+\mathrm{Im}\,\tilde{Y}(z)] \qquad (2.19)$$

Where $\dfrac{d\tilde{\tilde{Z}}}{dz}=\tilde{Z}$, $\dfrac{d\tilde{Z}}{dz}=Z$, and $\dfrac{d\tilde{Y}}{dz}=Y$

Thus, according to Equations 2.8 obtain (Sanford 2003):

$$\sigma_x=\mathrm{Re}\,Z-y(\mathrm{Im}\,Z'+\mathrm{Im}\,Y')+2\,\mathrm{Re}\,Y \qquad (2.20a)$$

$$\sigma_y=\mathrm{Re}\,Z+y(\mathrm{Im}\,Z'+\mathrm{Im}\,Y') \qquad (2.20b)$$

$$\tau_{xy}=-\mathrm{Im}\,Y-y(\mathrm{Re}\,Z'+\mathrm{Re}\,Y') \qquad (2.20c)$$

2.3 The Crack Tip Stress Field

For a central crack problem (as shown in Figure 2.1), the complex analytic functions are as follows (Sanford 2003):

$$Z(z) = \frac{\sigma z}{\sqrt{Z^2 - a^2}} \quad \text{and} \quad Y(z) = 0 \tag{2.21a}$$

$$Z'(z) = -\frac{\sigma a^2}{(z^2 - a^2)^{3/2}} \tag{2.21b}$$
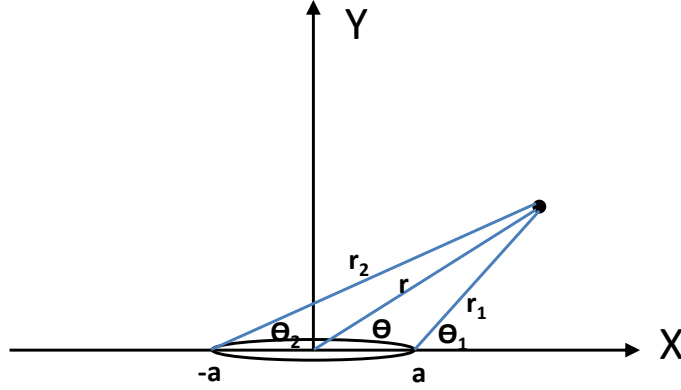
Figure 2.1 Coordinate Systems for a Central Crack

For convenience, the polar coordinates are introduced at the two singularity points (i.e., two crack tips):

$$z - a = (x - a) + iy = r_1 e^{i\theta_1} \tag{2.22a}$$

$$z + a = (x + a) + iy = r_2 e^{i\theta_2} \tag{2.22b}$$

Thus, according to Equation 2.20 obtain (Sanford 2003):

$$\sigma_x = \frac{\sigma r}{\sqrt{r_1 r_2}} \cos\left(\theta - \frac{\theta_1 + \theta_2}{2}\right) - \frac{\sigma a^2}{(r_1 r_2)^{3/2}} r_1 \sin\theta_1 \sin\frac{3}{2}(\theta_1 + \theta_2) \tag{2.23a}$$

$$\sigma_y = \frac{\sigma r}{\sqrt{r_1 r_2}} \cos\left(\theta - \frac{\theta_1 + \theta_2}{2}\right) - \frac{\sigma a^2}{(r_1 r_2)^{3/2}} r_1 \sin\theta_1 \sin\frac{3}{2}(\theta_1 + \theta_2) \tag{2.23b}$$

14

$$\tau_{xy} = \frac{\sigma a^2}{(r_1 r_2)^{3/2}} r_1 \sin\theta_1 \cos\frac{3}{2}(\theta_1 + \theta_2) \tag{2.23c}$$

When the attention is focused on one of the crack tips and a small region, we have (Sanford 2003):

$$r_2 \approx 2a \text{ and } \theta_2 \approx \theta \approx 0 \tag{2.24}$$

Substituting Equations 2.24 into Equations 2.23 gives:

$$\sigma_x = \frac{\sigma\sqrt{\pi a}}{\sqrt{2\pi r_1}} \cos\frac{\theta_1}{2}\left[1 - \sin\frac{\theta_1}{2}\sin\frac{3\theta_1}{2}\right] \tag{2.25a}$$

$$\sigma_y = \frac{\sigma\sqrt{\pi a}}{\sqrt{2\pi r_1}} \cos\frac{\theta_1}{2}\left[1 + \sin\frac{\theta_1}{2}\sin\frac{3\theta_1}{2}\right] \tag{2.25b}$$

$$\tau_{xy} = \frac{\sigma\sqrt{\pi a}}{2\pi r_1} \cos\frac{\theta_1}{2}\sin\frac{\theta_1}{2}\cos\frac{3\theta_1}{2} \tag{2.25c}$$

When we examine the equations about stress field of a crack tip, $\sigma\sqrt{\pi a}$ has a fixed value which is only related to applied load and the crack length, labeled as a constant K. The stress field of a crack tip is always the same for any cracked body of the same material, which is dominated by the inverse square root singularity (Sanford 2003). The magnitude of the singular term only depends on K, which varies with the geometry and type of loading. Thus, K is an important characteristics feature of the stress field of a crack tip, which is widely used in fracture and fatigue characterization.

3. CHEMICALLY STABILIZED SOILS

3.1 Soil Binders and Stabilized Soils

Subgrade soil stabilization has a major impact on the pavement performance and durability. The failure of sublayers of stabilized soil can be catastrophic, and it is expensive to remedy this failure. The most common binder used for soil stabilization is Portland cement. A polymer based binder is also a viable alternative. A number of studies have considered the use of polymer for soil stabilizations. Iyengar et al. (2012) investigated the mechanical performances of several stabilized soils with commercial polymers and found that polymer-stabilized soils have comparable or superior performance compared to cement-stabilized. There are various types of polymers, but many are variations of polyacrylamide (PAM) and its derivatives. In this research, a polymer binder and Portland cement are used for soil stabilization. The polymer used is a polyacrylamide based hydrocarbon chain, which is engineered and synthesized by the research team in the laboratory (as shown in Figure 3.1).
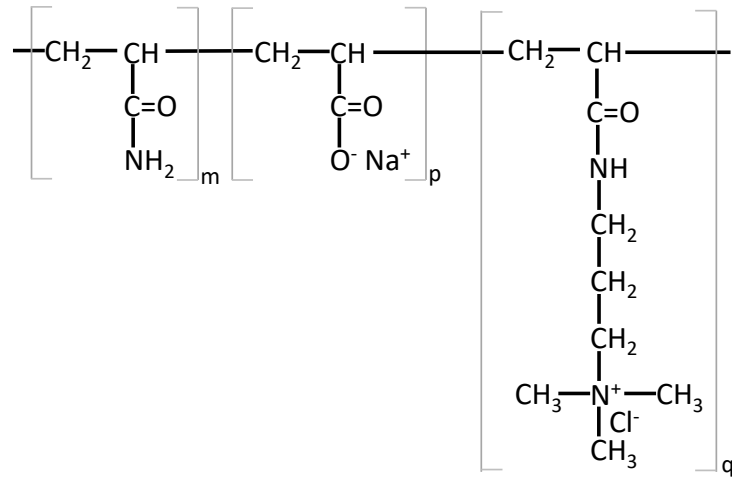
(a)
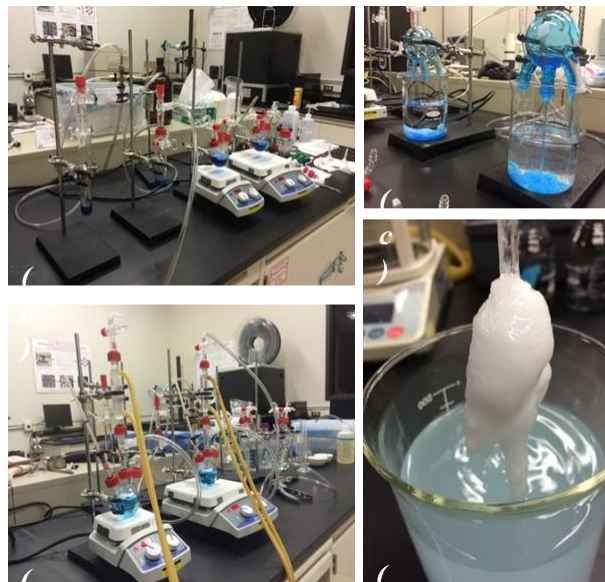
(b)

Figure 3.1 The Polymer Used in the Test: (a) the Structure of the Polymer (Hanley et al. 2014), and (b) the Polymer Synthesized in the Laboratory

Three stabilized soils including cement-stabilized sand, cement-stabilized limestone and polymer-stabilized limestone are tested. The sand is a fine-grained quartz

sand, and all the materials used pass the No. 40 standard sieve. The Portland cement dosage for all "cement" stabilized samples was 9 % by weight of dry soil. The polymer dosage is 2% of aqueous solution (the ratio of polymer to water by weight was one-to-one or a 50% blend of polymer in water) by weight of dry limestone. The optimum moisture contents (OMCs) for the stabilized soils are determined according to AASHTO T99 and presented in Table 3.1.

Table 3.1 Optimum Moisture Contents for Stabilized Soils

Stabilized soils	OMC (%)
Limestone + Cement (9%)	11.5%
Limestone + Polymer (2%)	11%
Sand + Cement (9%)	12.5%

3.2 Resilient Modulus of Cement and Polymer Stabilized Soils

Resilient modulus is an important mechanical property of base course and subgrade soils, which is widely used in the mechanistic-empirical design of pavement structures. This section is to characterize resilient modulus of cement and polymer stabilized soils for comparison. High resilient modulus is favorable to the durability of pavement system.

Resilient modulus test is widely used to characterize material stiffness using triaxial test method by applying cyclic loads in the laboratory. The test is performed in accordance with the AASHTO T307 which outlines the procedure to determine the resilient modulus of subgrade soils. Figure 3.2 illustrate the stresses, strains and loading

configuration used in the resilient modulus test. The resilient modulus is calculated using the following equation:

$$M_r = \frac{\sigma_d}{\varepsilon_r} \qquad (3.1)$$

Where σ_d is the deviatoric stress and ε_r is the axial resilient strain (or recoverable strain).

A cylindrical sample with a height of 150 mm and a diameter of 150 mm was compacted according to ASTM D698 for the resilient modulus test (as shown in Figure 3.3a). After compaction, the samples treated with cement or lime were wrapped in a plastic wrap with about 10 mL of free water to ensure proper moisture for pozzolanic reactions, and then cured at 40 °C for 7 days before the testing according to the guidelines established in the mixture design protocol provided by the NCHRP – w144 by Little et al. (2009) for both cement and lime stabilization mixture design considerations. The samples treated with Terpolymer were not wrapped and curing at 40 °C for 28 days.

For the testing, Figure 3.2 shows the apparatus used which include an IPC 100mm Rapid Triaxial Tester (RaTT) cell installed into a UTM-25kN hydraulic testing frame and two linear variable differential transformers (LVDTs). The LVDTs are accurate to capture the axial recoverable strain of the sample under cyclic loads. As per AASHTO T307, the sample is first pre-conditioned by applying 1000 loading cycles. After pre-conditioning, 100 cycles of load are applied at a constant confining pressure of 41.4 kPa and a deviatoric stress of 41.4 kPa. The cyclic loading is in the form of a haversine load pulse with a 1.5-sec. load duration and 1.5-sec. rest period.

$\sigma_1 - \sigma_3 = Deviator\ Stress$

σ_3

σ_3

Total Strain

Resilient Strain

Plastic Strain

Deviator Stress, $\sigma_1 - \sigma_3$

Axial Strain (in./in.)

(a)   (b)
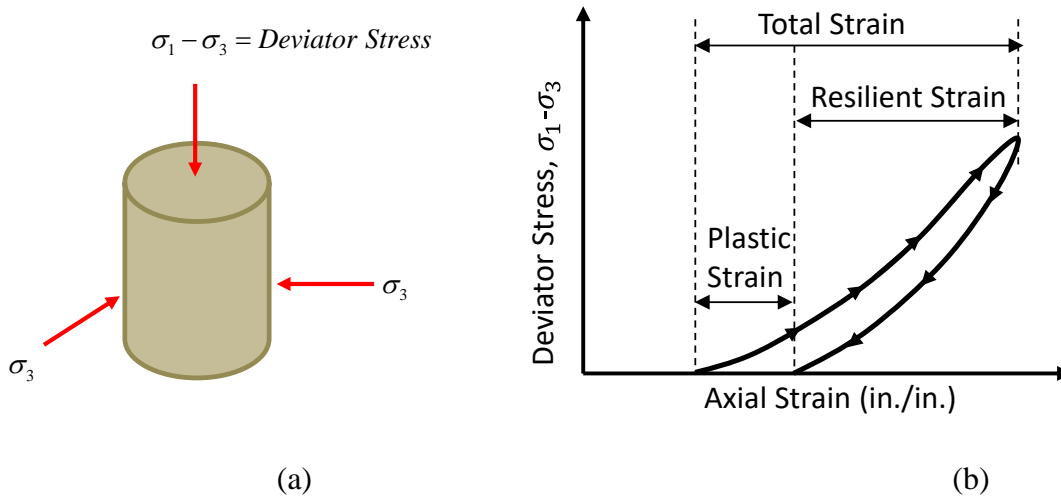
Figure 3.2 Resilient Modulus Test: (a) Deviatoric Stress and Confining Pressure, and (b) Resilient Strain

(a)   (b)   (c)
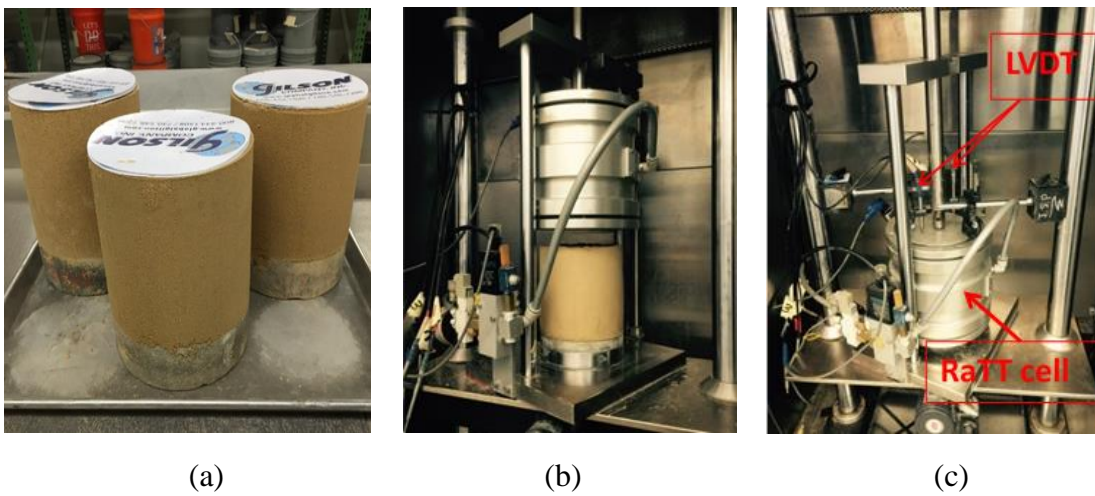
Figure 3.3 Resilient Modulus (RM) Test: (a) Compacted Samples, (b) Test Apparatus and a Sample, (c) a Sample in Testing

The resilient modulus test was performed on three replicates for each case and the results are presented in Figure 3.4. It is observed that the limestone samples treated with Terpolymer exhibit a much larger resilient modulus than the others, a 50% increase compared with the cement treated limestone. It should be noted that sand without

20

treatment is difficult to be compacted in the laboratory as there is no much cohesion between sand grains, and thus only sand treated with cement is presented here. When looking at the coefficient of variation (COV), all the cases have an acceptable COV (smaller than 30%) since the soils are heterogeneous and the compaction and curing for different replicates could cause such variations.
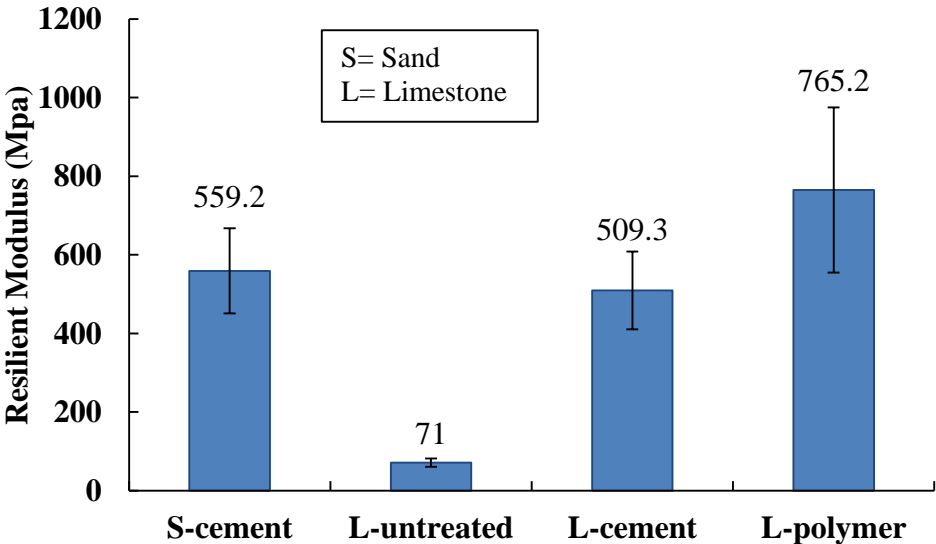
Figure 3.4 Resilient Modulus for Different Soils before and after Treatment with Lime or Cement or Terpolymer

4. FRACTURE CHARACTERIZATION OF CHEMICALLY STABILIZED SOILS USING MONOTONIC SCB TEST*

4.1 Problems

Stability of materials comprising pavement sublayers has a significant impact on the long-term performance of pavement systems (1). A typical pavement structure is composed of a surface layer, base layer and subgrade. Portland cement, lime or polymers are used to treat underlying materials (aggregates and soils) to provide a stabilized base course with a better support for the surface layer. However, the rigid matrix often developed with cementitious and pozzolanic stabilizers often produces chemically stabilized materials (CSMs) that are susceptible to fracture and fatigue. Fracture-susceptible paving materials compromise the life and sustainability of the pavement structure. Thus, an appropriate test method to characterize the fracture resistance of the stabilized soils is essential for design of pavement materials and structures.

Indirect tensile (IDT) tests and Compact Tension (CT) tests have been used to characterize fracture resistance of stabilized soils in a number of previous studies (Little 1987; Crockford et al. 1987; Harison et al. 1993; Sobhan et al. 2002; Piratheepan et al. 2010; Paul et al. 2010). The CT test is a reliable tension test, but sample preparation is complicated and time-consuming due to complex specimen geometry as shown in Figure

_____

4.1a. The IDT testing is simple, but its indirect tension mode resulting in multiple cracks instead of a single crack and high concentration of loads at two loading points may compromise the accuracy of the measurement, as shown in Figure 4.1b. The semi-circular bending (SCB) test is a simple three-point bending test (as shown in Figure 4.1c), which was first used to assess fracture properties of rocks and has been widely used in the area of asphaltic materials by several researchers (Molenaar et al. 2002; Li et al. 2004; Van et al. 2008; Kim et al. 2012; Im et al. 2014). The SCB test has several advantages compared to the IDT and DCT tests: (1) simple test procedure and setup; (2) easy and efficient sample preparation; (3) a sensitive fracture test; and (4) good repeatability.

(a)

(b)

(c)
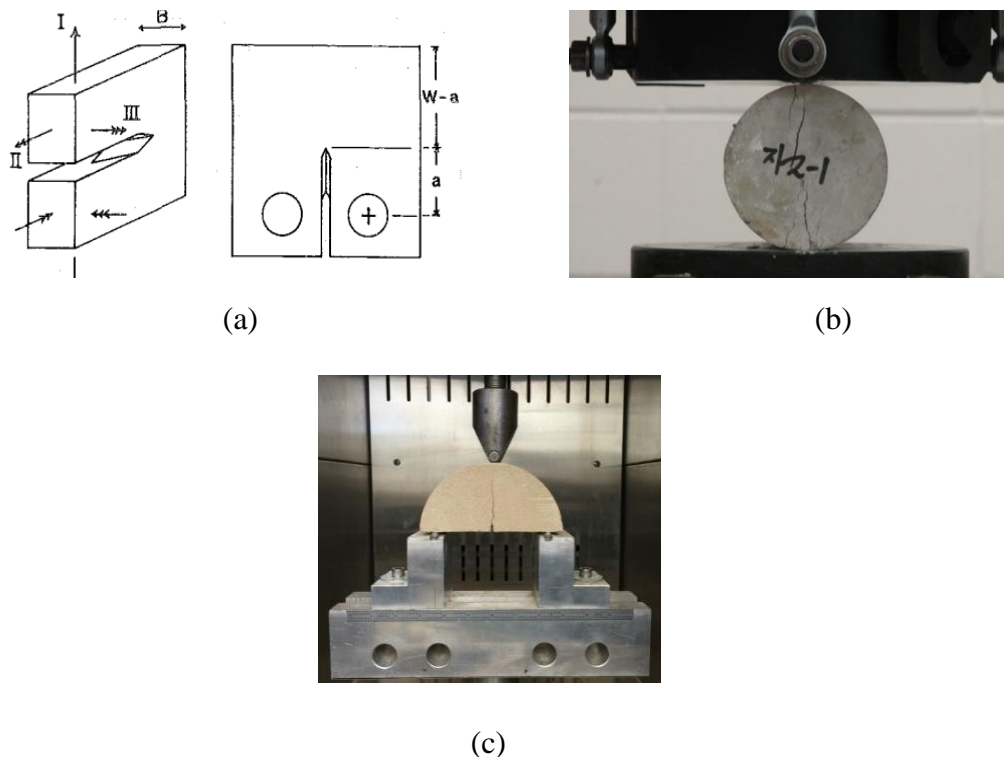
Figure 4.1 Three Fracture Tests: (a) Compact Tension Test (Reprinted from Crockford et al. 1987) (b) Indirect Tension Test (Reprinted from Choi et al. 2013), and (c) Semi-circular Bending Test

Another benefit for using the SCB geometry is that the parameter of stress intensity factor based on the linear elastic fracture mechanics can be used for test data analysis since the mathematical function for calculating stress intensity factor has been established. Fracture mechanics parameters such as fracture toughness (namely stress intensity factor) and fracture energy are widely used to characterize fracture resistance of materials. Based on linear elastic fracture mechanics (LEFM) and many experimental studies, researchers have identified several factors that may affect the fracture toughness: specimen thickness, notch length and loading rate (Nagai et al. 1981; Iqbal et al. 2007; Schmidt 1976; Khan et al. 2000; Lim et al. 1994; Bazant et al. 1992). Certain studies have shown that specimen thickness has a distinct effect on fracture toughness (Nagai et al. 1981; Iqbal et al. 2007; Schmidt 1976). Iqbal et al. (2007) evaluated the effect of thickness on fracture toughness of brittle rocks and found that the fracture toughness increased with decreasing thickness. This is not surprising as it is well established , based on fracture testing of metals, that as the thickness of a compact tensile sample increases, it mode 1 fracture toughness decreases as it moves toward plane strain. Schmidt (1976) studied the fracture toughness of limestone and found that it increased with increasing thickness However, a number of studies have shown that the specimen thickness does not significantly affect the fracture toughness of more rigid materials (Khan et al. 2000; Fowell et al. 1990; Chong et al. 1987; Singh et al. 1990). The impact of notch length is not so well established. Khan et al. (2000) found that the fracture toughness initially increased to a maximum value and then decreased with the increase of notch length. Lim et al. (1994) studied the fracture toughness of a soft rock and reported that when the notch length exceeded than 3 mm, the

fracture toughness tended to reach a constant value. As expected, loading rate has an effect on the fracture toughness. Bazant et al. (1992) found that the fracture toughness of concrete increased with increasing loading rate, and the effective length of the fracture process zone decreased with increasing loading rate, which means the material acts more brittle at higher loading rates. Lim et al. (1994) found the similar trend that the fracture toughness of a soft rock increased with the increase of loading rate. Based on the aforementioned discussions, the effects of such test variables as specimen thickness, notch length, and loading rate on the SCB test results require investigation.

4.2 Development of SCB Test Methodology for Fracture Characterization of Stabilized Soils

The SCB test is based upon a simple three-point bending configuration (as presented in Figure 1). The SCB specimen is subjected to a monotonic load with a constant rate of displacement. The diameter of the specimens used in this study is 150 mm. Crack propagates along the notch in the centerline of the specimen under loading, which is evident in Figure c. The SCB test methodology for chemically stabilized soils has not been established. This section presents the test protocol including the method of sample preparation and data analysis methods.

4.2.1 Method of Sample Preparation

Figure 4.2 presents the compaction process for the samples used in the SCB test. The treated soils were prepared at their optimum moisture contents (OMCs) according to AASHTO T99. The OMCs and MDDs (maximum dry densities) for cement-stabilized

sand, cement-stabilized limestone and polymer-stabilized limestone are 12.5% and 1.79 g/cm3, 11.5% and 1.93 g/cm3, and 11% and 2.00 g/cm3, respectively. The samples were then compacted using the standard compaction effort following ASTM D 698 and using a mechanical compactor as shown in Figure 2b. After compaction, a tool as shown in Figure 4.2c was used to level the top surface of the compacted sample. The last step was to extract the compacted sample from the mold. Figure 3 shows the compacted samples for cement-stabilized sand, cement-stabilized limestone and polymer-stabilized limestone.

The cement-stabilized samples were wrapped in plastic with about 10 mL of free water and cured in an oven at 40 °C for 7 days according to the guidelines established in the mixture design protocol provided by the NCHRP w144. The added 10 mL of free water was to ensure the availability of moisture to support pozzolanic reactions. The polymer-stabilized samples without plastic wrap were cured in an oven at 40°C for 28 days.

After curing, the cylindrical samples were saw cut and notched to produce SCB specimens. Figure 4.4 demonstrates the sample fabrication process. A compacted sample was cut into two SCB specimens using a single blade saw. A notch was then cut into the SCB specimen. In this study, a total of four SCB specimens for each material were fabricated and tested.

(a) (b) (c) (d)
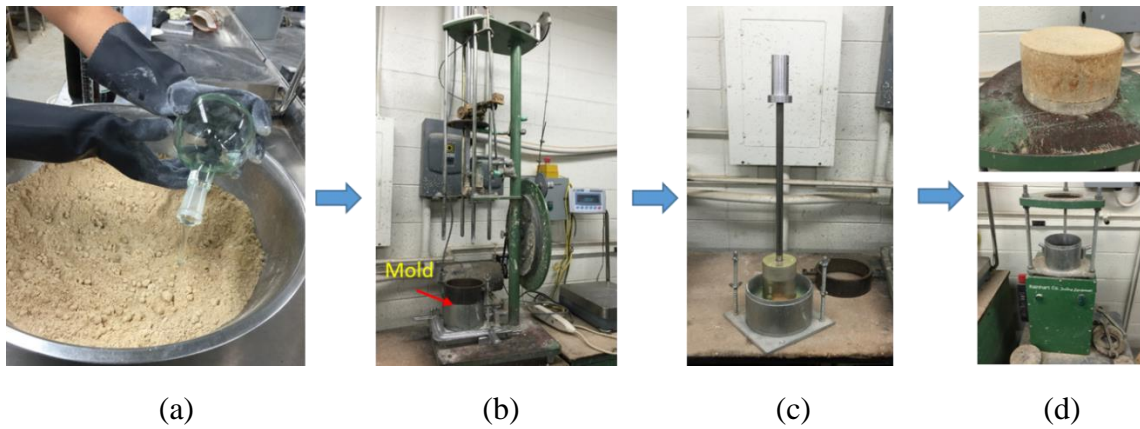
Figure 4.2 The Compaction Process: (a) Adding Compaction Moisture, (b) Mechanical Compactor, (c) Level Top Surface of a Compacted Sample, and (d) Extract the Compacted Sample from the Mold

(a) (b) (c)
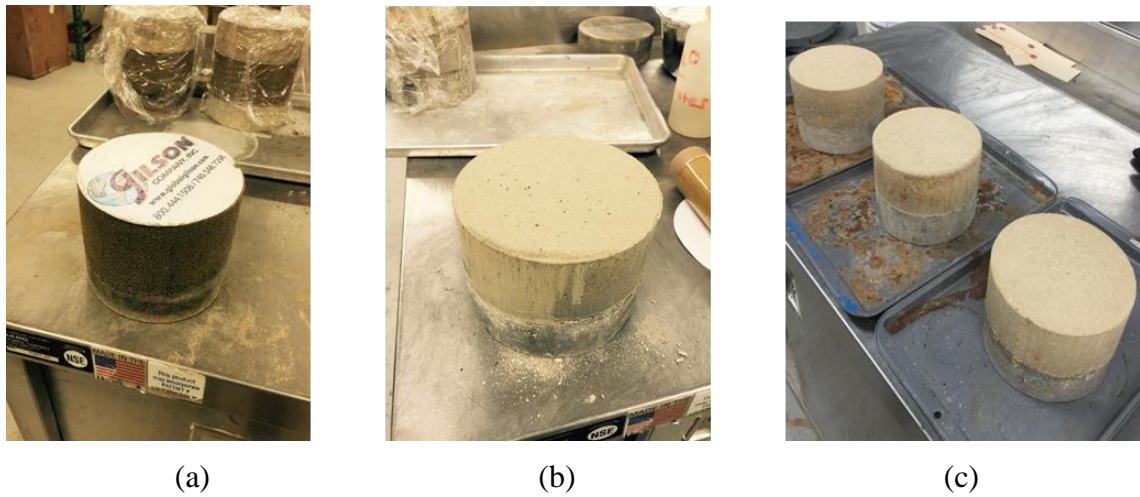
Figure 4.3 Compacted Samples: (a) Cement-stabilized Sand, (b) Cement-stabilized Limestone, (c) Polymer-stabilized Limestone
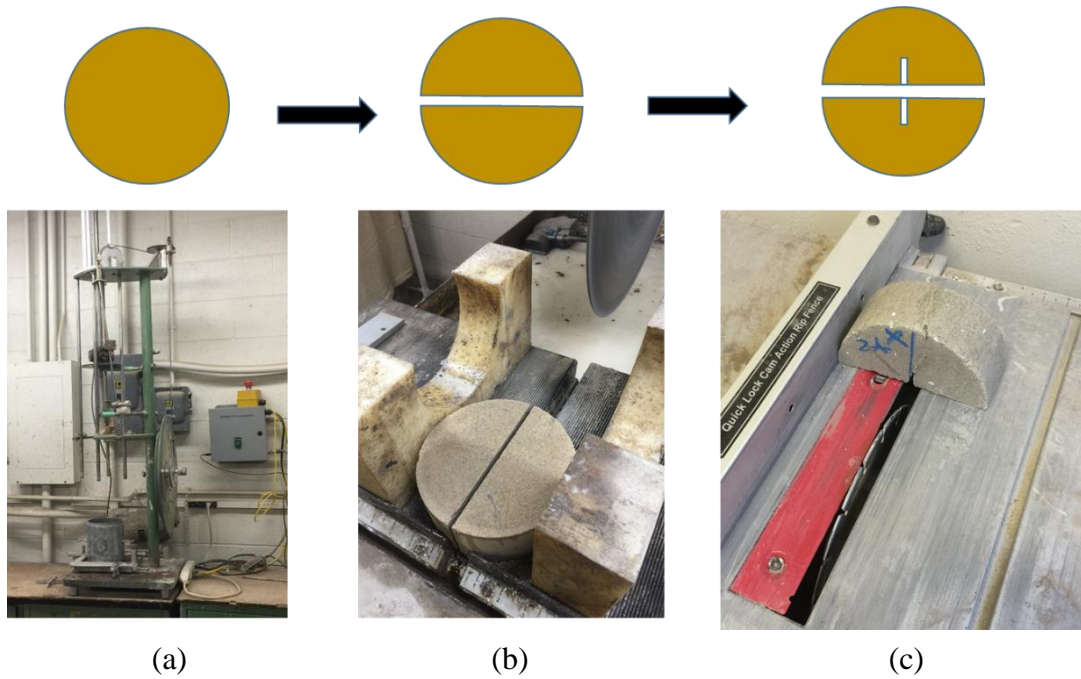
Figure 4.4 SCB Specimen Production Process: (a) Compact a Cylindrical Sample, (b) Cut the Compacted Samples (after Curing) into Halves, and (c) Make a Notch

4.2.2 Data Analysis Method

Two parameters, fracture energy and fracture toughness (i.e., stress intensity factor), are chosen to characterize the fracture resistance of the stabilized soils. Fracture energy is widely used for fracture potential assessment for inelastic or viscoelastic materials such as asphalt mixtures, which, like these stabilized soil, are heterogeneous materials. Fracture energy was based on a more "global" concept that interprets fracture potential over a greater analysis region. On the other hand, as opposed to viscoelastic asphalt mixtures, both cement-stabilized and polymer-stabilized soils are brittle materials, which means that LEFM is more applicable. Thus, fracture toughness was also selected as a candidate fracture parameter.

Fracture energy is calculated by dividing fracture work with ligament area, as expressed in the following equations:

$$G_f = \frac{W_f}{A_{lig}}$$
(4.1)

where G_f = fracture energy (J/m^2)

W_f = work of fracture (J), the area under load-displacement curve,

$W_f = \int P du$,

P = applied load (N),

u = load point displacement (LPD),

A_{lig} = ligament area (m^2), the fracture surface area; $A_{lig} = (r - a) \times t$, r, a, t are specimen radius, notch length (m) and specimen thickness, respectively.

Fracture toughness (K_{IC}) is obtained as the stress intensity factor K_I at the critical load P_c. The maximum load during the test is assumed to be P_c. K_{IC} is computed using the following equation (Lim et al. 1994):

$$\frac{K_{IC}}{\sigma_0 \sqrt{\pi a}} = Y_{I(0.8)}$$
(4.2)

where $\sigma_0 = \dfrac{P_c}{2rt}$

P_c = the critical load;

r = specimen radius (m);

t = specimen thickness (m);

a = notch length (m);

$$Y_{I(0.8)} = 4.782 + 1.219\left(\frac{a}{r}\right) + 0.063\exp\left(7.045\left(\frac{a}{r}\right)\right),$$ which is the geometric factor.

4.3 Effects of Test Variables on the Monotonic SCB Test Results

Numerous studies have investigated fracture toughness of materials using LEFM, and these studies have indicated that a number of test variables affect fracture toughness. A better understanding of the effects of these test variables on the SCB test results is essential for effective material characterization. The test variables including specimen thickness, notch length and loading rate were addressed. Experiments discussed in this section used to evaluate the effects of testing variables were conducted on quartz sand stabilized with Portland cement.

4.3.1 Specimen Thickness

Based on LEFM, the fracture toughness decreases to a lower constant value with an increase of the thickness (Roylance 2001). The constant toughness is regarded as a material property since it does not change with a change in thickness. In order to evaluate the effect of specimen thickness on fracture properties, three thicknesses of 40, 50 and 60 mm compared. Other testing variables (i.e., notch length = 15 mm, loading rate = 1 mm/min) were selected based on information from the literature. The SCB test results are presented in Figure 4.5 and Figure 4.6. As can be seen from these figures, a variation in specimen thickness from 40 to 60 mm does not have a substantial impact on either fracture energy of fracture toughness. The data indicate that fracture toughness values are, for practical purposes, constant over this range of specimen thicknesses. Although no

significant difference is observed in the fracture properties and coefficient of variance (COV) between different thicknesses, it is observed that the 60-mm thick specimens exhibit good repeatability based on the load-displacement curves. Therefore a thickness of 60 mm was selected for the experimental testing.
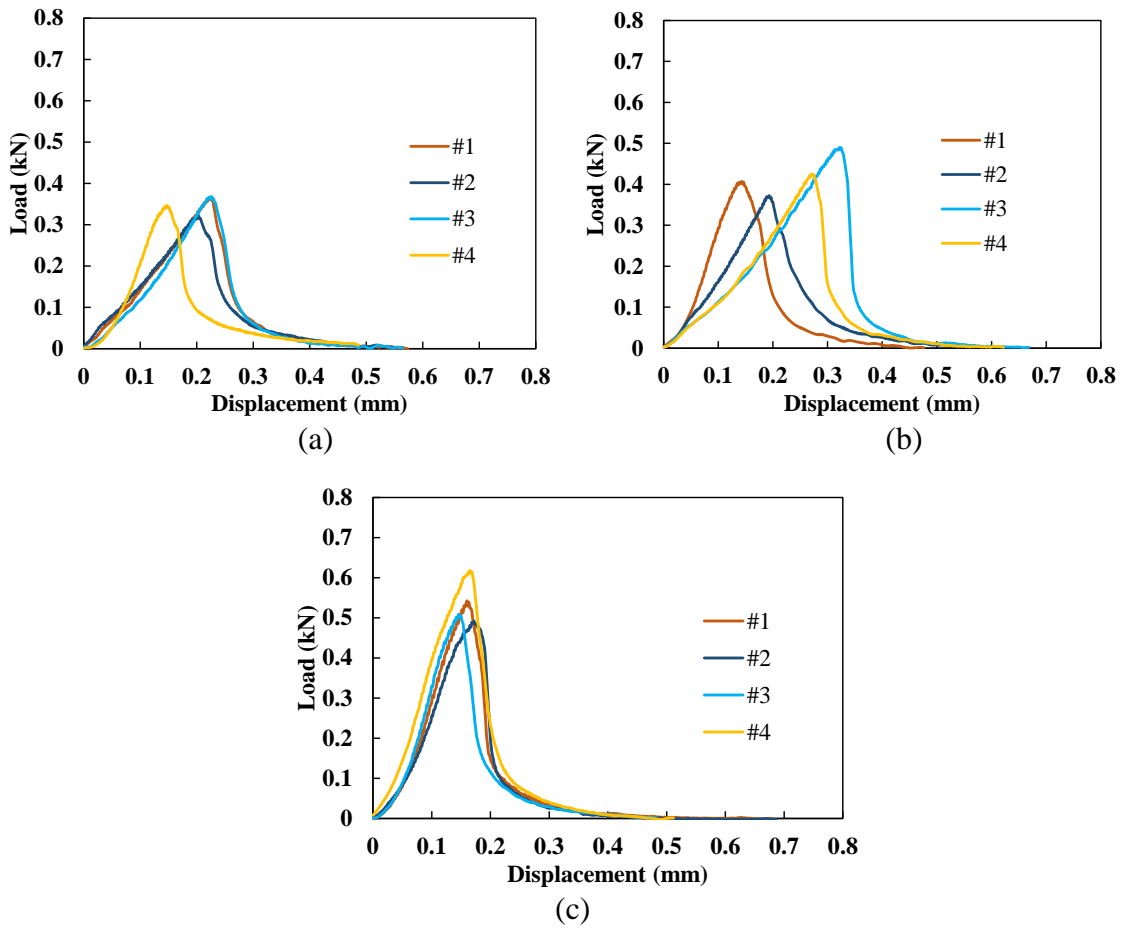
Figure 4.5 SCB Load-displacement Curves for Different Thicknesses of Specimens: (a) 40 mm, (b) 50 mm, (c) 60 mm
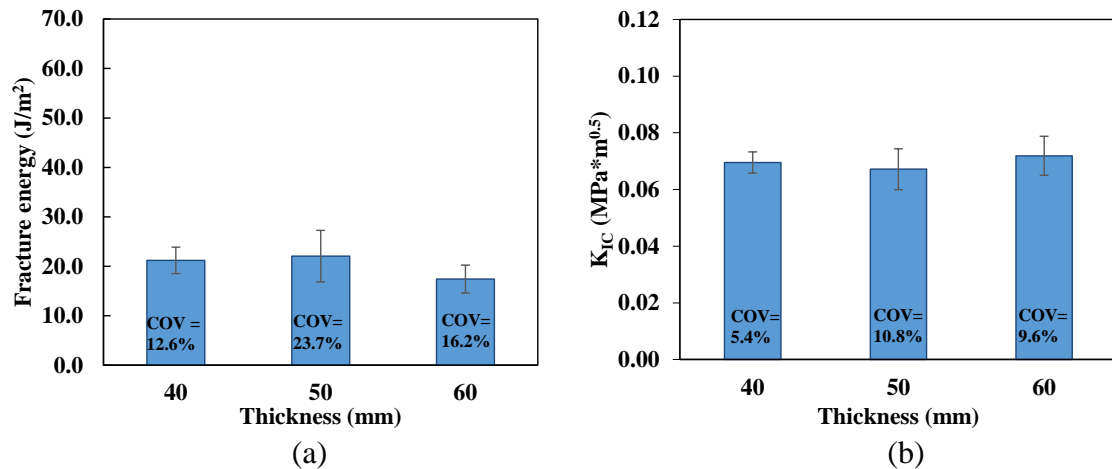
Figure 4.6 Fracture Properties for Different Thicknesses of Specimens: (a) Fracture Energy, and (b) Fracture Toughness

4.3.2 Notch Length

Previous studies indicate that notch length affects the fracture toughness of materials such as rocks (Lim et al. 1994; Khan et al. 2000). For viscoelastic material such as asphalt mixtures, fracture energy decreases linearly with the increase of the notch length (Nsengiyumva et al. 2015). In order to evaluate the effect of notch length on fracture properties, specimens with four different notch lengths (i.e., 0, 15, 25 and 35 mm) were prepared and tested. A loading rate of 1.0 mm/min was initially chosen. Figure 6 presents load-displacement curves and fracture properties. As seen in Figure 6 the peak load decreases with the increase of notch length. The specimens without the notch (i.e., notch length = 0 mm) showed the highest peak load and fracture energy; and when examining the specimens after testing, the crack(s) deviated from the centerline of the specimen in most cases, which could cause an overestimation of fracture energy and unrepeatable load-displacement curves (as shown in Figure 4.7a). Thus, un-notched specimens are not a good option for the SCB test.

When comparing fracture energy test results for specimens with notch lengths of 15, 25 and 35 mm, the notch length does not have a significant effect on the fracture energy. However, the fracture energy values for specimens with a notch length of 35 mm are on average value than both of the 15 and 25 mm cases. The trend is clear that fracture toughness decreases with an increase of notch length. The authors conclude that the notch length of the SCB specimen has an effect on the fracture properties of cement-stabilized sand, but more testing is needed to validate this statement. It can be seen that all three notch lengths of 15, 25 and 35 mm show comparable COVs, but the authors recommend using the 15 mm notch length as the shorter notch length gives the specimen a larger fracture ligament to sufficiently capture the fracture properties of the stabilized soils. Therefore, the notch length of 15 mm was chosen for this test.
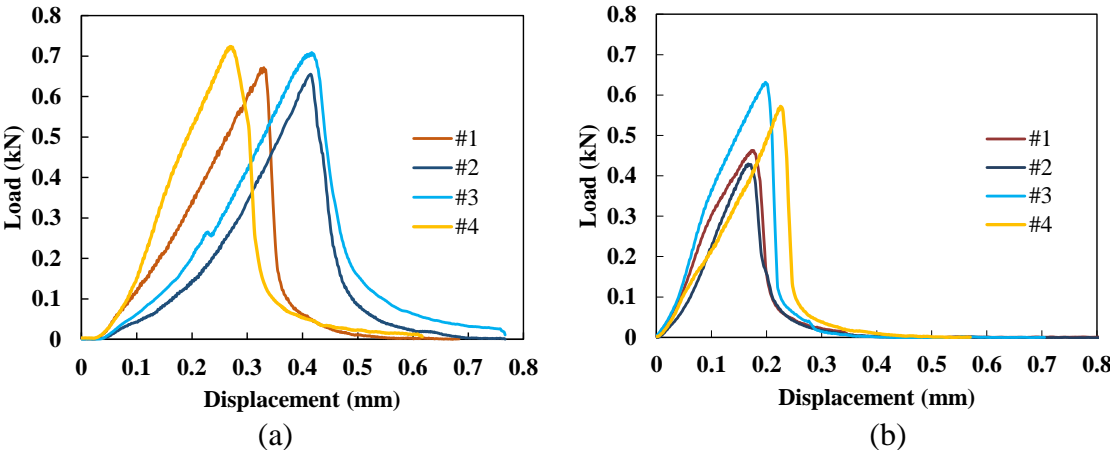
Figure 4.7 SCB Load-displacement Curves for Different Notch Lengths: (a) 0 mm, (b) 15 mm, (c) 25 mm, (d) 35 mm

(c)

(d)
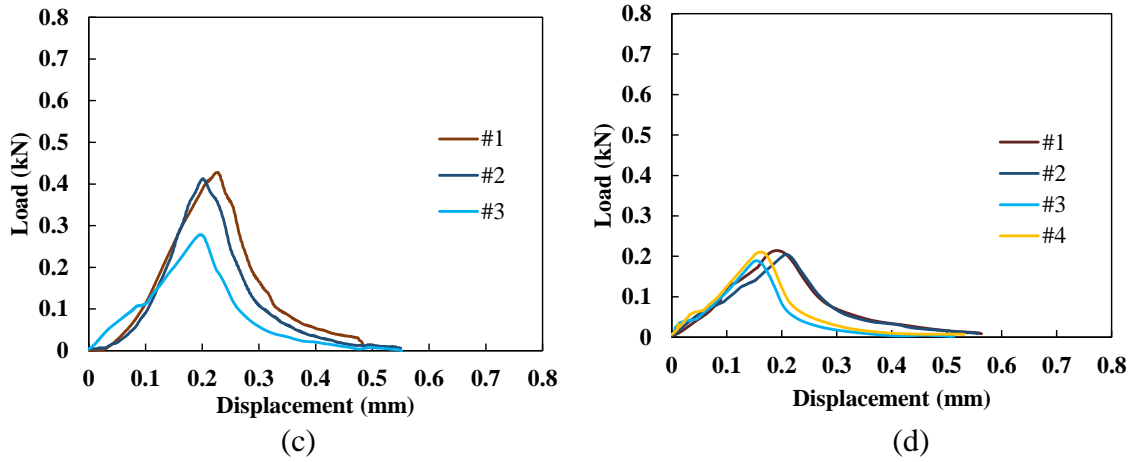
Figure 4.7 Continued.

(a)

(b)
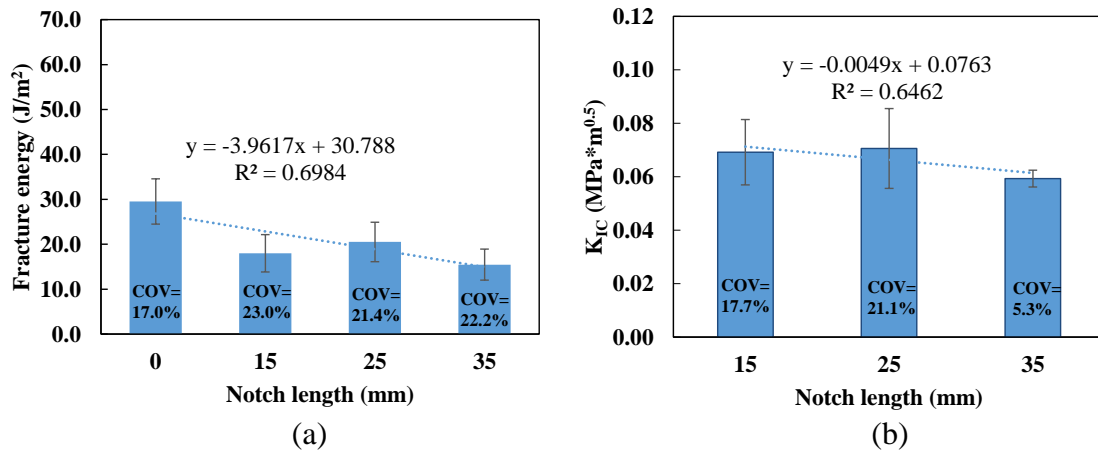
Figure 4.8 Fracture Properties for Different Notch Lengths: (a) Fracture Energy, and (b) Fracture Toughness

4.3.3 Loading Rate

Some studies have demonstrated that fracture toughness increases with increasing loading rate (Lim et al 1994; Byzant et al. 1992). To evaluate the effect of loading rate on fracture properties, three loading rates (i.e., 0.5, 1.0 and 5.0 mm/min) are used. The test results are presented in Figure 4.9 and Figure 4.10. As can be seen the loading rate has a significant effect on the fracture energy and fracture toughness. The fracture energy

34

decreased with increasing loading rate, while the fracture toughness increased with increasing loading rate. Although the trends are opposite, the results are still reasonable as fracture energy and fracture toughness are two different concepts used to describe the fracture resistance of materials. Fracture energy is an average value based on energy equilibrium, which does not represent the stress state at the crack tip. However, fracture toughness represents the stress state of the crack tip. When loading rate is increased, the peak load, which is used to calculate fracture toughness, increases resulting in higher fracture toughness. Therefore, when calculating fracture energy and fracture toughness at various loading rates, the trends could be different and even opposite to each other. For comparison, a moderate loading rate of 1.0 mm/min was selected. Furthermore, the 1.0 mm/min loading rate shows more repeatable curves than the other two loading rates.
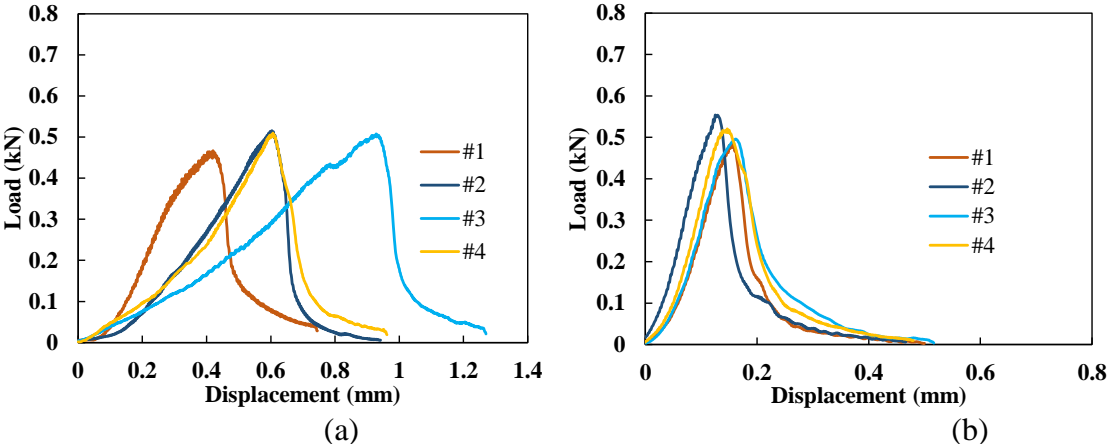
Figure 4.9 SCB Load-displacement Curves and Fracture Properties for Different Loading Rates: (a) 0.5 mm/min, (b) 1.0 mm/min, (c) 5.0 mm/min

(c)

Figure 4.9 Continued

(a)

$y = -21.263x + 67.725$
$R^2 = 0.9312$

(b)

$y = 0.0153x + 0.0453$
$R^2 = 0.888$
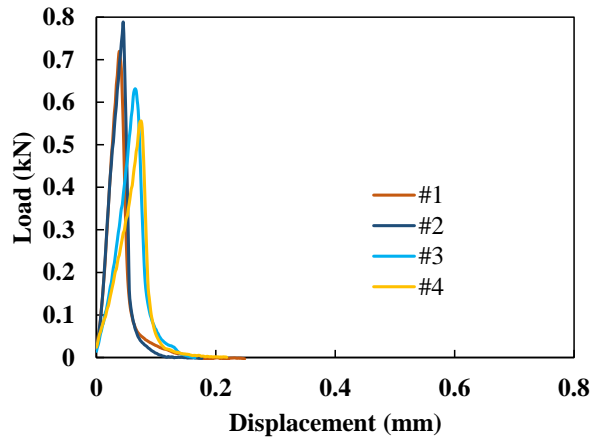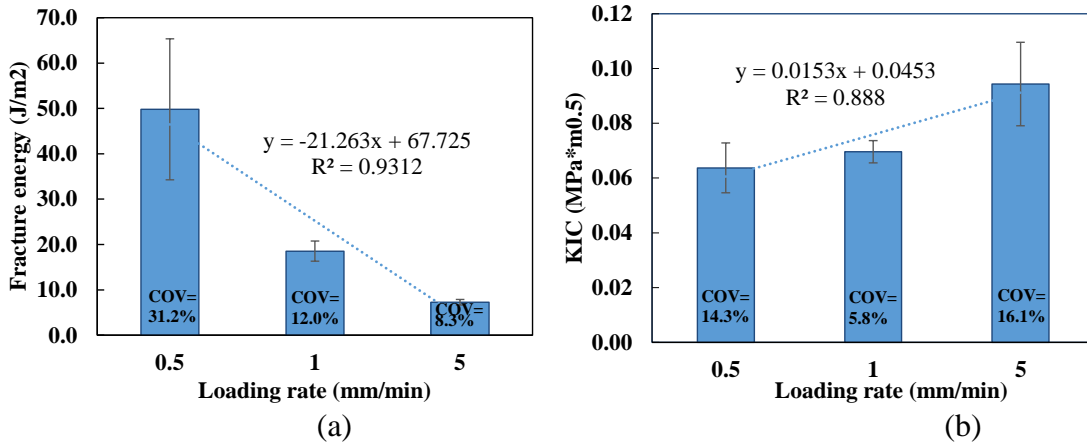
Figure 4.10 SCB Load-displacement Curves and Fracture Properties for Different Loading Rates: (a) Fracture Energy, and (b) Fracture Toughness

4.4 Fracture Characterization of Different Types of Stabilized Soils

The selected values of test variables (i.e., specimen thickness = 60 mm, notch length = 15 mm and loading rate = 1.0 mm/min) previously discussed were used to evaluate the fracture resistance of three different types of stabilized soils (i.e., polymer-stabilized limestone, cement-stabilized limestone and cement-stabilized sand). Figure 4.11

shows the SCB specimens after testing and the load-displacement curves. As observed cracking propagates along the centerline of the SCB specimens. The load-displacement curves for all the three cases show good repeatability, which further validates that the selected values of the test variables are appropriate. The polymer-stabilized limestone has the largest peak load while the cement-stabilized sand shows the lowest value. The fracture properties obtained from the test results are also presented in Figure 8. It is clear that the SCB test is able to differentiate among the fracture properties of the different stabilized soils. Polymer-stabilized limestone exhibited the largest fracture energy and fracture toughness, which is twice as large as that for the other two stabilized materials. In addition, the three materials rank consistently in terms of both fracture energy and fracture toughness.

Although this terpolymer resists fracture very well compared to the more brittle cement stabilized materials, its weakness is in its sensitivity to moisture damage. This is primarily due to the hydrophilic nature of the polymer due to its potential to interact with water via hydrogen bonding and/or the fact that water molecules are more strongly attracted to the surface of soil particles than the terpolymer. Nonetheless, the terpolymer provides better fracture resistance compared to cement stabilized soils in the state of nominal moisture content (near compaction optimum) but is likely to exhibit damage as moisture reaches high levels near saturation. This is an issue that is being addressed separately by the author and that is specifically to amend the polymer design to make it resistant to moisture effects, hydrophobic in nature.
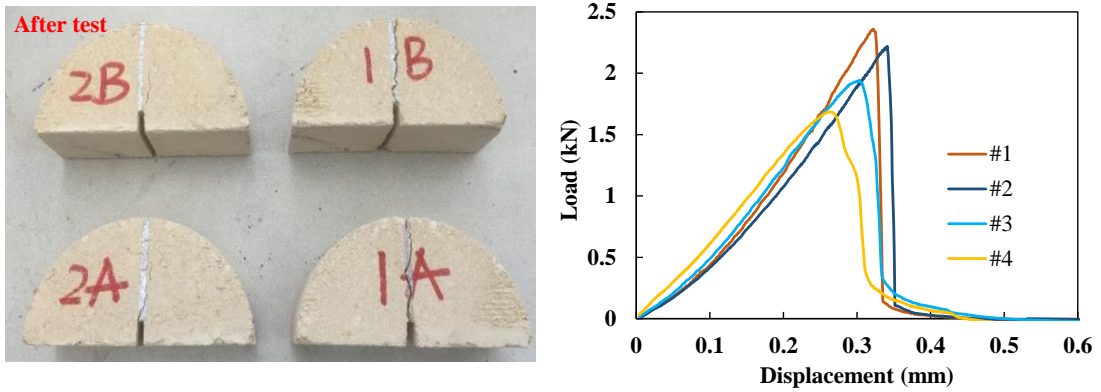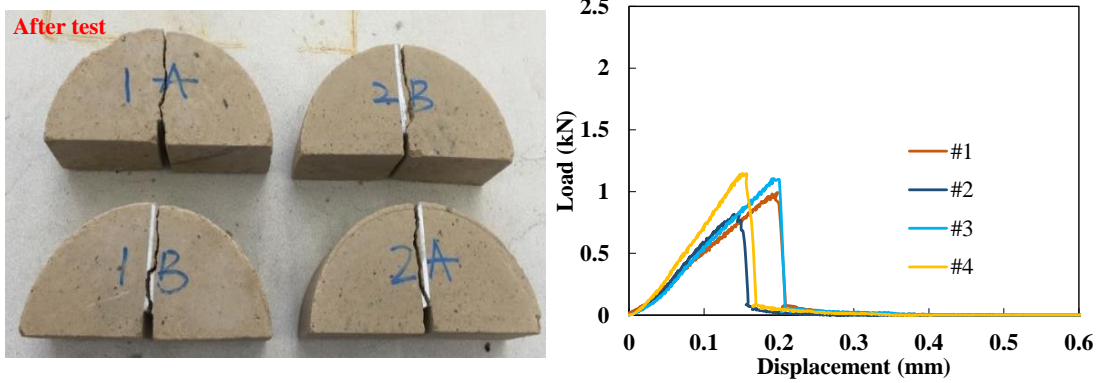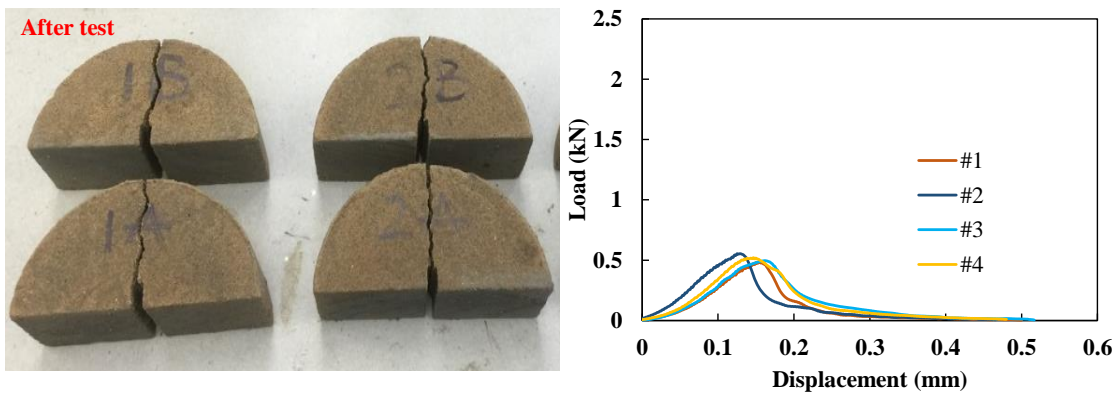
Figure 4.11 SCB Specimens after Test and Load-displacement Curves for Different Stabilized Soils: (a) Polymer-stabilized Limestone, (b) Cement-stabilized Limestone, (c) Cement-stabilized Sand
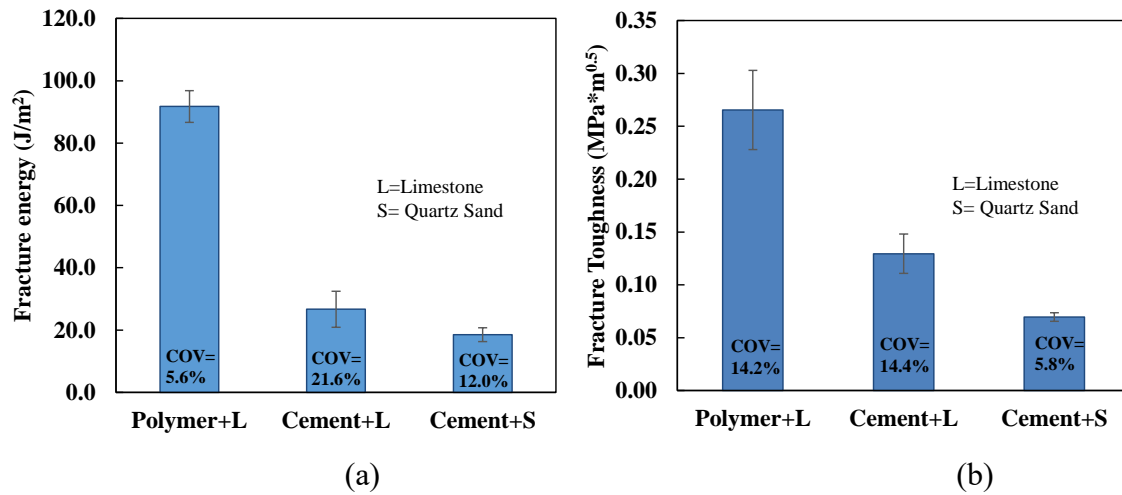
Figure 4.12 Fracture Properties for Different Stabilized Soils: (a) Fracture Energy, and (b) Fracture Toughness

4.5 Numerical Simulation of the SCB Test Results Using the Cohesive Zone Model

A number of studies have used cohesive zone models to characterize the fracture properties of various engineering materials (Im et al 2014; Kim et al. 2005; Song et al. 2006; Li et al. 2010; Aragao et al. 2011). As shown in Figure 9, the local fracture properties of different stabilized soils were obtained by integrating the SCB test results presented above. A three-dimensional finite element model in which zero-thickness cohesive elements were embedded along the center of the model was created to simulate the SCB fracture tests. Six-node linear triangular prism elements (C3D6) and three-dimensional eight-node cohesive elements (COH3D8) were selected for the bulk specimen and the cohesive zone, respectively. The mesh size and design was determined based on a sensitivity analysis conducted by Aragao et al. (2012). Young's modulus (E) was obtained by comparing the initial slope of the experimental results to that modeled in simulations where SCB fracture was not considered. Poisson's ratio (v) was assumed to be 0.35 for

the three stabilized soils. The elastic properties determined were used for the six-node linear triangular prism elements. The three-dimensional eight-node cohesive elements were incorporated with a bilinear cohesive zone model. As shown in Figure 4.13, the cohesive zone fracture energy (Γ_c), locally estimated fracture toughness, can be calculated by computing the area below the bilinear traction-separation curve with peak traction (T_{max}) and critical displacement (δ_c) as follows:

$$\Gamma_c = \frac{1}{2} T_{max} \delta_c \qquad\qquad (4.3)$$

In the cohesive zone model, recoverable linear elastic behavior is assumed until the traction (T) reaches the peak traction (T_{max}) when a corresponding separation (Δ) becomes a non-dimensional displacement (λ). Once damage initiates (i.e., Δ is equal to λ), T varies from T_{max} to zero, and the faces of the cohesive element are fully and irreversibly separated when Δ reaches δ_c. Two independent cohesive zone properties (T_{max} and Γ_c) of the three properties above were obtained through the model calibration process that targets close agreement between the SCB test results and model simulations.

As can be seen in Figures 4.14, 4.15 and 4.16, the model simulations agree very well with the experimental results. Table 4.1 summarizes the predicted elastic and cohesive zone fracture properties for three different soils, indicating that among three stabilized soils, the polymer-stabilized limestone had the highest stiffness. It was also observed that the polymer-stabilized limestone required higher force to initiate crack than other two stabilized soils (cement-stabilized limestone and cement-stabilized sand). The finite element modeling presented in this study was used to identify true fracture properties

that are independent of loading condition and specimen geometry of the material. Thus, the cohesive zone fracture properties (T_{max} and Γ_c) can be used as basic material property inputs (similar to stiffness) to predict and/or analyze fracture-related performance of other tests in different testing geometries (mixtures and structures) without extra experiments.
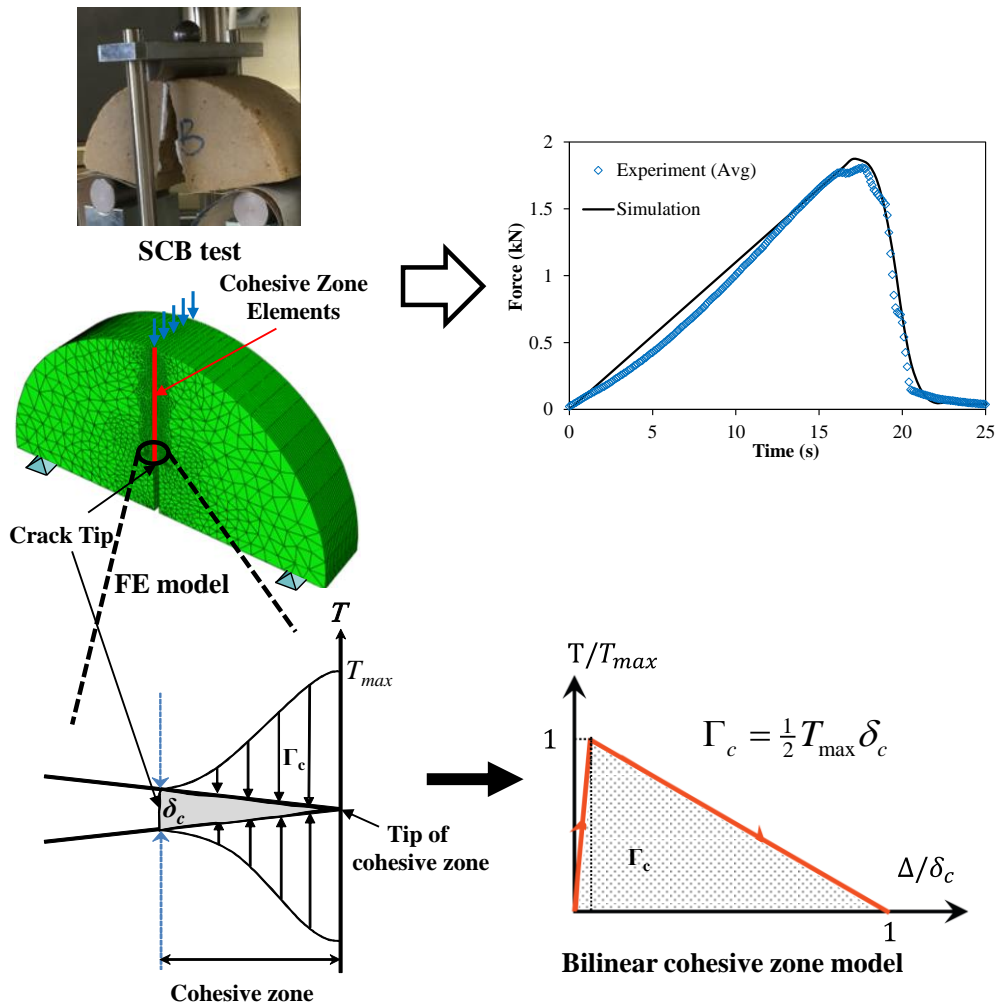
Figure 4.13 Schematic View of an Integrated Experimental-numerical Approach for Obtaining Fracture Properties by Incorporating with a Bilinear Cohesive Zone Model
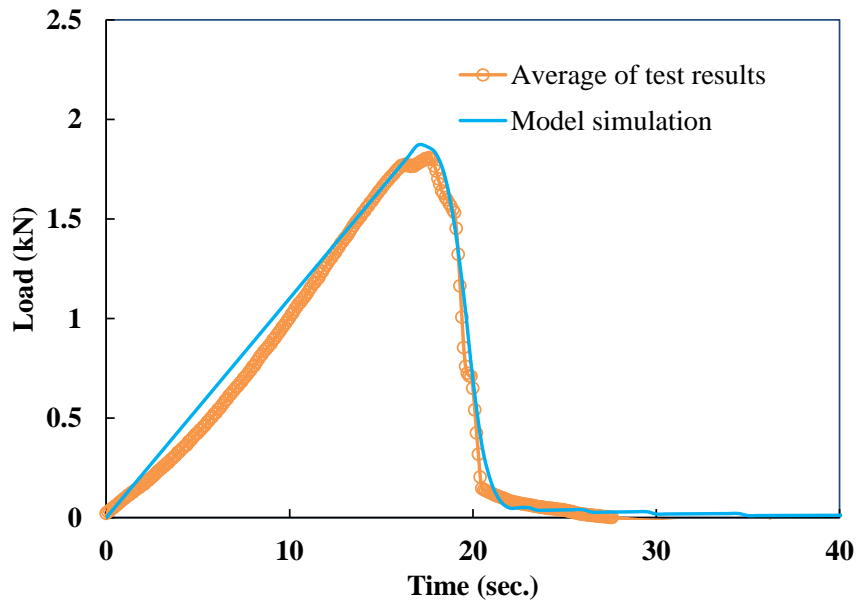
Figure 4.14 Experimental and Simulation Load-Time Curves for the SCB Test Results of Polymer-stabilized Limestone
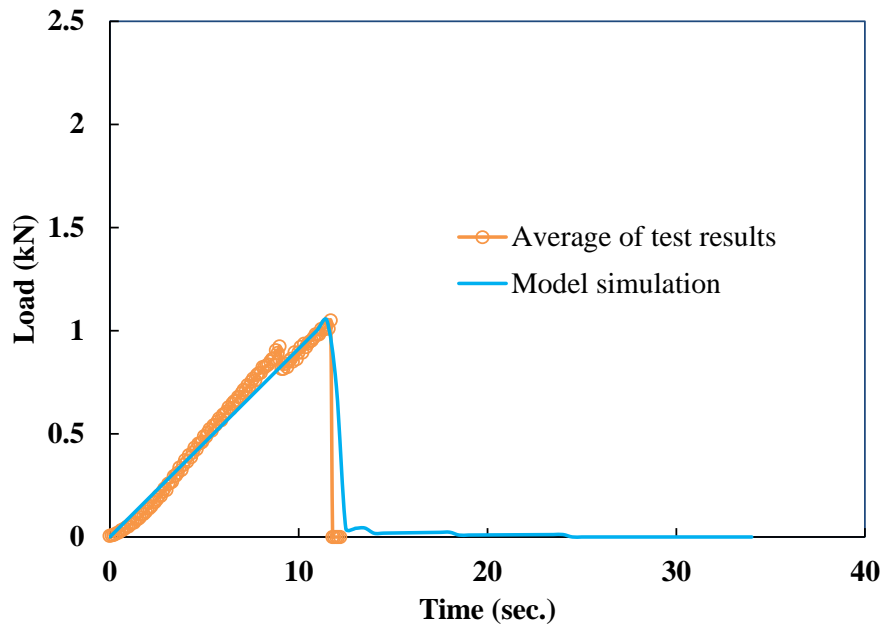
Figure 4.15 Experimental and Simulation Load-Time Curves for the SCB test Results of Cement-stabilized Limestone
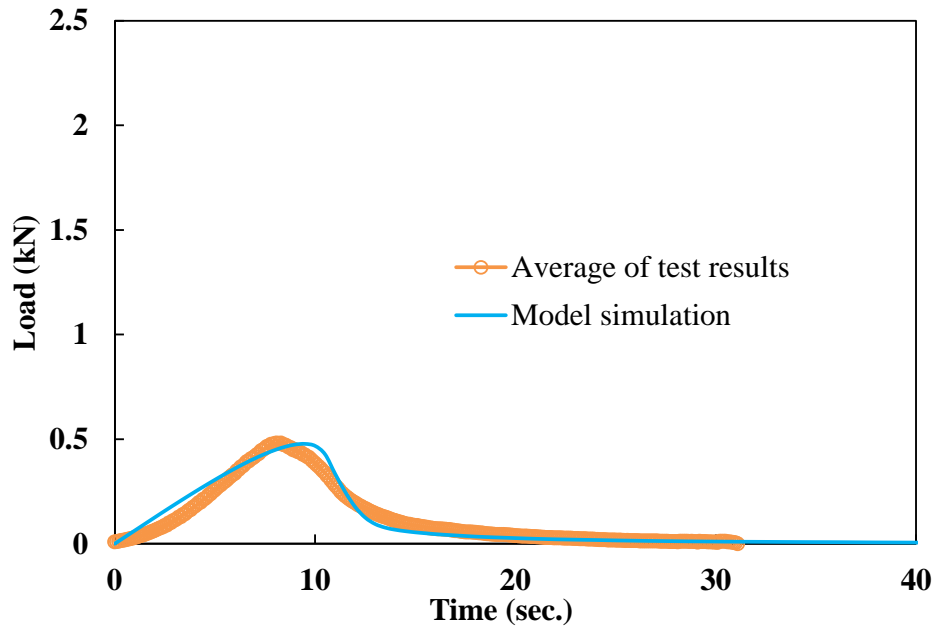
Figure 4.16 Experimental and Simulation Load-Time Curves for the SCB Test Results of Cement-stabilized Sand

Table 4.1 Summary of Predicted Elastic and Fracture Properties

Type of Stabilized Soils	Elastic Properties		Fracture Properties		
	E (MPa)	v	T_{max} (MPa)	Γ_c (J/m^2)	δ_c (mm)
Polymer-stabilized Limestone	700		3.70	30.0	0.016
Cement-stabilized Limestone	580	0.35	2.15	1.0	0.001
Cement-stabilized Sand	400		0.25	18.0	0.144

5. FATIGUE CHARACTERIZATION OF CEMENT STABILIZED SOILS USING CYLIC SCB TEST

5.1 Background of Fatigue Crack Growth

Fatigue is one of major distresses occurring in the materials and structures. It is estimated that more than 80 percent of all brittle fractures are preceded by a period of crack growth in fatigue (Sanford 2003). Characterization of fatigue is important because fatigue crack-growth portion is a major part of a structure's overall lifetime. Sanford indicated that the primary mechanism of fatigue on the microscale is dislocation motion occurring within the damage process zone. As the load is small in fatigue, the damage process zone is well contained with the singularity dominated zone of linear elastic fracture mechanics. Thus, the mechanism of fatigue is governed by the stress state within the singularity dominated zone, which can be fully characterized by the stress intensity factor K (Sanford 2003).

A material or structure generally experience three states of fatigue crack growth, as shown in Figure 5.1. Stage I is the process of crack initiation. Stage II is a stable crack growth portion, which accounts for the major part of the whole fatigue crack growth process. When the fatigue crack grows and approaches to the critical crack length, the crack grows rapidly, which is the process of Stage III, and the specimen eventually fails when satisfying the fracture criterion (i.e., $K_{max} > K_{IC}$).

44
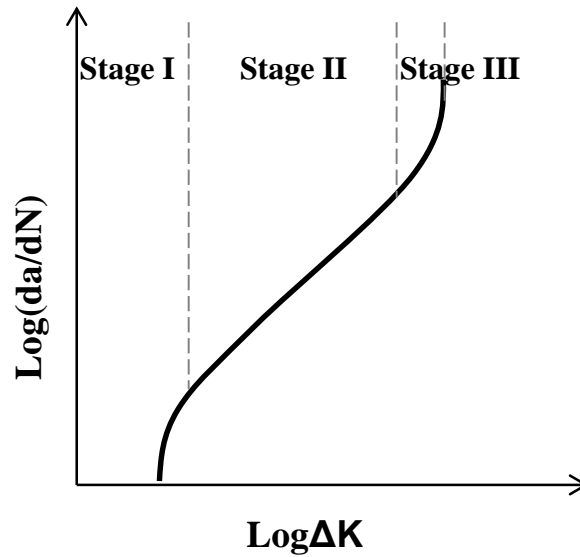
Figure 5.1 Three Stages of Crack growth

Characterization of Stage II crack growth is useful and important for predicting fatigue life of a structure in service since Stage II accounts for the major portion of fatigue crack growth. The theory of brittle fracture (e.g., K_{IC}) is derived from laws of physics, whereas the mathematical description of Stage II fatigue crack growth is based on the phenomenological method of analysis. The most popular model to characterize Stage II fatigue crack growth is Paris's law, which was proposed by Paris and Erdogan in 1963, as expressed in Equation 1:

$$\frac{da}{dN} = A(\Delta K)^n \tag{5.1}$$

where,

a = crack length;

N = load cycle;

A and n = material coefficients; and

ΔK = range of stress intensity factor.

As aforementioned, the mechanism of fatigue is governed by the state of stress within singularity dominated zone, which can be characterized by stress intensity factor K. Thus, the Paris's law describes the relationship between crack growth rate and stress intensity factor.

5.2 Compliance Method

The concept of compliance method is derived from linear elastic fracture mechanics. Figure 5.2 shows an example that a plate containing a crack with the length of a is subjected to an increasing load p, and at the same time the loading point has an increasing deflection δ. If the plate is linearly elastic, the relationship of p and δ is linear, as illustrated in Figure. The slope of the line is defined as the stiffness of the plate, and C_a is the compliance of the plate with a crack length of a. The expression for δ is:

$$\delta = C_a p \tag{5.2}$$

When the original crack length of a extends to a new crack length of a + da, a new linear relationship of p and δ is illustrated in Figure. As can be seen in Figure, each crack length corresponds to a specified compliance. The method of using compliances to determine crack lengths is named the compliance calibration method.
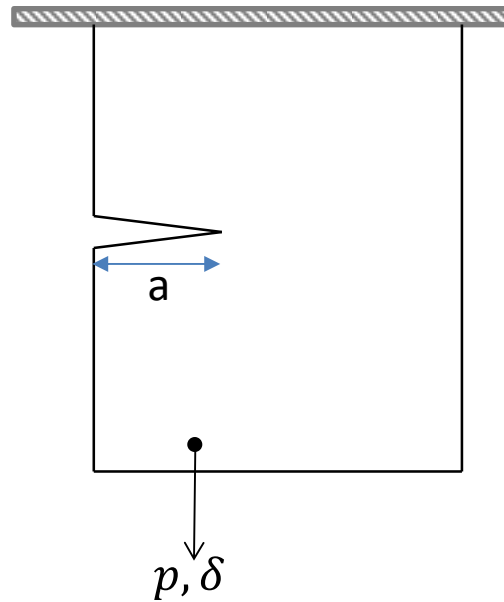
(a)
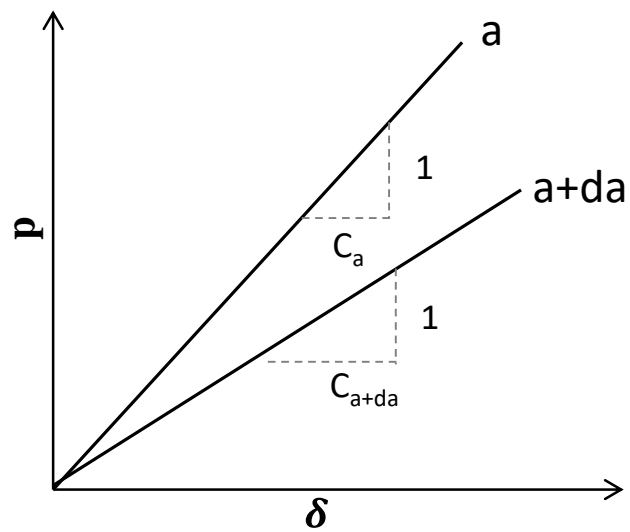
(b)

Figure 5.2 (a) A Plate Subjected to an Increasing Load, (b) Load-deflection Diagram

In order to characterize fatigue crack growth properties, determining crack length is an important step. However, it is difficult to directly measure crack lengths because

cracks in the specimen could be invisible. Thus, it is important and challenging to find a proper method to determine crack lengths. Swartz et al. (1982) investigated four techniques to monitor crack growth in plain concrete beams, which are photoelastic coating, crack-propagation gages, visual inspection and compliance calibration. He found that photoelastic-coating technique was inappropriate because of the stiffening effect on crack formation. Cracking gauge was not reliable because sometimes it did not work even though the crack was visible. The visual inspection and compliance calibration have the similar results, but visual inspection relies strongly on the judgement of the observer and most of cases the cracks are invisible. Thus, compliance calibration method could be the most reliable and effective method among the four techniques as it is derived from linear elastic fracture mechanics.

5.3 Development of the Cyclic SCB Fatigue Test Based on the Compliance Calibration Method

Compliance calibration method has successfully applied to metallic materials and nonmetallic materials such as rock, mortar, plain and fiber-reinforced concrete (Swartz et al. 1978; Velazco et al. 1980; Wecharatana et al. 1982). In addition, the semi-circular specimen has been used for fracture testing for a sufficient length of time to demonstrate the advantages of its simple specimen geometry and high efficiency of sample preparation. It is promising to develop a new fatigue method with use of both the compliance calibration method and the semi-circular specimen geometry. Thus, this section is to

48

propose the method of the cyclic SCB fatigue test based on the compliance calibration method.

The cyclic SCB test set-up is presented in Figure 5.3. As can be seen, the cracking mouth opening displacement (CMOD) is measured by a linear variable differential transformer (LVDT) mounted on a semi-circular specimen. As illustrated in Figure 5.4a, each notch length corresponds to a specified compliance. The first step is to establish a calibration curve representing the relationship between compliances and corresponding notch lengths (as shown in Figure 5.4a). The compliance is defined as the slope of the curve of CMODs versus loads. The compliance calibration curve is experimentally determined as follows:

(1) mark a notch length on the surface of a specimen;

(2) cut the notch at the center of the bottom of the specimen;

(3) mount the LVDT on the specimen;

(4) apply a small load for 10 cycles;

(5) remove the specimen from the fixture in the machine, and extend the notch length to the next marking and repeat the steps.

After obtaining the calibration curve, a specimen with a notch length of 15 mm is used for the cyclic fatigue test, as shown in Figure 5.3. In the testing, the CMOD and applying loads are recorded at the same time. As the loading cycles proceed, the crack propagates along the centerline of the specimen, and each propagated crack length corresponds to a specified compliance. The compliance is increased due to an increase of the crack length. Figure 5.4b illustrates the test results including applied load, CMOD and loading cycles.

49

When the compliances corresponding to different loading cycles are determined, the corresponding crack lengths can be determined based on the calibration curve.
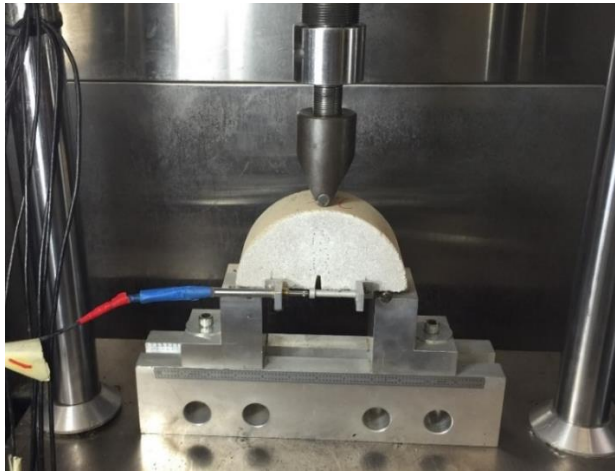
Figure 5.3 The Cyclic SCB Test Set-up
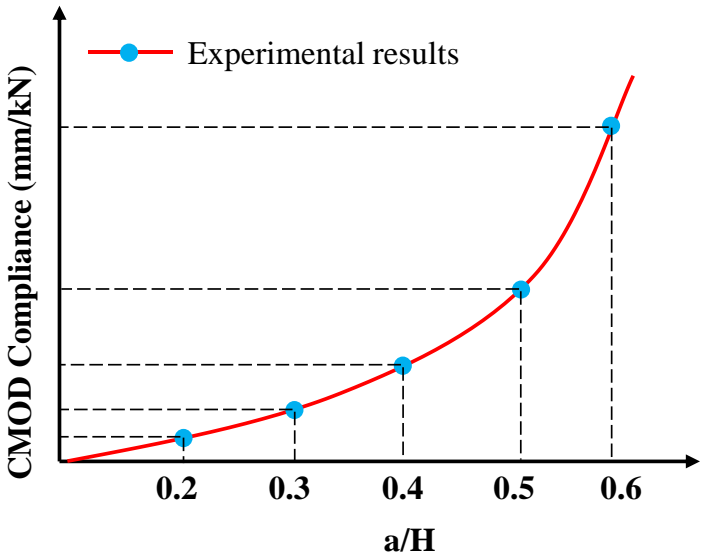
(a)

Figure 5.4 SCB Cyclic Fatigue Test: (a) Calibration Curve and (b) Example of Load versus CMOD at Different Loading Cycles
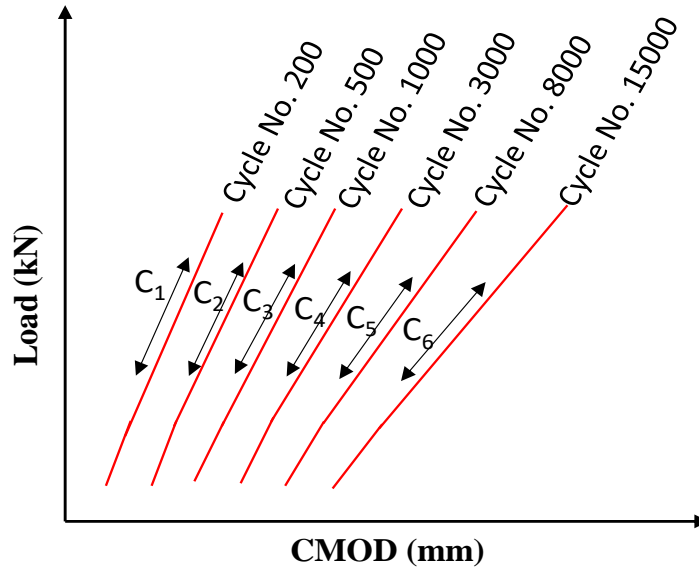
(b)

Figure 5.4 Continued

A stable crack growth in the specimen is a premise for crack growth rate characterization. However, not all the loading levels can achieve the stable crack growth, especially for brittle materials such as cementitious materials. Schimidt (1976) indicated that when maximum fatigue loads exceeded 85 percent of the breaking load for limestone, a steady increase in compliance was observed. He also noticed that when the fatigue loads were below 85 percent of the breaking load, the crack growth apparently ceased. Based on a number of experiments performed on cement stabilized materials, the author noticed that when the maximum fatigue loads were below 85 percent of the breaking load, there was no stable crack growth. It was noticed that the loads for stable crack growth were in the range of 85 to 95 percent of the breaking load. When the fatigue loads were larger than 95 percent of the breaking load, the specimen failed in a short time, and the fatigue test

seems the fracture test. The range of loads for stable crack growth is narrow, and each stabilized specimen has a certain variation in the strength (i.e., breaking load or peak load) due to compaction. Although the average breaking load was used for calculating the applied load for the specimen, it was observed that the calculated load was out of the true range (based on the true breaking loads) for some specimens. In other words, the applied load was either smaller than 85 percent of the true breaking load resulting in unstable crack growth or greater than 95 percent resulting in a fast failure.

In order to overcome this difficulty, a relatively small load (e.g., 70 percent of the average of the breaking load) is initially applied for 1000 cycles. If the specimen does not fail, increase the load by a small increment for another 1000 cycles，and repeatedly increase the load until the specimen fails. It should be noted that the load mentioned herein is referred as the maximum of cyclic load with a haversine function. The crack growth rate parameters (i.e., Paris's law coefficients) are material property, and thus they are independent of the applied load. After several load levels, the specimen fails ultimately. This test procedure has two major advantages as follows:

(1) It solves the problem that for some specimens the applied load based on the calculation could be out of the best load range (based on the true breaking load) for a stable crack growth.

(2) Increased loads can greatly reduce the testing time and make the test highly efficient comparing with the case of a single load.

5.4 Determination of Crack Growth Rate of Cement Stabilized Sand

5.4.1 Characteristics of Compliances under Different Loading Cycles for Cement Stabilized Sand

The cracking mouth opening displacement at fracture is typically around 0.025 mm. In order to accurately measure the displacement, a linear variable differential transformer is used, which is accurate to 0.001mm. In addition, the time interval between two adjacent data points is important, which determines how many data points are collected per second. If there are no sufficient data points for a loading-unloading cycle, the compliance determined may be inaccurate. The time interval between two adjacent data points is 0.0166 second, and a total of 60 data points are collected per load-unloading cycle, which give sufficient data points for accurate determination of the compliance.

The cyclic load pulse is a haversine waveform, and it is expected that the CMOD response is haversine and there is no lag for CMOD response (as shown in Figure 5.5) since the specimen exhibits the linear elastic response. When plotting the load versus CMOD curve, a clear linear relationship with a very high coefficient of correlation (i.e., $R> 0.97$) is observed. The compliance is an inverse of the slope of the load versus displacement curve. As the crack length increases with an increase of loading cycle, a steady increase in compliance is noted in Figure 5.5. The cyclic fatigue test is stress-controlled, and with the proceeding of crack growth the stress intensity factor increases. As a result, the crack growth rate increases with an increase of loading cycle. The evidence for this phenomenon is definitive in Figure 5d (i.e., Cycle #2300). For the cases of Cycle #100, Cycle #800 and Cycle #1800, the loading-displacement curve matches the

unloading-displacement curve well because the crack growth rate is small, whereas for the case of Cycle #2300, the crack growth rate is much larger as the loading-displacement curve does not match the unloading-displacement curve due to the larger crack growth after a loading-unloading cycle.

In the load-CMOD curve, the slope of the loading line is different from the slope of unloading line when the crack growth rate is large. In order to be consistent, the compliance is determined from the initial portion of the loading line, as illustrated in Figure 5.6. As can be seen in the figure, the linear function fits to the data very well, and the coefficient of correlation is 0.99.
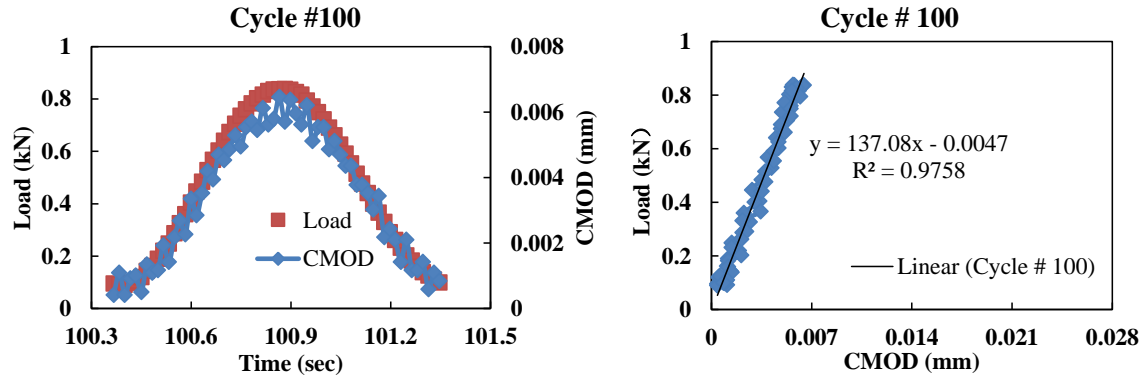
(a)

Figure 5.5 Test Results for Cement-stabilized Sand including Load Pulse, CMOD Response and Slope of Load-CMOD Curve at Different Load Cycles: (a) Cycle #100, (b) Cycle #800, (c) Cycle #1800, and (d) Cycle #2300
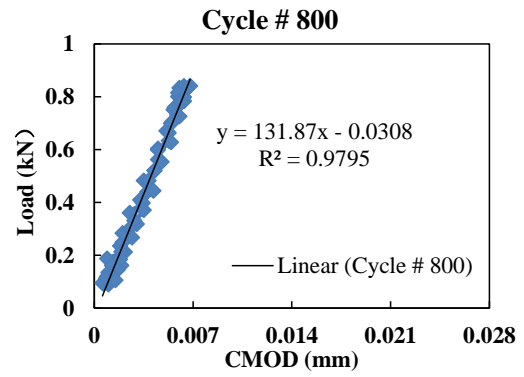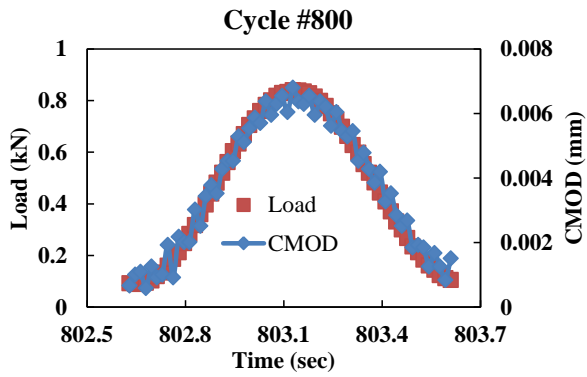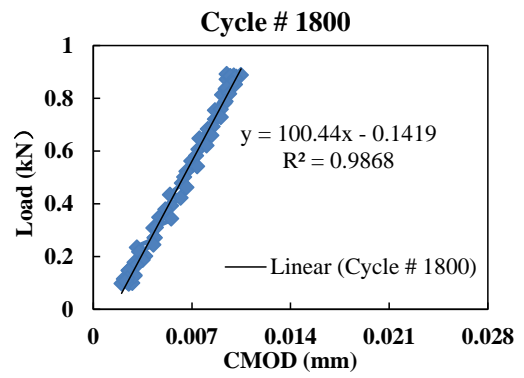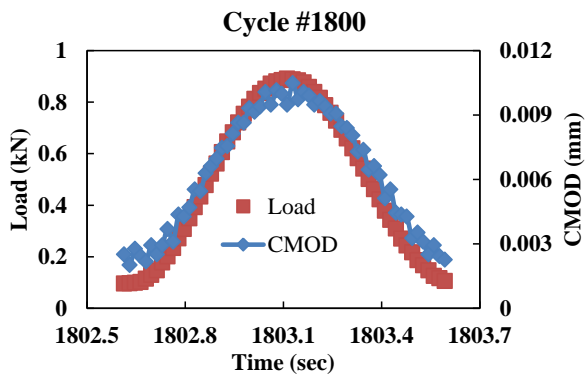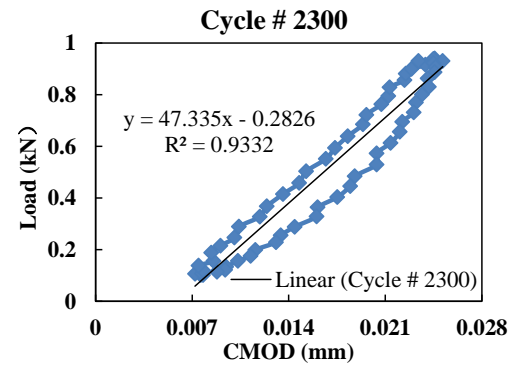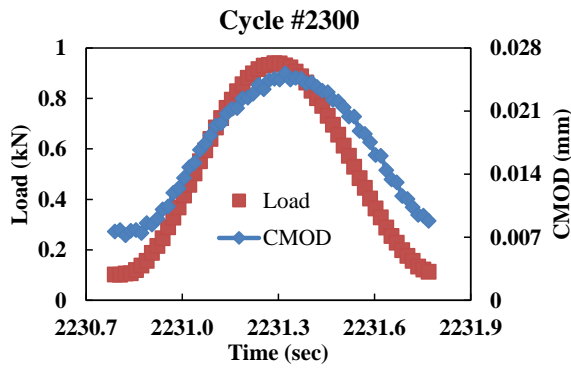
Figure 5.5 Continued

Figure 5.6 Compliance Determined from the Initial Portion (Highlighted Red Color) of the Loading Line

5.4.2 Characterization of Crack Growth Rate of Cement Stabilized Sand

Due to the difficulty of optical and other direct measurements, the compliance calibration method is used to determine the crack length. The compliance calibration curve was determined from the experiments, as shown in Figure 5.7. The crack length has a clear correlation with compliance based on a second degree polynomial, which is indicated by a high coefficient of correlation (i.e., $R^2 = 0.97$).

In the cyclic loading test, the compliance increases with an increase of loading cycle. With use of the correlation between crack length and compliance (i.e., compliance calibration curve), the crack length corresponding to each load cycle is determined. And thus, the crack growth rate da/dN is calculated as well as the stress intensity factor ΔK. By fitting a linear function to the data of log (da/dN) versus log (ΔK), the Paris's law coefficients of A and n are determined. The test results of crack growth rate versus stress intensity factor are presented in Figure 5.8 to 5.12. Based on the literature, the coefficient of correlation for the fitting was lower than 70% when determining the Paris's law

coefficients. However, the test results presented herein show that all the five samples have a high coefficient of correlation (i.e., $R^2 \geq 84\%$), which indicates that the proposed SCB fatigue protocol based on the compliance method is promising for characterization of crack growth rate. Table 5.1 presents a summary of crack growth rate parameters for cement stabilized sand.
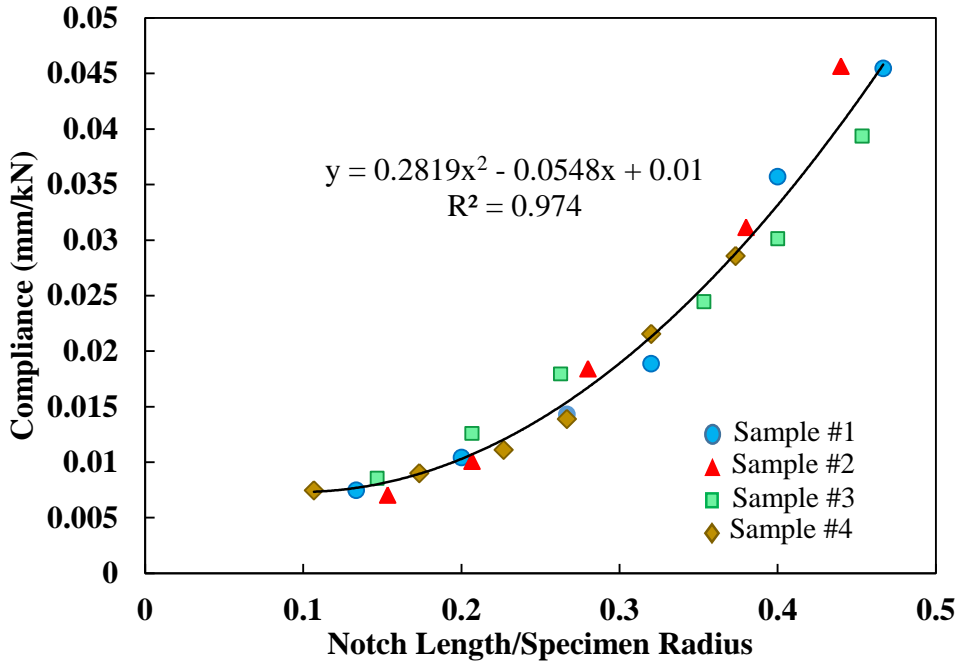
Figure 5.7 Compliance Calibration Data Measured from the Experiments for Cement-stabilized Sand

Figure 5.8 Crack Growth Rate versus Stress Intensity Factor for Sample #1

Figure 5.9 Crack Growth Rate versus Stress Intensity Factor for Sample #2

Figure 5.10 Crack Growth Rate versus Stress Intensity Factor for Sample #3
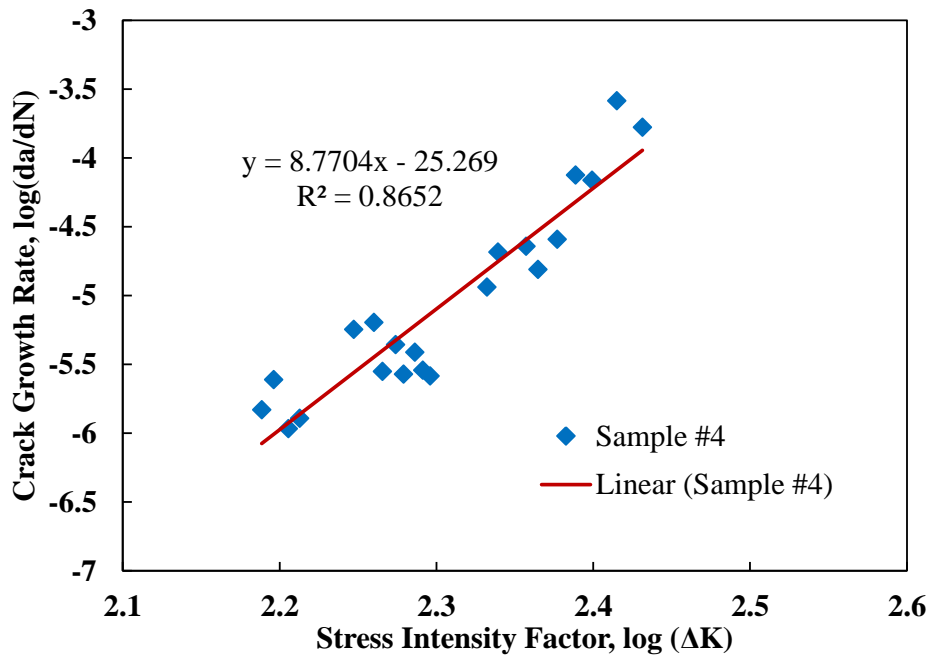
Figure 5.11 Crack Growth Rate versus Stress Intensity Factor for Sample #4
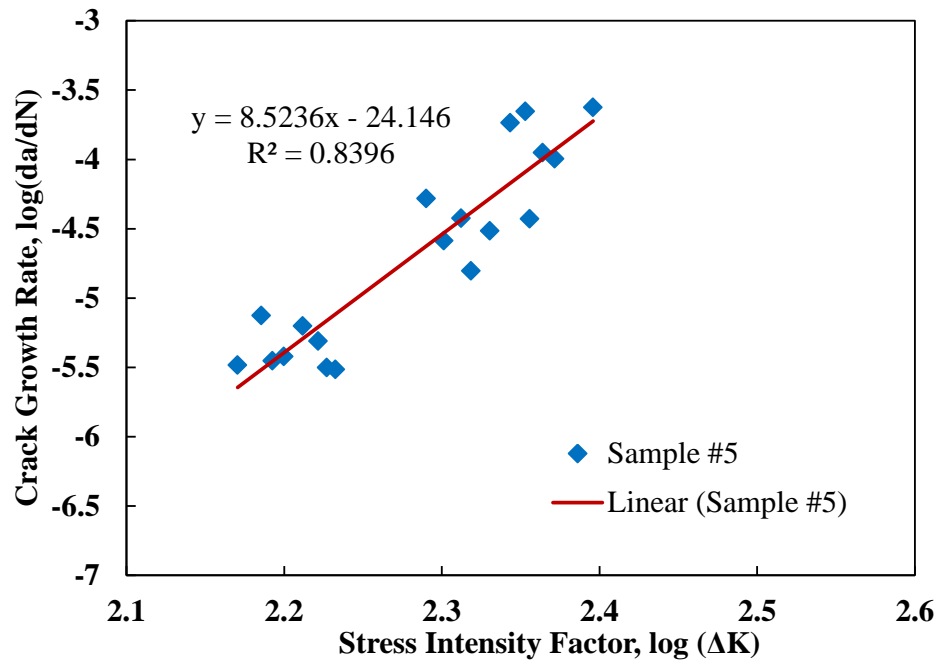
Figure 5.12 Crack Growth Rate versus Stress Intensity Factor for Sample #5

Table 5.1 Paris's Law Coefficients of A and n for Cement-stabilized Sand

Sample ID	A	n
Sample #1	8.39E-18	5.02
Sample #2	3.14E-17	5.21
Sample #3	1.32E-24	8.41
Sample #4	5.38E-26	8.77
Sample #5	1.32E-24	8.41
Average	7.96E-18	7.17
COV	N/A	26.2%

5.5 Determination of Crack Growth Rate of Cement Stabilized Limestone

5.5.1 Characteristics of Compliances under Different Loading Cycles for Cement

Stabilized Limestone

Figure 5.13 presents the test results including load pulse, CMOD response and slope of load-CMOD curve at different load cycles. The load pulse is haversine, and expectedly, the measurement of CMOD is haversine as well. There is no lag observed between the load pulse and CMOD response. In Figure, the slope of load-CMOD curve is determined from both of the loading and unloading lines. It is evident that the compliance increases with an increase of load cycles since the slope of load-CMOD curve decreases and the compliance is an inverse of the slope. When the number of load cycles is low (e.g., Cycle #100 and Cycle #500), the slope of the loading line is very close to the slope of the unloading line as the crack growth rate is small. However, when the number of load cycles is high, the crack length is much larger than that at the beginning due to crack propagation. Also, the cyclic test is stress-controlled, which means that the stress intensity factor is much larger, and the crack growth rate is larger as well. Thus, it is evident in Figure 5.13d that the loading line is separated from the unloading line after a loading-unloading cycle.

The compliance method is based on the theory of linear elasticity, and the initial portion of the loading line is more linear than the other portions of the load-CMOD curve. Thus, the compliance is determined from the initial portion of the loading line, as illustrated in Figure 5.14. It can be seen that the coefficient of correlation is very high (i.e., $R^2=0.99$) for the linear regression.
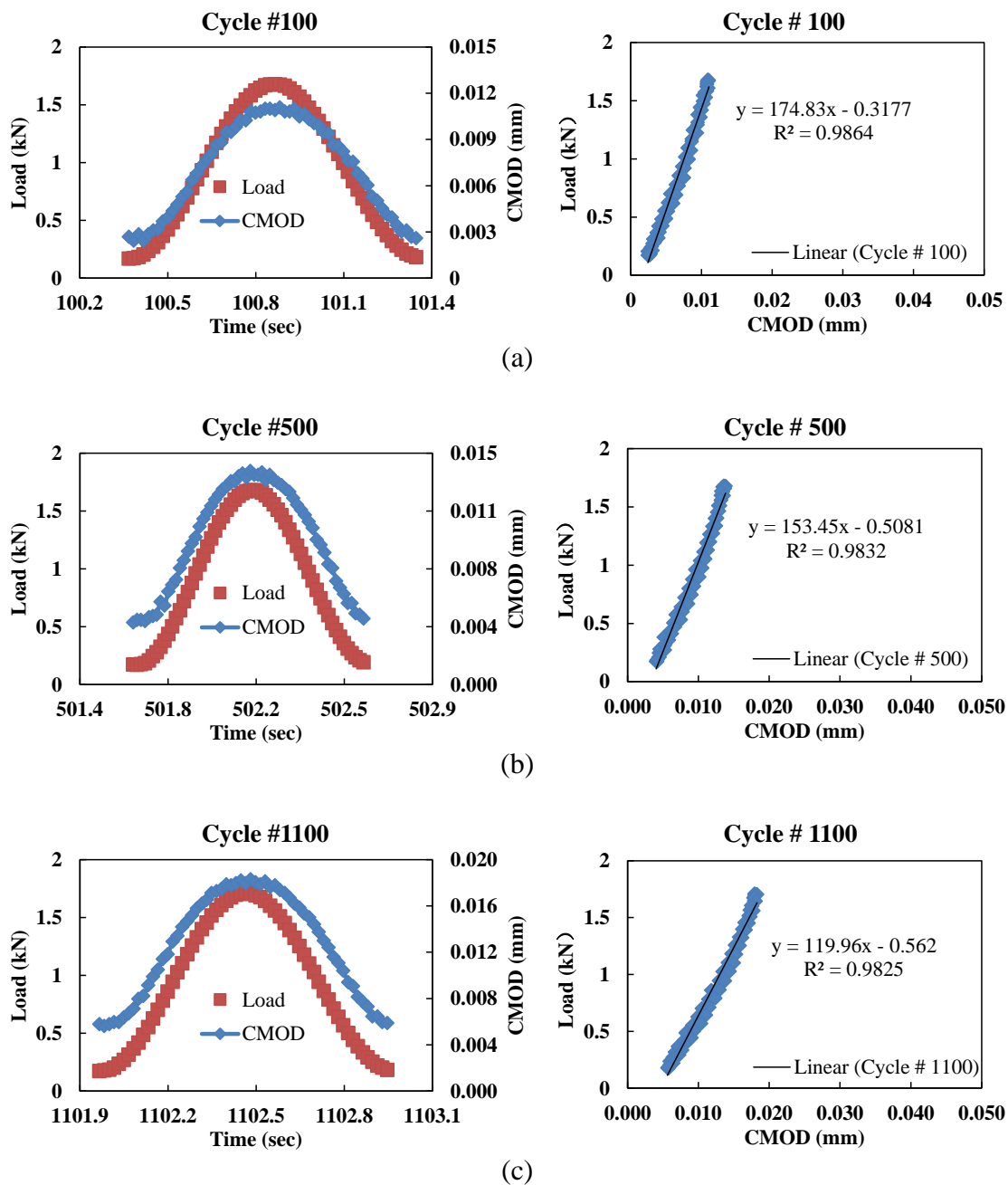
Figure 5.13 Test Results for Cement-stabilized Limestone including Load Pulse, CMOD Response and Slope of Load-CMOD Curve at Different Load Cycles: (a) Cycle #100，(b) Cycle #500, (c) Cycle #1100, and (d) Cycle #1700
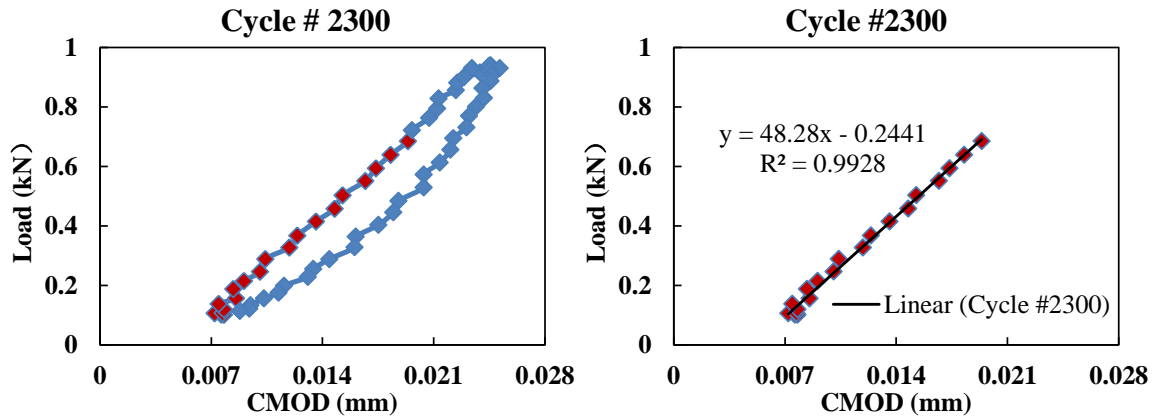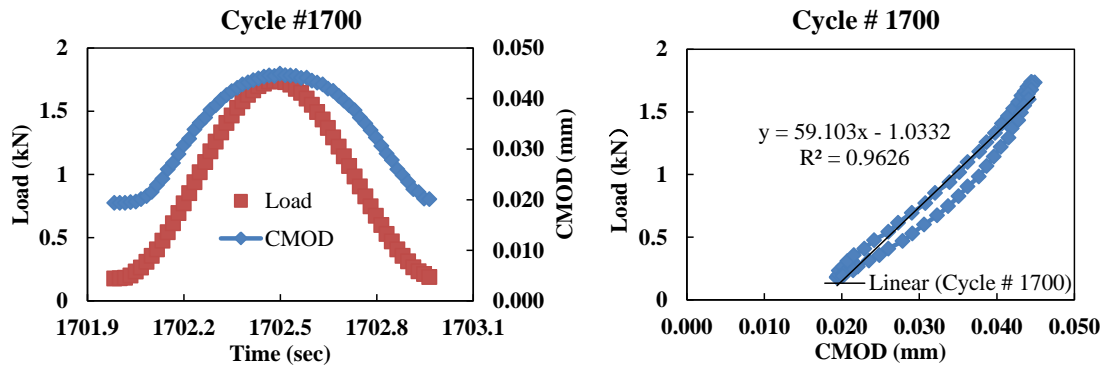
(d)

Figure 5.13 Continued
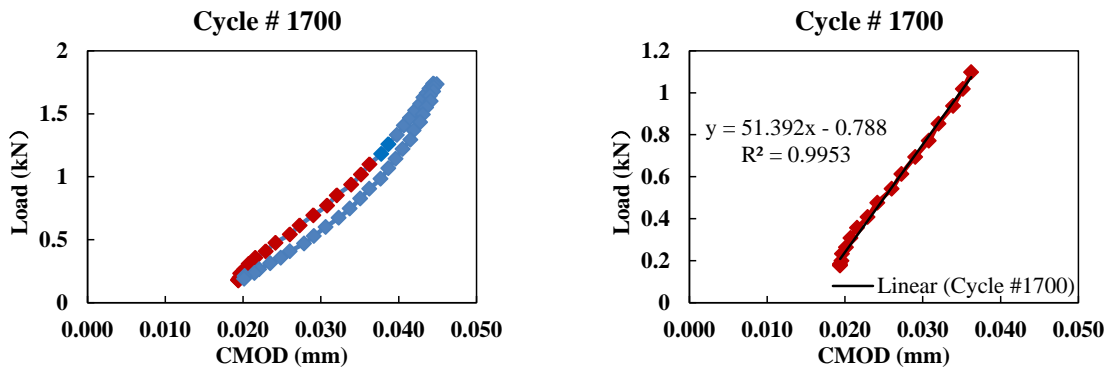
Figure 5.14 Compliance Determined from the Initial Portion (Highlighted Red Color) of the Loading Line

5.5.2 Characterization of Crack Growth Rate of Cement Stabilized Limestone

The procedure for determining crack growth rate parameters is presented in Section. Figure 5.15 presents the compliance calibration curve measured from the experiments for cement stabilized limestone. As can be seen, a second degree polynomial nicely fits the experimental data with a high coefficient of correlation (i.e., $R^2=0.99$). Figure 5.16 to 5.20 present the test results of crack growth rate versus stress intensity factor for five samples. As can be observed in the figures, the linear function fits the data

well with a high coefficient of correlations (i.e., $R^2 \geq 0.89$). The Paris's law coefficients are determined based on the fittings summarized in Table 5.2.
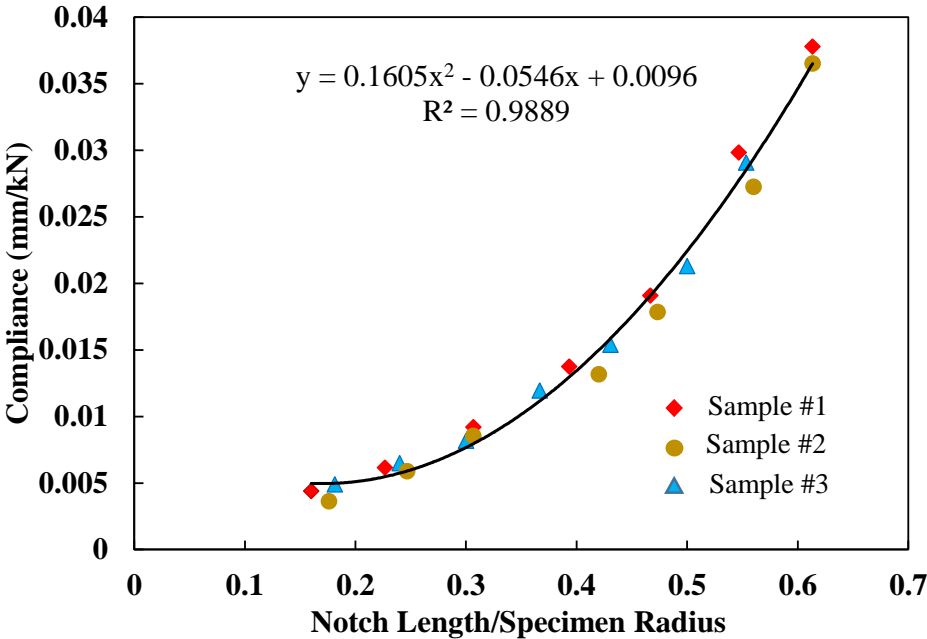
Figure 5.15 Compliance Calibration Data Measured from the Experiments for Cement-stabilized Limestone
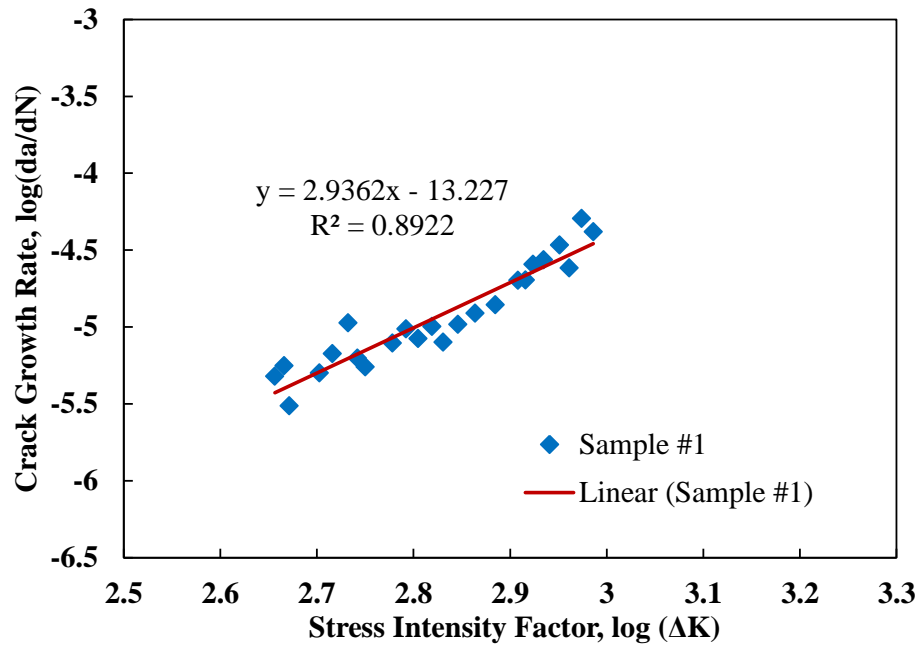
Figure 5.16 Crack Growth Rate versus Stress Intensity Factor for Sample #1
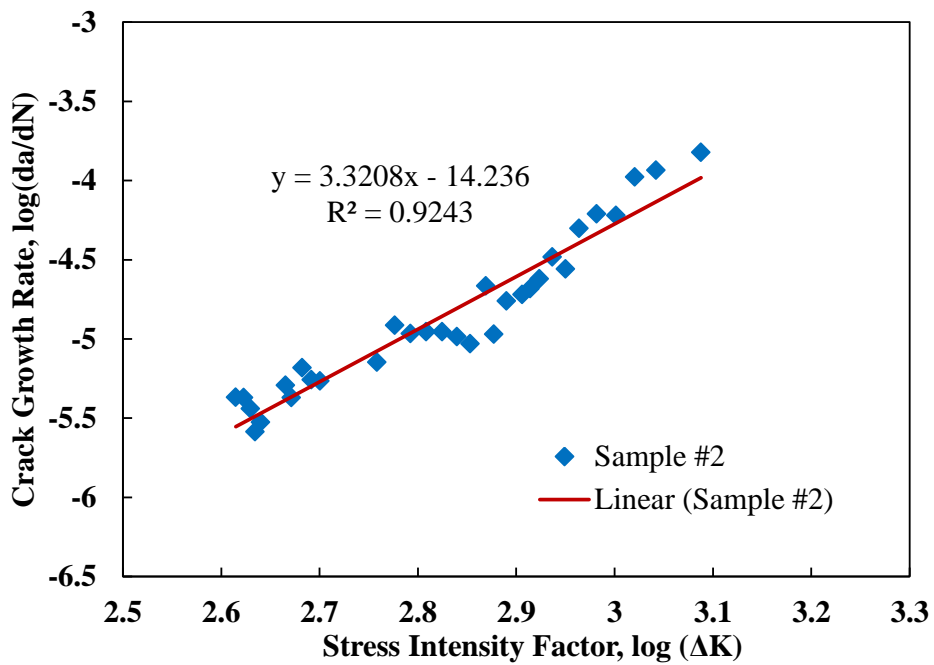
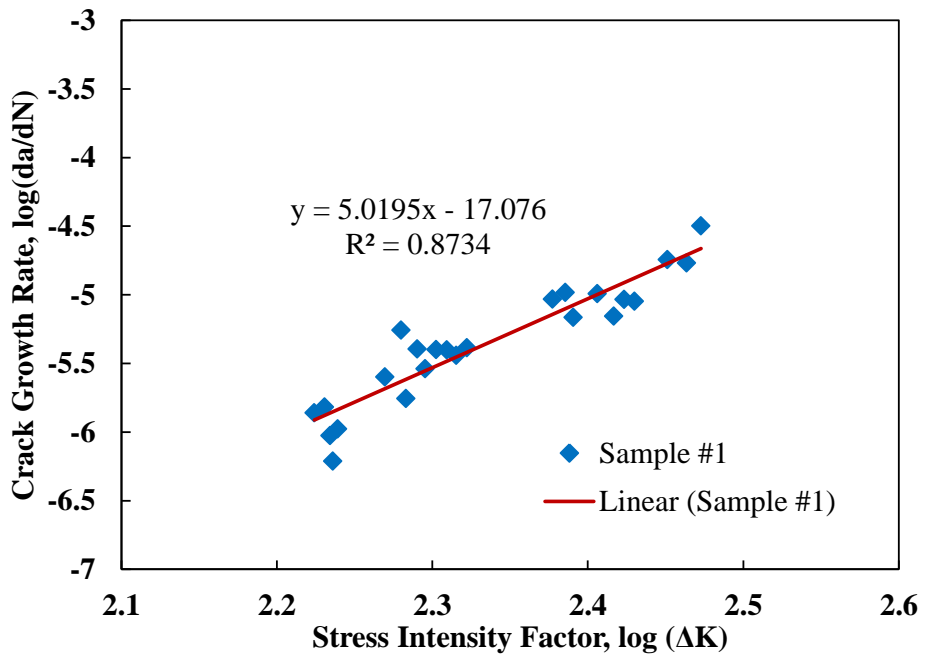**Figure 5.17 Crack Growth Rate versus Stress Intensity Factor for Sample #2**
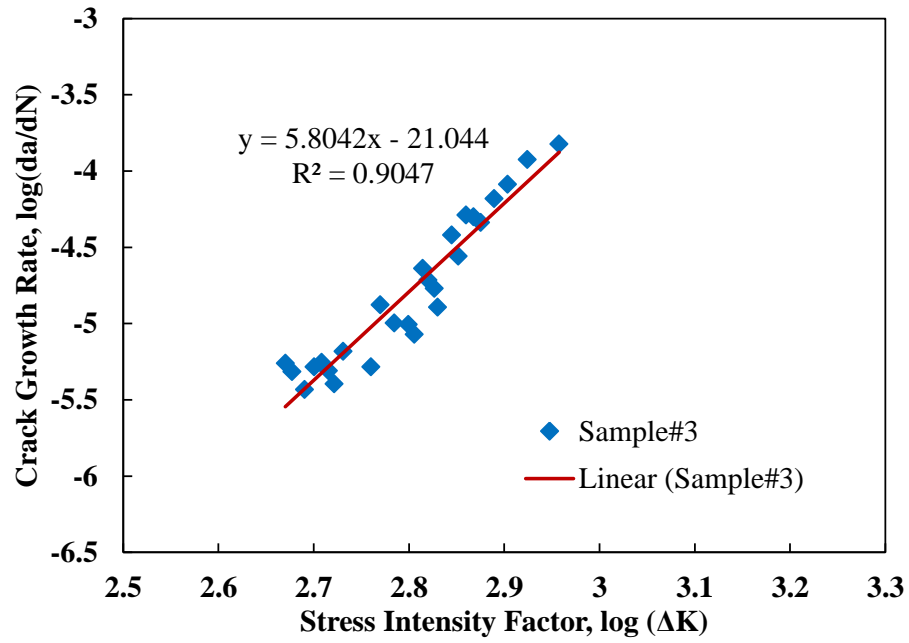
Figure 5.18 Crack Growth Rate versus Stress Intensity Factor for Sample #3
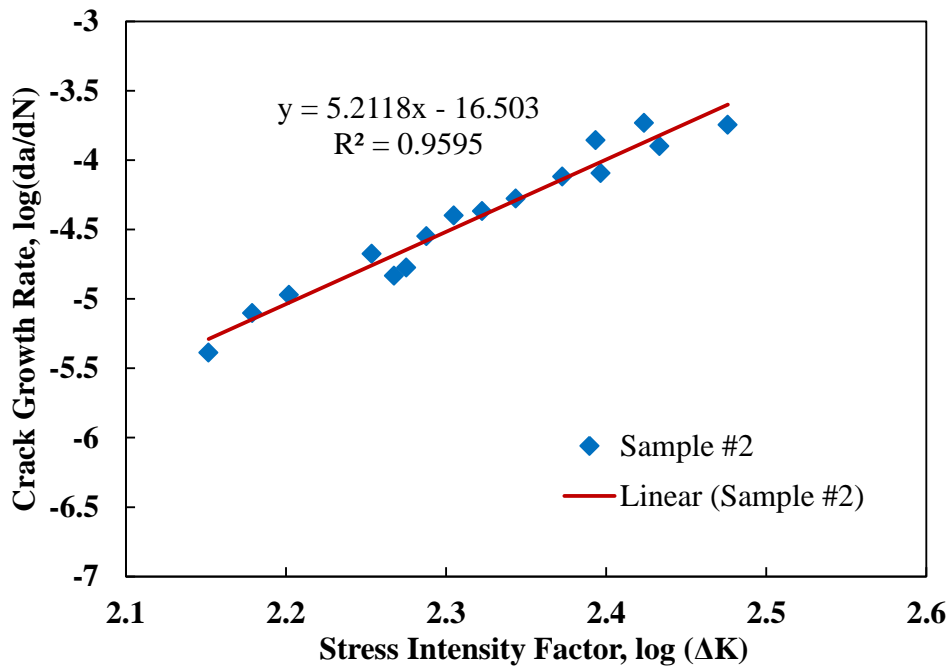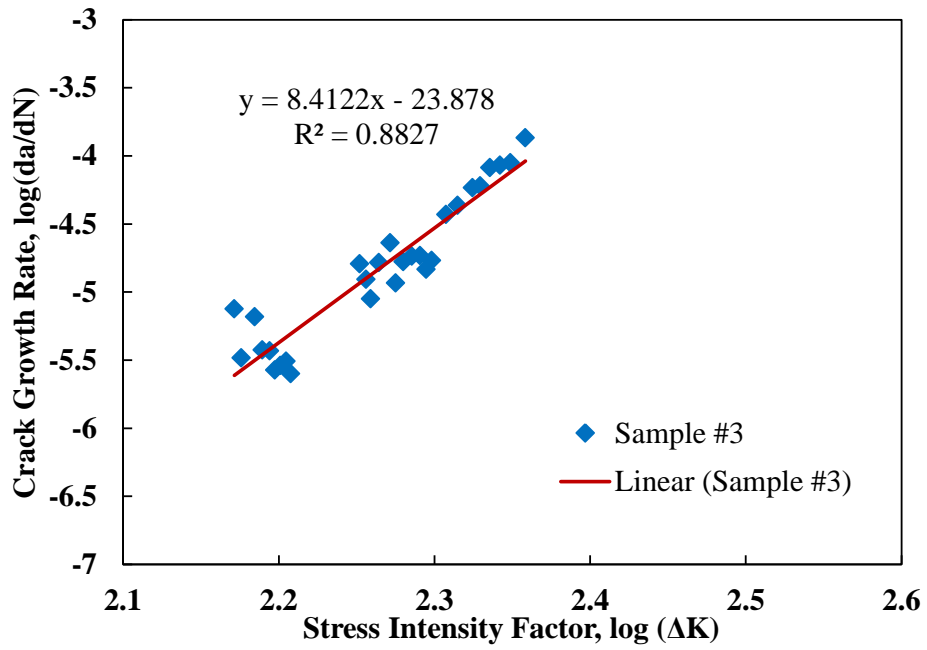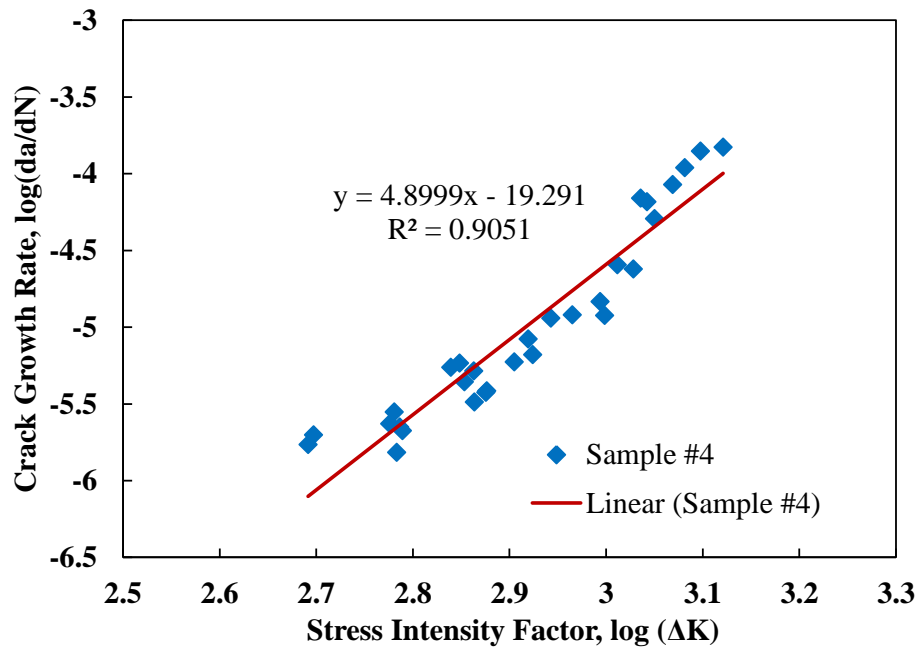

Figure 5.19 Crack Growth Rate versus Stress Intensity Factor for Sample #4
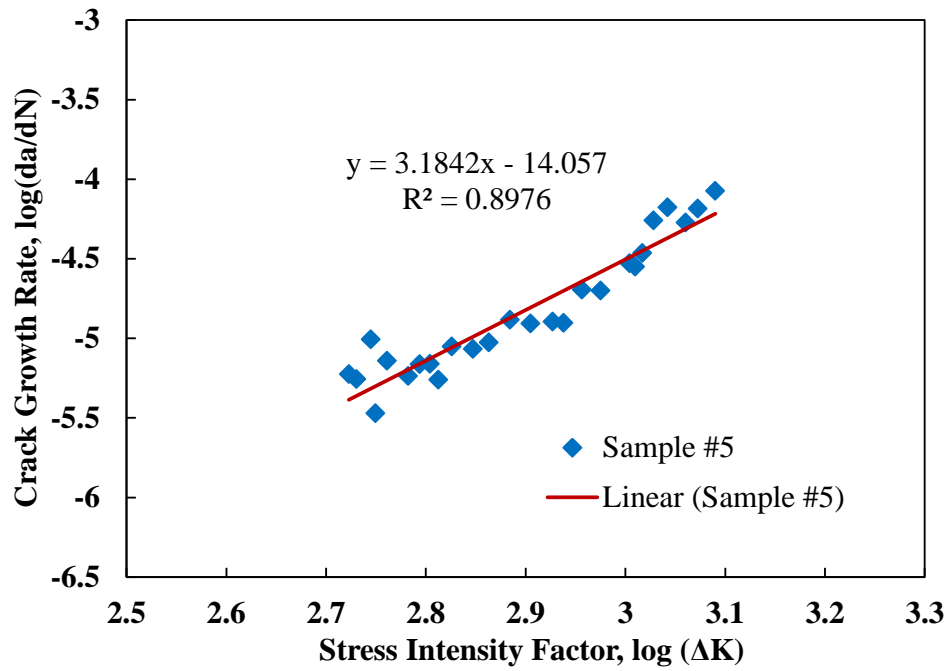
Figure 5.20 Crack Growth Rate versus Stress Intensity Factor for Sample #5

Table 5.2 Paris's Law Coefficients of A and n for Cement-stabilized Limestone

Sample ID	A	n
Sample #1	5.93E-14	2.94
Sample #2	5.81E-15	3.32
Sample #3	9.04E-22	5.80
Sample #4	5.12E-20	4.90
Sample #5	8.77E-15	3.18
Average	1.48E-14	4.03
COV	N/A	31.2%

6. SULFUR EXTENDED ASPHALT (SEA)

6.1 Background

An abundance of low-cost elemental sulfur as the by-product of the oil and gas refinery process has driven the increasing interest in the use of sulfur to partially replace conventional asphalt binder for asphalt pavement. When adding the sulfur into asphalt, chemical reactions are occurring between asphalt and sulfur, and these chemical reactions change the asphalt composition. Petrossi et al. (1972) found that the naphthene-aromatics were transformed into asphaltenes through dehydrogenation and cyclization at 140 °C. Parvez et al. (2013) found that C-S bond increased due to the addition of sulfur with use of the FTIR. However, the addition of more sulfur into asphalt does not always mean more chemical reactions. Several studies indicated that when the added dosage of sulfur by weight of asphalt binder is more than a threshold, there are two states of sulfur existing in the asphalt: chemically bonded sulfur and free sulfur (Lee 1975; Nicholls 2009; Yu et al. 2009). These studies found that the proportion of chemically bonded sulfur was typically around 15% to 20% by weight of asphalt binder. The free sulfur acts as a filler to strengthen the asphalt binder.

A number of studies have indicated the use of SEA offers a great benefit to improve rutting resistance of asphalt mixtures (Bayomy et al. 1987; Lu et al. 2005; Al-Mehthel et al. 2010; Tran et al. 2010; Cooper III et al. 2011). Field trial sections showed the SEA pavements had a comparable or superior rutting performance compared to the control pavements (Beatty et al. 1987; Bayomy et al. 1987; Al-Mehthel et al. 2010). However,

the major concern for SEA pavements is fatigue cracking. Cooper III et al. (2011) compared three mixtures, two hot-mix asphalt (HMA) and one WMA. Mixture One used an unmodified asphalt binder (i.e., PG 64-22), Mixture Two used a polymer-modified binder (i.e., PG 70-22), and Mixture Three was a WMA that used a sulfur additive and a PG 64-22 binder. SCB and bending beam fatigue test results showed that sulfur-modified mixture was more susceptible to fracture than the conventional mixtures. Arora et al. (1994) carried out a pavement performance evaluation survey of three SEA test roads constructed in Saudi Arabia and each test road had a control section of conventional pavement. Test Road 1 and Test Road 3 used a sulfur/asphalt ratio of 30/70 by weight, whereas a higher ratio of 45/55 was used in Test Road 2. The field performance survey showed that the most predominant distress in the SEA test sections are the load-associated alligator cracking and the climate-associated block cracking and transverse cracking. More cracking was observed in the SEA sections than in the control sections. Tran et al. (2010) comprehensively studied sulfur modified asphalt with the addition of Thiopave pellets and compared with the control mixtures. The bending beam fatigue test results showed that the sulfur-modified asphalt (with PG 67-22) mixture had less fatigue life than the control mixtures with asphalt binders of PG 76-22 and PG 67-22.

Based on the literature review, the addition of sulfur into asphalt causes chemical reaction between sulfur and asphalt, and the extent of chemical reaction is related to different dosages of sulfur. These chemical reactions also change the rheological properties of sulfur-extended asphalt, which further altering the mechanical performances of sulfur-extend asphalt mixtures. Thus, characterization of rheological properties of

sulfur-extended asphalt at different dosages of sulfur is important for a better understanding of the mechanical performances of its mixtures.

6.2 Materials and Mixing Protocol for Producing SEA in the Laboratory

The constituents in the asphalt mixtures in this study were asphalt binder (PG 64-22), element sulfur and crumb rubber. The use of crumb rubber in asphalt concrete has shown a number of economic and performance benefits (Mull et al. 2002; Huang et al. 2004; Xiao et al. 2009). One of the most important is the increase in cracking and fatigue resistance. In order to improve cracking resistance of SEA, crumb rubber and elemental sulfur are blended together with asphalt binder. The percentage of crumb rubber used in this study was 11% by weight of asphalt.

Asphalt binder was first blended with crumb rubber, and then blended with elemental sulfur at four different dosages by weight of asphalt (i.e., 0%, 15%, 30% and 45%). Figure 6.1 shows the elemental sulfur and crumb rubber. The gradation of crumb rubber is presented in Table 6.1.

| (a) | (b) |

Figure 6.1 (a) Elemental Sulfur, and (b) Crumb Rubber

Table 6.1 Gradation of Grade C Crumb Rubber

Sieve Size	1.18 mm (#16)	600 µm (#30)	425 µm (#40)
% Passing	100	90-100	45-100

A high shear mixer is used for the mixing process as shown in Figure 6.2. In order to control the mixing temperature, a heating mantle with a temperature control device is used. For sulfur-extended asphalt, the mixing temperature is about 140 ℃. During the mixing process, the elemental sulfur is added gradually into hot asphalt, especially for 30% and 45 % dosages. It should be noted that the specific gravity of sulfur is twice as big as that of asphalt. When adding a large amount of sulfur at one time, the sulfur could fall down to the bottom of the container, which could cause the insufficient mixing with asphalt. The mixing duration is 1 hour for all the sulfur-extended asphalts.

For sulfur-rubber modified asphalt, the mixing procedure is different from the sulfur-extended asphalt. The crumb rubber is firstly mixed with asphalt at 180 ℃ for 10 minutes, and then, the container with the asphalt is sealed from the top and put in an oven at 180 ℃ for 1 hour in order to allow the rubber to swell. After swelling, the elemental sulfur is added into asphalt at 140 ℃ for mixing. The mixing duration for the addition of elemental sulfur is 1 hour.
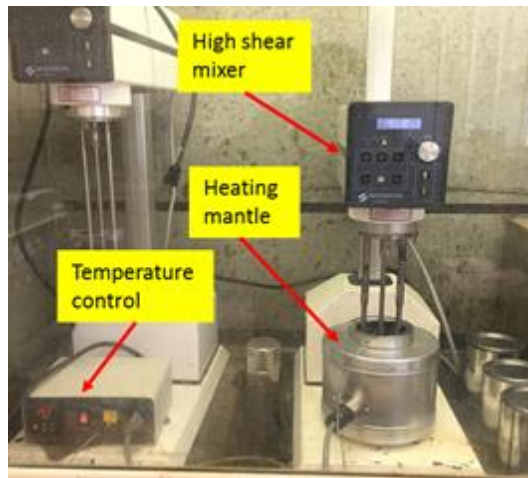
Figure 6.2 Equipment Used for the Mixing Process

A Nikon Labophot 2-POL transmitted light microscope with magnification range 4–40X is used to examine the samples of sulfur-extended asphalt. As can be seen in Figure 6.3, when the mixing time is too short (i.e., 10 minutes), the mixing is not complete. After 60 minutes, the color is smooth and consistent in the image which indicates that the sulfur is completely mixed with asphalt. Figure 6.4 presents the images of sulfur-extended asphalt with addition of crumb rubber and the control sample without sulfur. The color is completely black for the control sample without sulfur, while the sulfur-extended asphalts show the brown color and the crumb rubber is seen in the image.
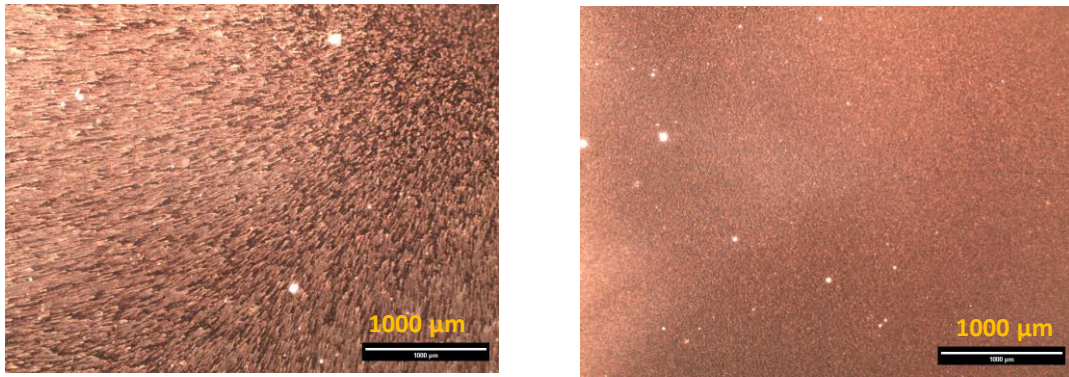
(a)   (b)

Figure 6.3 Microscopy Images of Sulfur-extended Asphalt (45% Sulfur Added by Weight of Neat Asphalt) at Different Mixing Time: (a) 10 Minutes, and (b) 60 Minutes
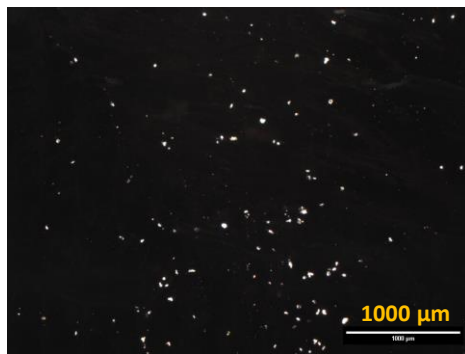
(a)
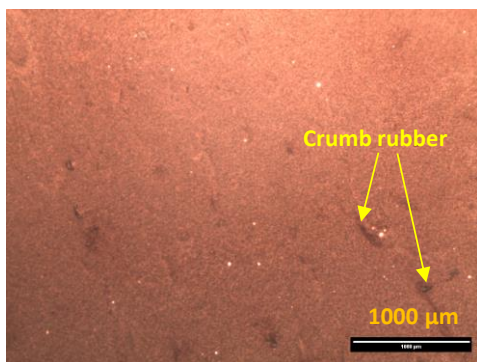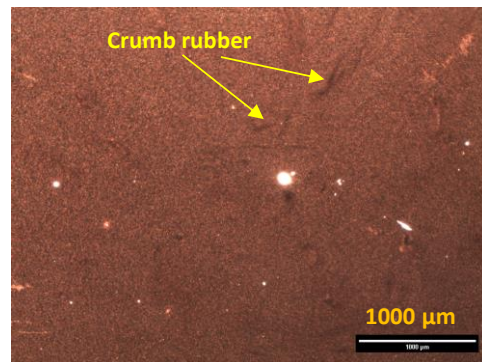
(b)   (c)

Figure 6.4 Microscopy Images of Sulfur-extended Asphalts after Mixing: (a) 0% Sulfur + 11% Crumb Rubber, (b) 30% Sulfur + 11% Crumb Rubber, and (c) 45% Sulfur + 11% Crumb Rubber

6.3 Characterization of Rheological Properties of SEA

6.3.1 Laboratory Test Method

Table 6.2 presents the standardized laboratory tests used to characterize asphalt properties in various aspects of different temperatures, aging and purpose. Dynamic Shear Rheometer (DSR) high temperature grade test is used to characterize both the elastic and viscous behaviors of original or Rolling Thin Film Oven (RTFO) aged asphalt binders at high temperatures, which is commonly used to indicate the highest service temperature of a pavement. Bending Beam Rheometer (BBR) test is used to characterize the properties of Pressure Aging Vessel (PAV) aged asphalt related to the lowest service temperature of a pavement. Multiple Stress Creep and Recovery (MSCR) test is used to characterize the non-recovery and recovery properties of RTFO aged asphalt at high temperatures. The non-recovery property is used to indicate the resistance of asphalt to shear flow. The rotational viscosity test is used to measure the flow characteristics of asphalt to determine the mixing and compaction temperatures. The details of these tests are given in the following subsections.

Table 6.2 Laboratory Tests to Characterize Asphalt Properties

Test	Standard	Purpose
DSR High Temperature grade (original and RTFO aged asphalts)	AASHTO M320 AASHTO T240 for RTFO aging	Asphalt properties related to rutting resistance at high temperature
BBR Test (PAV aged asphalt)	AASHTO TP1 AASHTO PP1 for PAV aging	Asphalt properties related to a pavement's lowest service temperature
MSCR test	AASHTO TP 70-10	Asphalt non-recovery and recovery properties at high temperature
Viscosity Test	ASTM D4402	Asphalt property related to the workability during handling at hot mixing facility

The DSR High Temperature Grade Test

The DSR test is performed according to AASHTO M320. The test temperatures are controlled using a water bath in the DSR machine. An oscillatory sinusoidal shear stress is applied to asphalt binder samples to obtain the $|G^*|$ and δ properties. The test is performed at a frequency of 10 radians per second. High temperature PG grade is designed to address the pavement rutting performance.

The BBR Test

The BBR test is used to measure the deflections or creeps of the asphalt under a constant load at a constant low temperature according to ASSHTO TP1. The asphalt is aged in both a rolling thin film oven and the pressure aging vessel. An asphalt beam sample is used, and the beam theory is used to determine the stiffness of the sample. Two

parameters of creep stiffness (s) and creep rate (m) can be obtained from the test, which are used to determine the lowest service temperature of a pavement.

The MSCR Test

The MSCR test is performed using a DSR machine as per AASHTO TP 70-10. The test is typically conducted at high temperatures such as 64, 70, and 76 °C, respectively. Two stress levels of 0.1 and 3.2 kPa are applied on an asphalt binder sample for a total of ten cycles for each stress. For each cycle, a haversine shear load is applied to the sample for 1 s, followed by a 9-s rest period. The averages of non-recoverable creep compliance (J_{nr}) and percent recovery (R%) from 10 cycles for each stress are the output results, which are expressed in Equation 1 and 2, respectively:

$$J_{nr} = \frac{non-recoverable\ strain}{stress} \qquad (6.1)$$

$$R\% = \frac{Recoverable\ strain}{stress} \qquad (6.2)$$

The Viscosity Test

The viscosity test is a standard test method used to measure the viscosity of asphalt binders at a specified temperature using a Rotational Viscometer in accordance with ASTM D4402. For specification testing, the motor is set at 20 rpm. In this study, the testing temperature is 140 ℃. The output is in units of Pascal-seconds (Pa·s).

6.3.2 Test Results and Discussion

The DSR Test Results

The PG high temperature grades from the DSR test for both of sulfur-extended asphalt and sulfur-rubber modified asphalt are presented in Figure 6.5 and 6.6. It should be noted that the sulfur-extended asphalt and sulfur-rubber modified asphalt are indicated as "Without rubber" and "With 11% rubber", respectively in the figures.

For the original sulfur-extended asphalt, the sulfur dosage does not have a significant impact on the PG high temperature grade. It is noticed that the 15% dosage of sulfur decreases the high temperature grade. For the original sulfur-rubber modified asphalt, the 0% dosage of sulfur (i.e., the control sample) has a littler greater PG grade than the other asphalts with addition of sulfur, while the sulfur dosage does not have a significant effect on the PG grade of asphalts with addition of sulfur ranged from 15% to 45%. When comparing sulfur-extended asphalt and sulfur-rubber modified asphalt at the same dosage of sulfur, it can be seen that the addition of crumb rubber does increase the PG grade at least one standard grade.
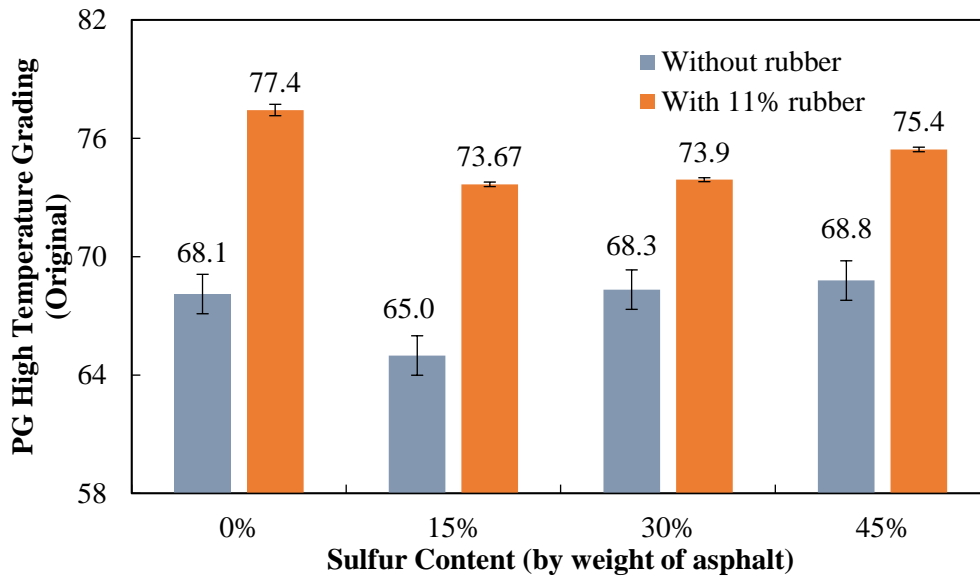
Figure 6.5 PG High Temperature Grade for Original Asphalt

For the RTFO aged sulfur-extended asphalt, there is a trend that the sulfur dosage increases the PG high temperature grade, but the increase is not significant for each increment of 15% sulfur dosage. For the sulfur-rubber modified asphalt, the control samples without addition of sulfur exhibited the largest PG high temperature grade; the addition of sulfur with the dosages ranged from 15% to 45% shows the lower PG grades than the control samples, while there is also a trend that the increase of sulfur dosage increases the PG grade. When comparing the sulfur-extended asphalt with sulfur-rubber modified asphalt, it can be seen that 0% sulfur-rubber modified asphalt has a much higher PG grade than the 0% sulfur-extended asphalt. For the other three sulfur dosages, the sulfur-rubber modified asphalts have a little higher PG grade than the sulfur-extended asphalts at the same dosage, but the differences are not significant between them.
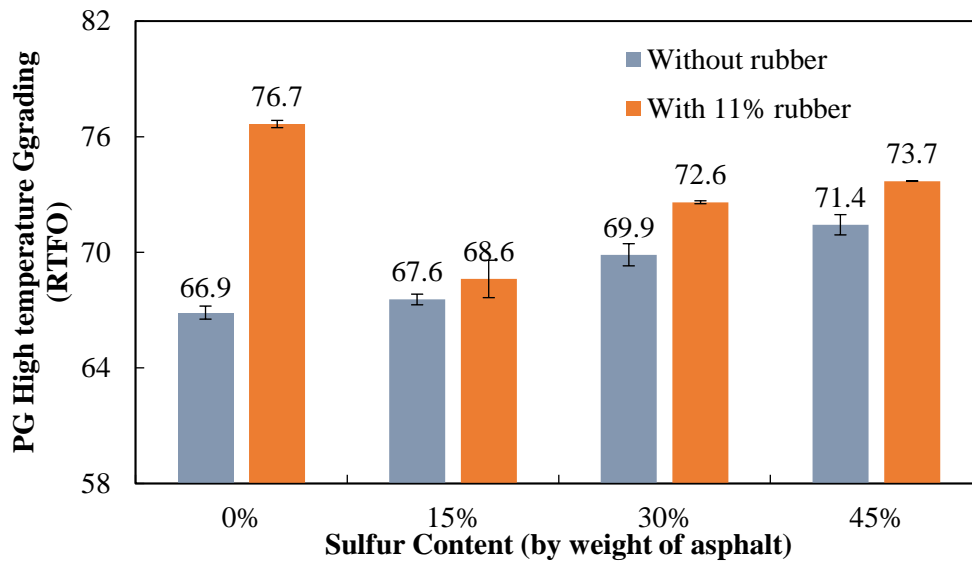
Figure 6.6 PG High Temperature Grade for RTFO Aged Asphalt

The BBR Test Results

Figure 6.7 presents the BBR low temperature grades for both of sulfur-extended asphalt and sulfur-rubber modified asphalt. The BBR test results indicate the lowest service temperature of a pavement. For the sulfur-extended asphalt, the increase of sulfur dosage significantly decreases the BBR low temperature grade. Especially for 45%, the PG low temperature grade dramatically drops to about a half of that for 30%. For the sulfur-rubber modified asphalt, there is also a significant trend that the increase of sulfur dosage decreases the PG low temperature grade. In addition, the sulfur-rubber modified asphalt has a higher PG low temperature grade than the sulfur-extended asphalt at the same dosage of sulfur, but for 0%, 15% and 30%, the differences are not significant.
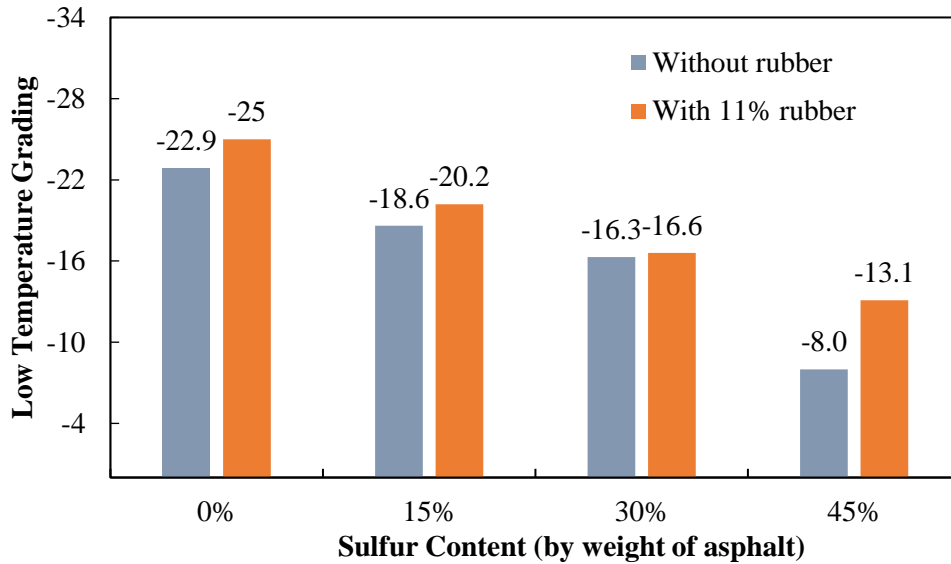
Figure 6.7 PG Low Temperature Grade for PAV Aged Asphalts

The MSCR Test Results

The J_{nr} and R% are the two output parameters of the MSCR test. The parameter of J_{nr} has a much better correlation with the rutting resistance of asphalt mixtures than the DSR high temperature grade, which has been verified in a number of studies (D'Angelo 2009; Zhang et al. 2015). The smaller the Jnr, the higher the rutting resistance of asphalt mixtures.

Figure 6.8 and 6.9 present the Jnr values for both of sulfur-extended asphalt and sulfur-rubber modified asphalt at two high temperatures of 64 and 70 °C. It can be seen that the trend of J_{nr} values for all the asphalts at 64 °C is similar with that at 70 °C. For the sulfur-extended asphalt, the 15% sulfur dosage has the largest J_{nr} values, while the 30% and 45% have the lowest J_{nr} values which means that they have a much higher rutting resistance than 0% and 15%. When comparing the J_{nr} values of 30% and 45%, there is no

significant difference observed. All the sulfur-rubber modified asphalts have a much lower J_{nr} values than the sulfur extended asphalts, which is not the case in the DSR high temperature grade. The 0% has the smallest J_{nr} among the sulfur-rubber modified asphalts, while the J_{nr} values for 15%, 30% and 45% are comparable.

(a)

(b)
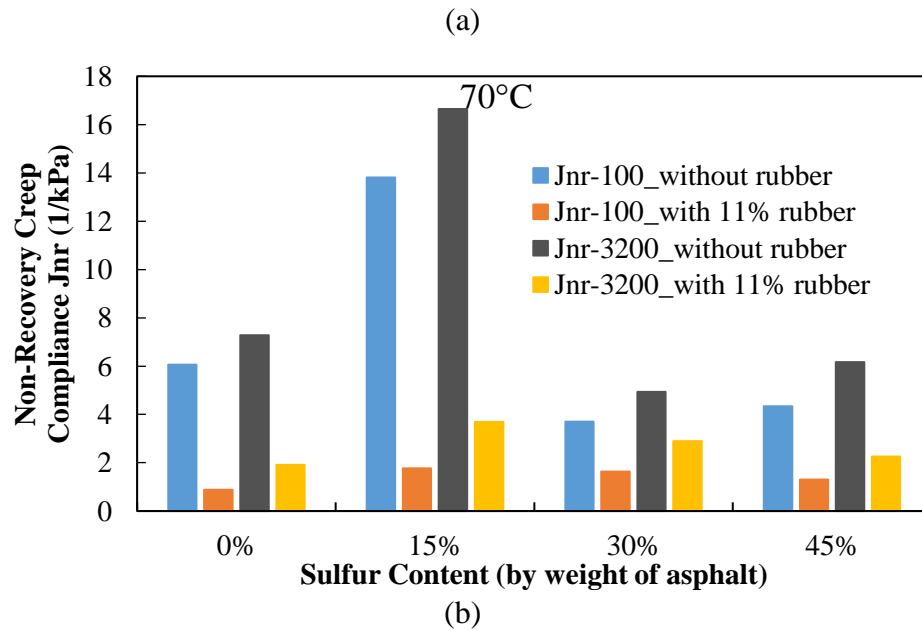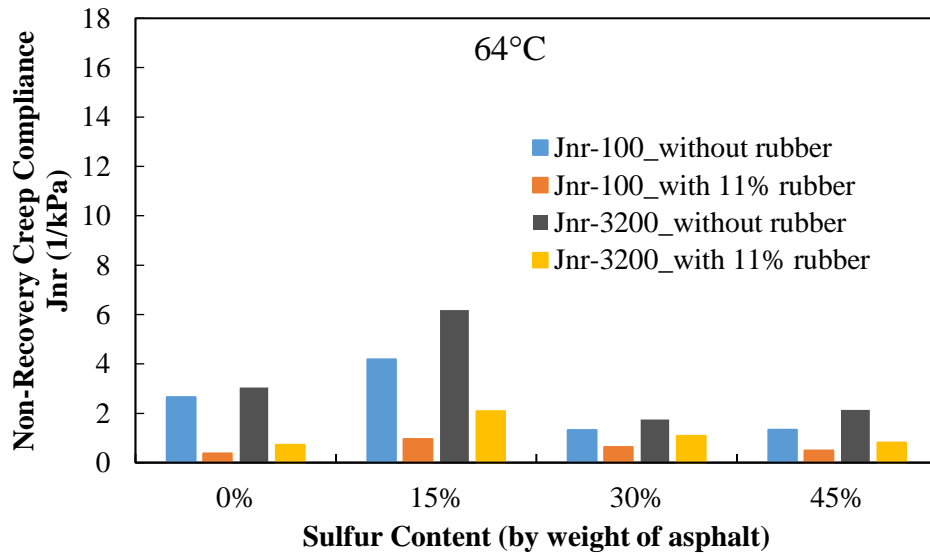
Figure 6.8 J_{nr} at Two Temperatures of (a) 64 °C and (b) 70 °C

Figure 6.9 presents the R% from the MSCR tests. It is hypothesized that the high elastic recovery of asphalt can contribute to a better fatigue resistance of asphalt mixture, but there is no clear relationship observed between them (Zhang et al. 2016). For sulfur-extended asphalts, the increase of sulfur dosage increases the R%, while the trend is opposite for the sulfur-rubber modified asphalt. The addition of crumb rubber significantly increases the R% compared with the sulfur-extended asphalts (without the addition of rubber).
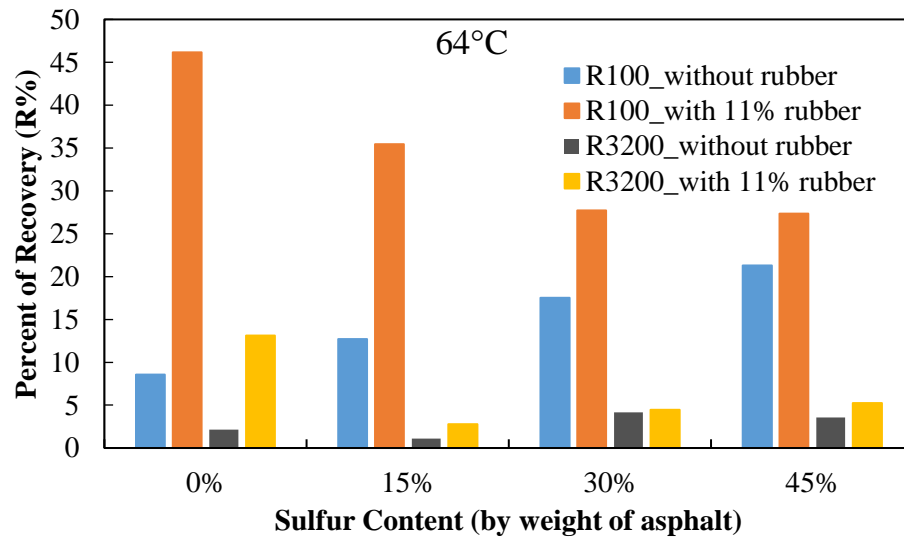
(a)

Figure 6.9 R% at Two Temperatures of (a) 64 °C and (b) 70 °C
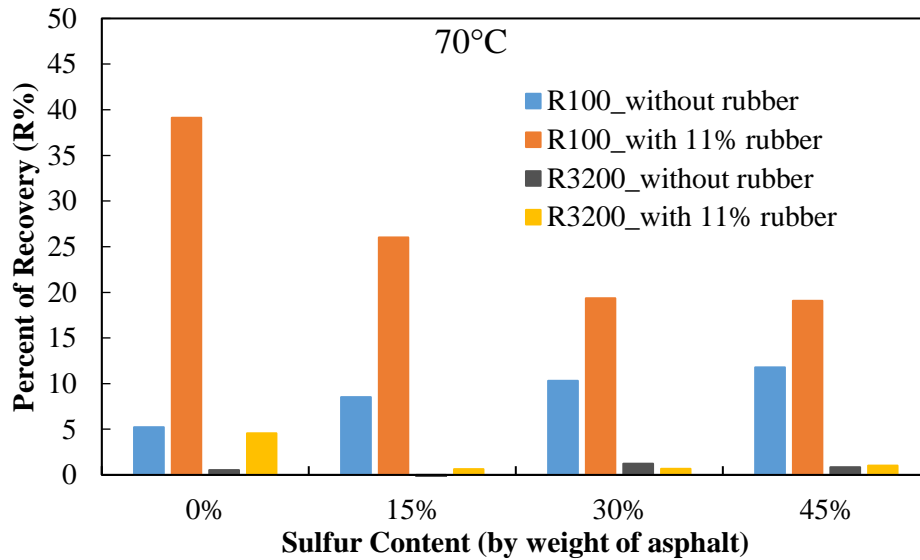
(b)

Figure 6.9 Continued

The Viscosity Test Results

The rotational viscosity test is used to describe the flow characteristics of asphalt at a specified temperature. Figure 6.10 presents the viscosity test results. As can be seen, for sulfur-extended asphalt, the addition of sulfur significantly decreases the viscosity compared with the control sample (0%); the viscosities for 15%, 30% and 45% are comparable. For sulfur-rubber modified asphalts, the addition of rubber significantly increase the viscosity. The 0% sulfur-rubber modified asphalt has a much higher viscosity than others, while the addition of sulfur greatly decreases the viscosity of sulfur-rubber modified asphalts.
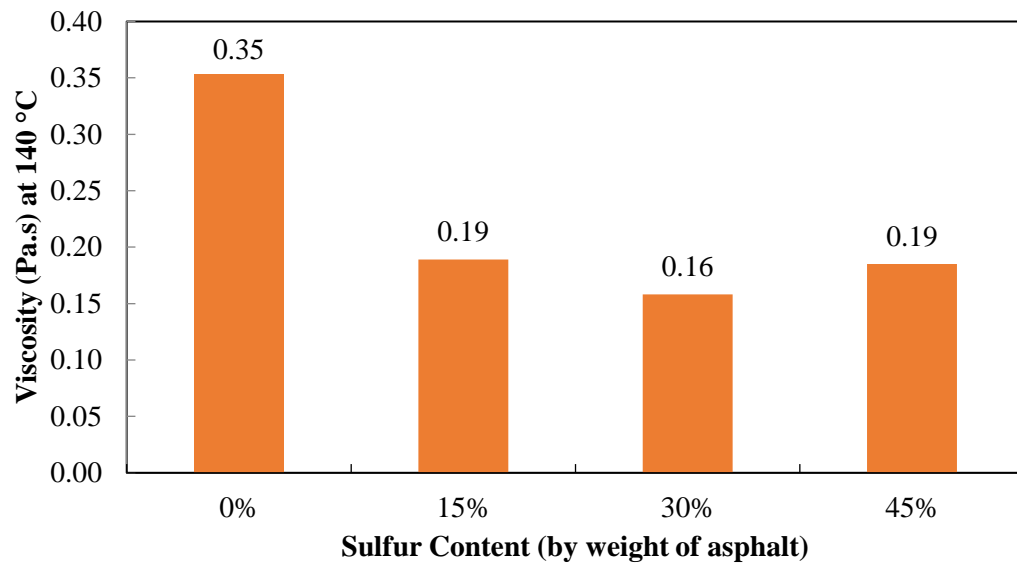
Figure 6.10 Rotational Viscosity Test Results at 140 °C for Sulfur-extended Asphalt (without Crumb Rubber)

7. FRACTURE CHARACTERIZATION OF SEA FAM MIXTURES USING THE MONOTONIC SCB TEST

Asphalt mixtures are heterogeneous composite, which have three primary phases: fine aggregate matrix (FAM), coarse aggregates and air voids. The FAM phase is responsible for compliance deformation in the asphalt concrete mixtures. Most importantly, FAM phase surrounds the stiff coarse aggregates, and cracks generally occur in the FAM phase. Different from the heterogeneity and discontinuity of asphalt mixtures, FAM phase is continuous and fine aggregates are well distributed in FAM mixture. Characterization of fracture properties of FAM is very helpful to understanding the fracture behavior of asphalt mixtures.

7.1 Materials and Mix Design

A Texas Type C asphalt mixture is used as the full mixture, which is a dense graded mixture meeting Texas Department of Transportation (TxDOT) specifications. Type C is widely used in Texas as a surface course and asphalt binder content used in this mixture was 5.2% by weight of mixture. The aggregate gradation is presented in Table 7.1.

Table 7.1 Aggregate Gradation

Sieve Size	Cum.% Passing	Lower Specification Limits	Upper Specification Limits
3/4"	100.0	95.0	100.0
3/8"	85.0	70.0	85.0
#4	60.0	43.0	63.0
#8	35.1	32.0	44.0
#30	15.7	14.0	28.0
#50	11.6	7.0	21.0
#200	3.6	2.0	7.0

The aggregates passing No. 16 (i.e., 1.18 mm) sieve are used for the FAM mixtures. Table 7.2 presents the FAM aggregate gradation.

Table 7.2 Aggregate Gradation for FAM

Sieve Size	Individual Retained %
#30	33.3
#50	17.4
#200	34.0
Pan	15.3

The FAM mix design followed the method used by Karki (2010). In order to determine the binder content for FAM, the first step is to calculate the weight of binder surrounding the coarse aggregates:

$$W_{bf,ret16} = SA_{ret16} \times W_{s,ret16} \times T_{f,ret16} \times G_b \times \rho_w \qquad (7.1)$$

Where $W_{bf,ret16}$ = the weight of binder surrounding the coarse aggregates,

$W_{s,ret16}$ = the weight of coarse aggregate in entire AC mixtures,

$T_{f,ret16}$ = the film thickness surrounding the aggregates retained on a No. 16 sieve,

G_b = the specific gravity of binder,

ρ_w = the density of water.

SA_{ret16} refers to the total surface area of the coarse aggregates retained on No.16 sieve, which is calculated by the following equation:

$$SA_{ret16} = \sum_{i=1}^{n} \frac{P_{p,ret16} \times CP_{i,ret16}}{100} \tag{7.2}$$

Where $P_{p,ret16}$ = the percentage of aggregate passing a specified sieve,

$CP_{i,ret16}$ = the surface area factor (m^2/kg) for the specified sieve, and n is the total number of sieves used for coarse aggregates.

The next step is to determine the weight of binder absorbed by coarse aggregates:

$$W_{ba,ret16} = \frac{W_b}{\% P_b} \times G_b \times \left(\frac{1}{G_{sb,ret16}} - \frac{1}{G_{se,ret16}} \right) \times 100 \tag{7.3}$$

Where $W_{ba,ret16}$ = the weight of binder absorbed by coarse aggregates retained on No.16 sieve,

$G_{sb,ret16}$ = the bulk specific gravity of coarse aggregates,

$G_{se,ret16}$ = the effective specific gravity of coarse aggregates.

The binder content for the full mixture is 5.2% by weight of mixture. The binder content for FAM is determined as 7.5% by total weight of fine aggregates.

7.2 Sample Preparation and Experimental Method

A superpave gyratory compactor is used to produce the cylindrical samples with a diameter of 150 mm and a height of 140 mm. Then, the samples are cut to produce cylindrical slices, and the slices are cut to produce two SCB specimen. Figure 7.1 shows the SCB specimens with a notch length of 15 mm after cutting.

Figure 7.1 SCB Specimens after Cutting

A Materials Testing System (MTS) is used for the fracture test. The SCB fracture tests are performed at two temperatures of 5 °C and -10 °C. The loading rates for 5 °C and -10 °C are 20 mm/min and 2 mm/min, respectively.

Fracture process zone (FPZ) is a nonlinear zone around the crack tip in brittle materials, which is a key characteristics of crack propagation. Many researchers have studies the FPZ of brittle concrete. However, very few work is related to asphalt mixture, especially the FAM. Thus, a digital image correlation (DIC) is used to measure the strain field of crack tip for FAM mixtures. Before testing, a SCB specimen is painted with white

background and black speckles, as shown in Figure 7.2. Figure 7.3 shows the speckled

specimen tested in the MTS with use of a DIC.

<table>
<tr><td>(a)</td><td>(b)</td></tr>
</table>

Figure 7.2 A Speckled Specimen: (a) before Painting, and (b) after Painting
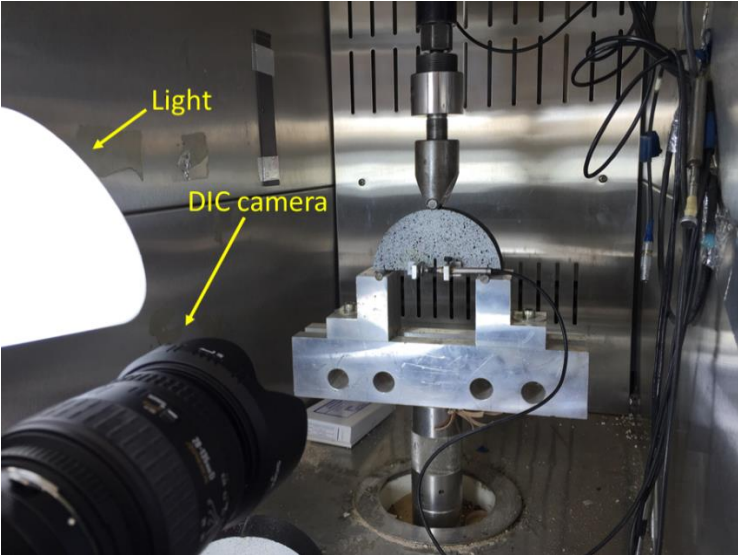
Figure 7.3 A Specimen Tested with Use of a DIC

7.3 SCB Fracture Test Results for FAM

The SCB monotonic fracture test results are presented in Figure 7.4 to 7.6. The load-displacement curves showed that 15S11R is different from the other three mixtures at both testing temperatures of 5°C and -10°C. 0S11R, 30S11R and 45S11R have the comparable curves. The same trend is also observed in the test results of fracture energy. 15S11R has a much larger fracture energy and lower peak load than the others, while 0S11R, 30S11R and 45S11R have the comparable fracture energies. It can be seen that all the mixtures behave brittle at -10°C and 5°C except that 15S11R behave ductile at 5°C.
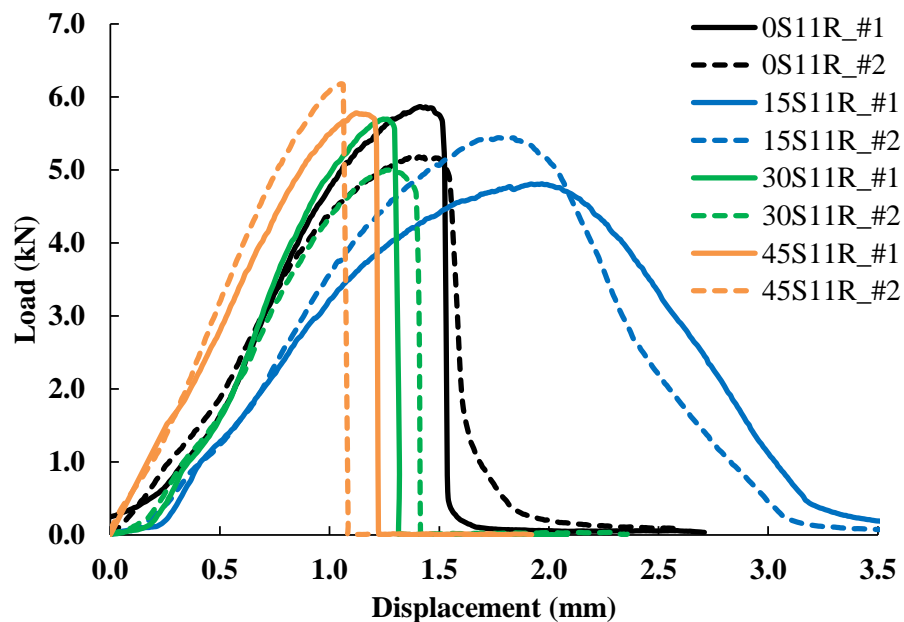
Figure 7.4 Load-displacement Curves at 5 °C *(Legend: 0S11R=0% sulfur+11% crumb rubber, 15S11R=15% sulfur+11% crumb rubber, 30S11R=30% sulfur+11% crumb rubber, 45S11R=45% sulfur+11% crumb rubber; #1 means Replicate #1, #2 means Replicate #2)*
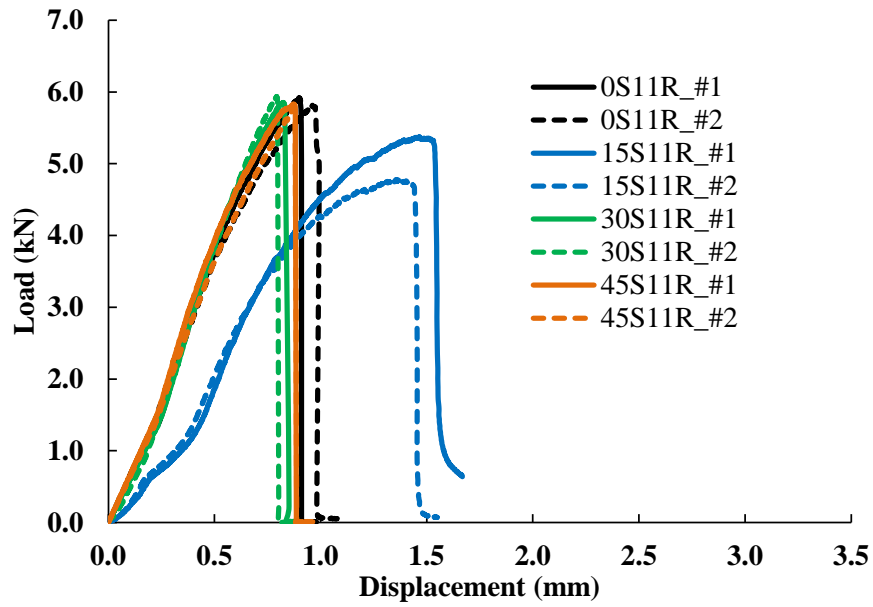
Figure 7.5 Load-displacement Curves at -10 °C
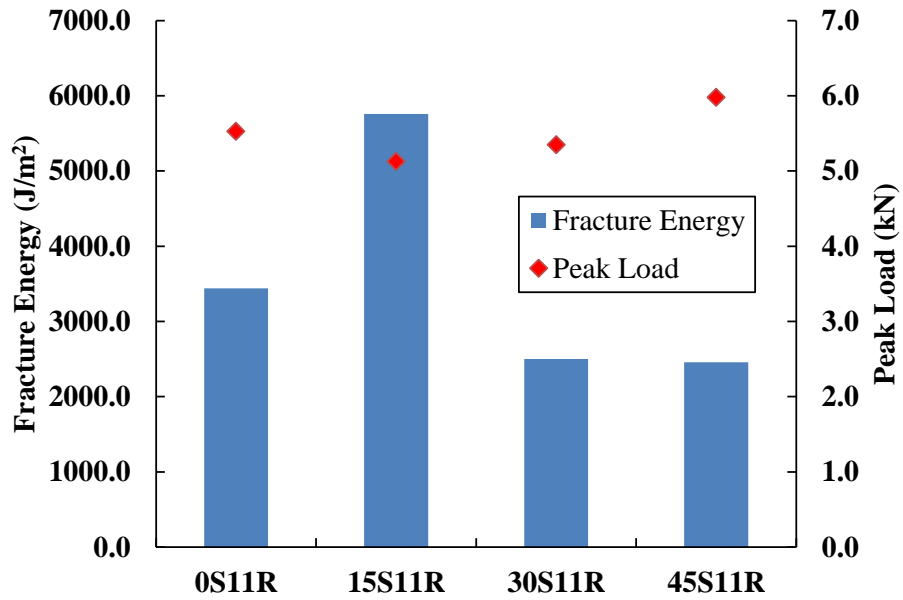
(a)

Figure 7.6 Comparison of Fracture Energy and Peak Load for Different SEA Mixtures: (a) at 5 °C, and (b) at -10 °C
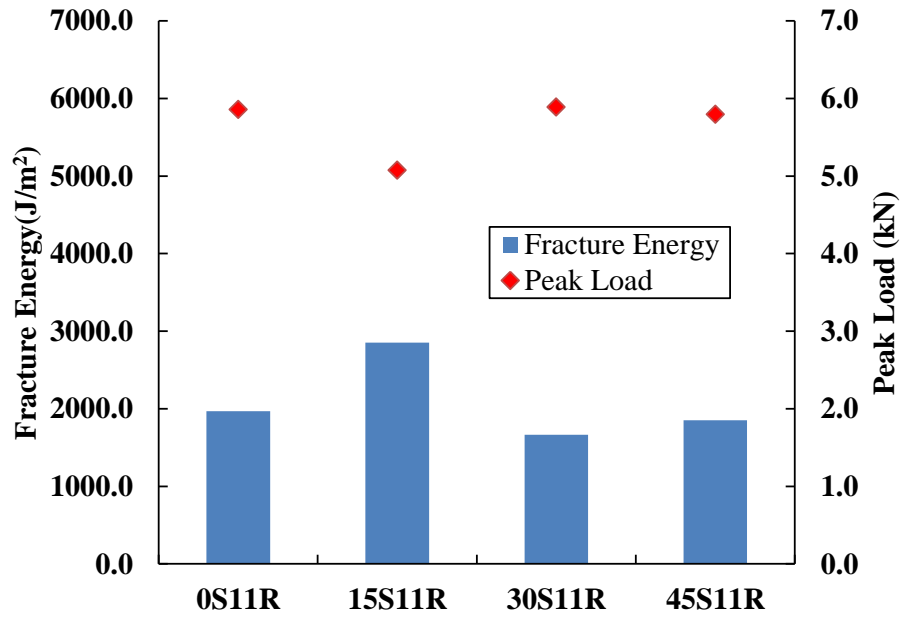
(b)

Figure 7.6 Continued

7.4 Characterization of Strain Field of a Crack Tip for FAM

Fracture process zone (FPZ) is a nonlinear zone around the crack tip in brittle materials, which is a key characteristics of crack propagation. A digital image correlation (DIC) is used to measure the strain field of FAM specimens at both 5 °C and -10 °C. Figure 7.7 shows comparisons of strain field of a crack tip and actual crack path. It can be seen that the strain field measured matches well the actual crack path in the specimen. Thus, the DIC is able to accurate to measure the strain field of a crack tip in the specimen.
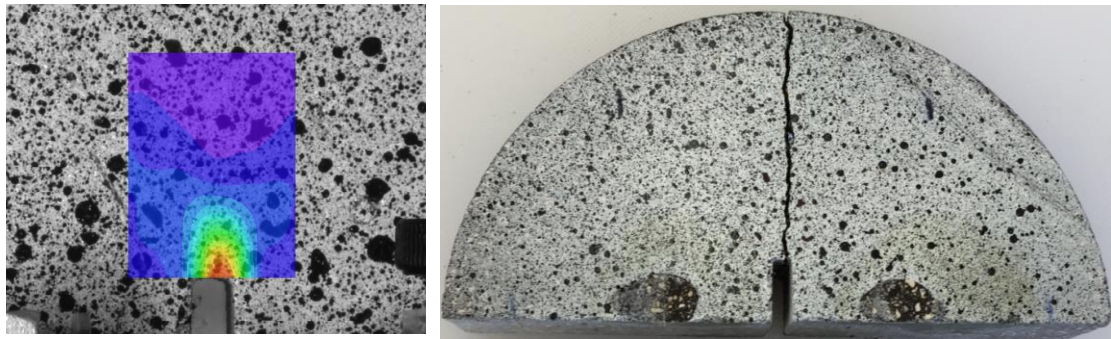
(a)

(b)

Figure 7.7 Comparison of Strain Field of a Crack Tip and Crack Path: (a) Crack in the Right Corner of Notch Front, and (b) Crack in the Left Corner of Notch Front

The horizontal strain fields of the crack tip at 5 °C and -10 °C are presented in Figure 7.8 and 7.9. Figure 7.10 shows the graphical compassion of maximum horizontal strain of different mixtures. It is obvious that 15S11R exhibited the largest maximum horizontal strain among the four mixtures at the two temperatures, which is consistent with the SCB test results. 30S11R and 45S11R have the comparable horizontal strain field at the two temperatures with 0S11R. When comparing the strain field at two temperatures. The strain field is more localized at the lower temperature than the higher temperature, and facture behavior is more brittle, which is also verified in Figure 7.5 that the load-displacement curve reaches the peak and instaneously drops. When correlating the

maximum horizontal strain to peak load (as shown in Figure 7.11) , it is found that the peak load has a fair correlation with maximum horizontal strain. Higher peak load means more localized strain field.

0.00037 0.0216	0.0023 0.0322
(a)	(b)
0.0020 0.0178	0.0014 0.0205
(c)	(d)
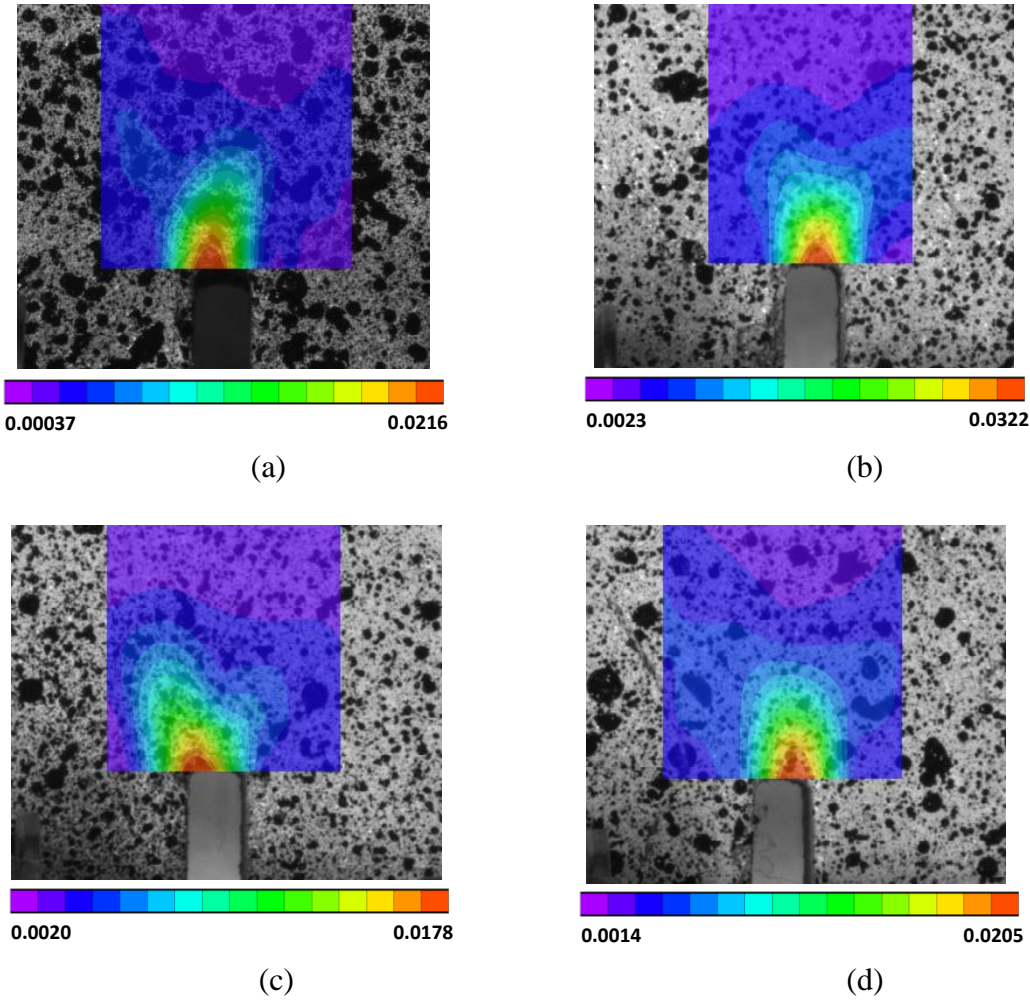
Figure 7.8 Horizontal Strain Field of the Crack Tip at Peak Load and 5 °C: (a) 0S11R, (b) 15S11R, (c) 30S11R, and (d) 45S11R
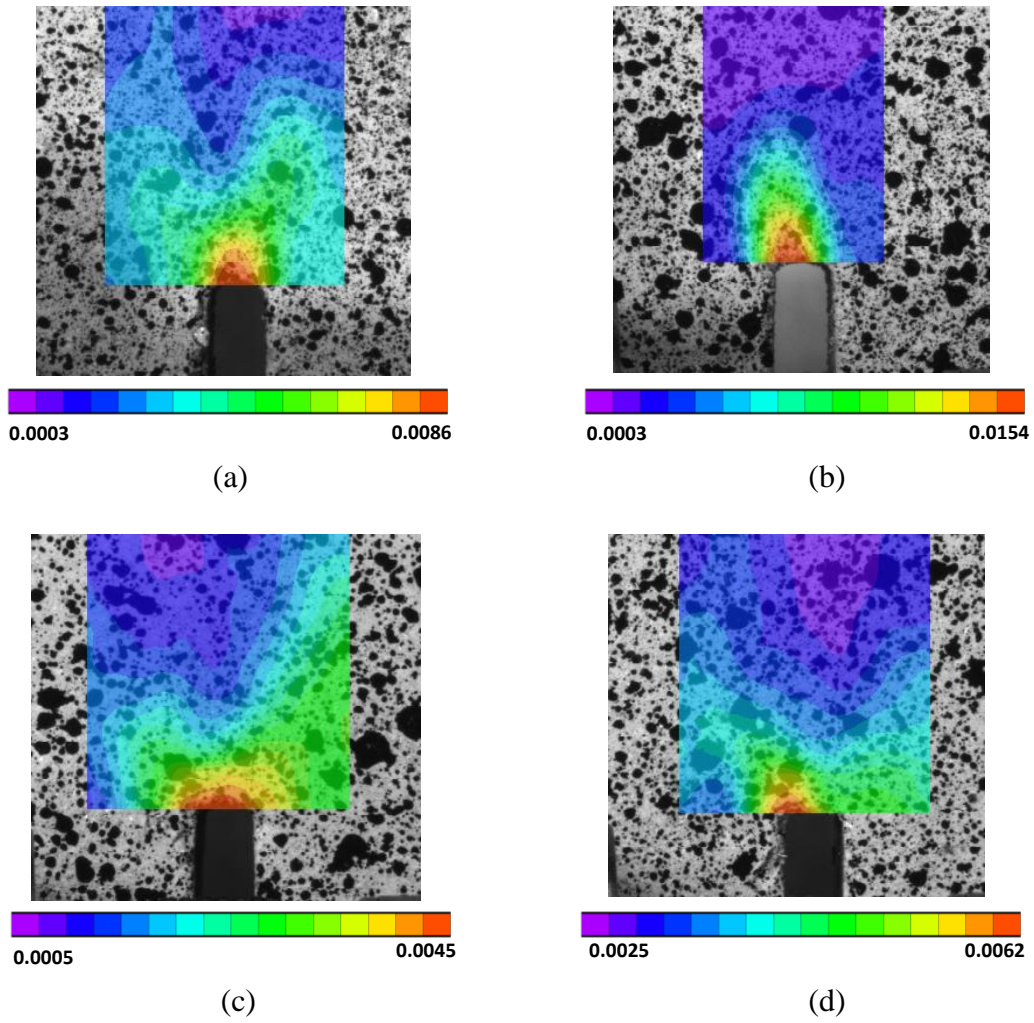
Figure 7.9 Horizontal Strain Field of the Crack Tip at Peak Load and -10 °C: (a) 0S11R, (b) 15S11R, (c) 30S11R, and (d) 45S11R
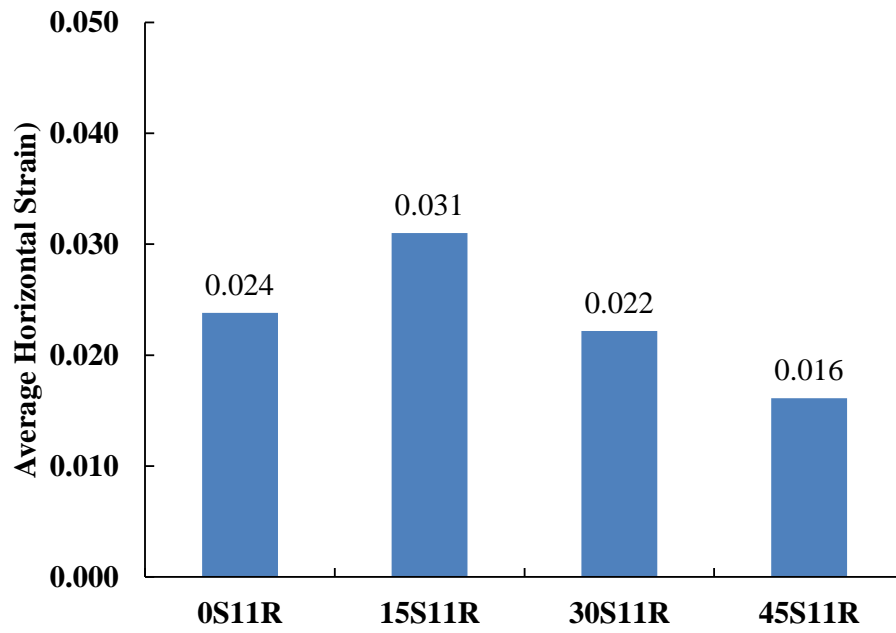
(a)
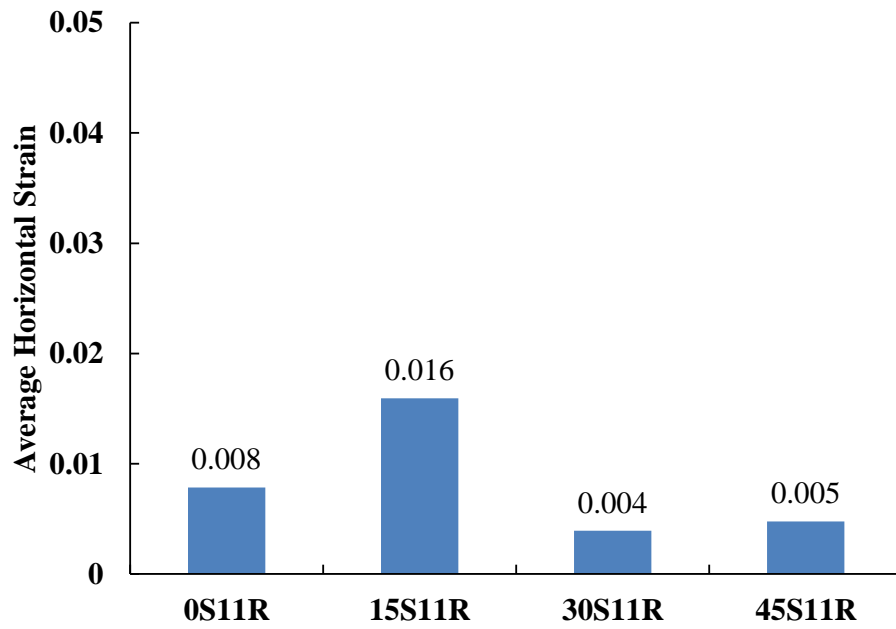
(b)

Figure 7.10 Average Maximum Horizontal Strain: (a) 5 °C and (b) -10 °C

(a)

(b)
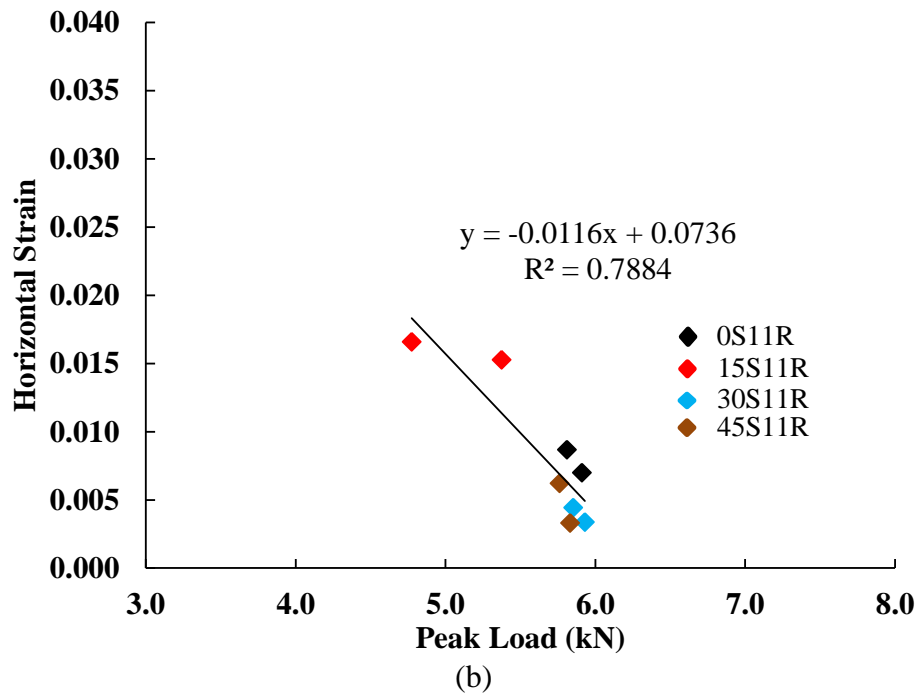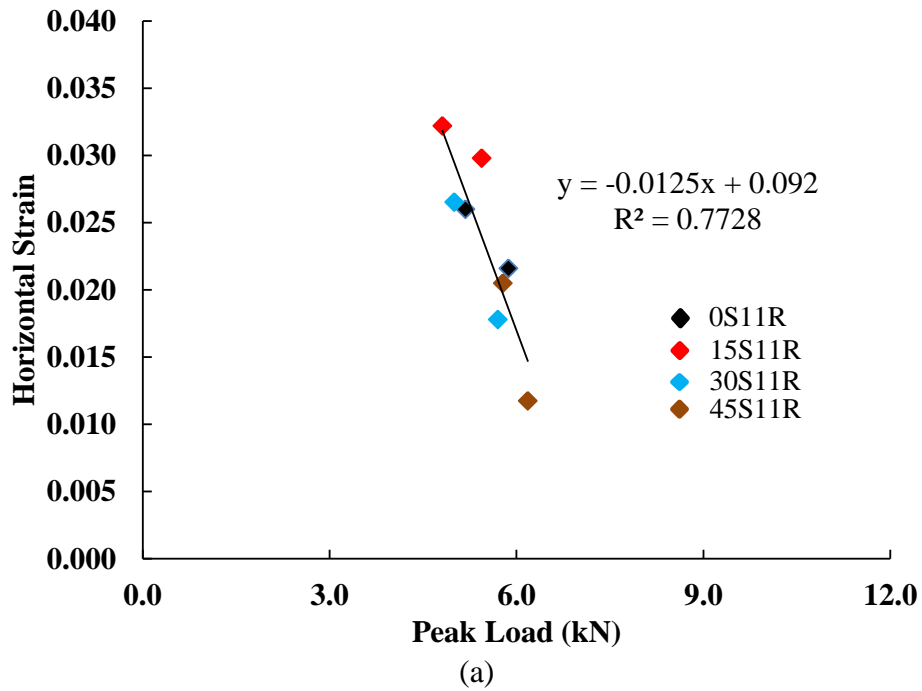
Figure 7.11 Correlations of Horizontal Strain and Peak Load: (a) 5 °C and (b) -10 °C

8. FATIGUE CHARACTERIZATION OF SEA MIXTURES USING THE CYCLIC SCB TEST

8.1 Background

Fatigue cracking is a major form of distress in asphalt pavement. Laboratory evaluation of fatigue behavior of asphalt mixtures is essential for mixture design and pavement structural design. Due to the composite nature of the material and its complexity, a number of fatigue tests have been proposed and used for evaluating fatigue resistance of asphalt mixtures. The major fatigue tests include bending beam fatigue (BBF), simplified viscoelastic continuum damage (S-VECD) test, Texas overlay test (OT), and repeated direct tension test. The BBF test can be run in either a strain-controlled or stress-controlled mode to determine the fatigue life of a beam specimen subjected to repeated flexural bending until failure (Tayebali 1996; Ghuzlan et al. 2000; Wagoner et al. 2005; Shu et al. 2008). The S-VECD test develops a damage characteristic curve of the asphalt mixture from direct tension cyclic fatigue testing, and the damage parameters are used with the mechanistic-empirical pavement design guide (MEPDG) or more advanced models to simulate pavement fatigue performance (Park et al. 1996; Daniel et al. 2002; Underwood et al. 2012). The OT test is a strain controlled test used to determine the failure cycles of a specimen glued onto two metallic plates-one mobile and the other fixed during the testing process (Lytton 1989; Zhou et al. 2007). The repeated direct tension test is a strain controlled test to obtain Paris' law or failure cycles of a cylindrical specimen subjected to repeated tension (Luo et al. 2013).

All these fatigue tests have their advantages and disadvantages. The S-VECD modeling is based on continuum mechanics, which is incapable of characterizing fracture properties (i.e., cracking growth rate). Characterizing crack propagation of asphalt mixtures is helpful for optimizing the mixture design and predicting cracking performance of asphalt pavements. Bending bean fatigue (BBF) and overlay tests (OT) are capable of capturing crack propagation, but they are highly variable (Walubita et al. 2012). Roque et al. (1999) developed a method based on the simple IDT test to characterize crack growth rate of asphalt mixture. However, the disadvantages of that method are that multiple cracks occur along the centerline of IDT specimen instead of a single crack, and the method for determining crack length may not be reliable.

A simple specimen geometry used for laboratory tests has benefits including high efficiency of sample preparation using material. Most importantly, the simple specimen geometry may reduce the variability of testing results. The semi-circular specimen has been used for fracture testing for a sufficient length of time to demonstrate the advantages of its simple specimen geometry a single crack occurring in the specimen. With the advantages, developing a method based on the cyclic semi-circular bending test is useful and promising. For characterizing crack growth rate, the difficulty is the measurement of crack length during testing. A study conducted by Huang et al. (2013) applied the cyclic SCB test to asphalt mixtures for evaluating cracking resistance. In his study, crack length was determined based on a relationship between the vertical loading displacement and crack length which was established using numerical simulation. In order to accurately measure crack length, a digital image correlation (DIC) system was utilized. Previous

99

studies have also shown the success of this method in identifying cracking and measuring displacements (Seo et al. 2004; Zhang 2010; Im et al. 2014).

8.2 Experimental Method

The cyclic SCB test set-up with a DIC system is shown in Figure 8.2. The test was performed in the environmental chamber of a UTM-25 machine. Before testing, a speckled specimen is prepared, which is shown in 8.1. In order to measure the crack mouth opening displacement (CMOD), two LVDTs are attached on the surfaces of a SCB specimen with a measuring span of 10 mm. The DIC camera was connected to a computer which captured an image each second during testing. Figure 8.2b shows an image of crack propagation which was captured by the DIC system. The test mode was stress-controlled, and a haversine load applied to the SCB specimen with a frequency of 5 Hz. The test was performed at 21°C.

Figure 8.1 A SCB Specimen with Speckles
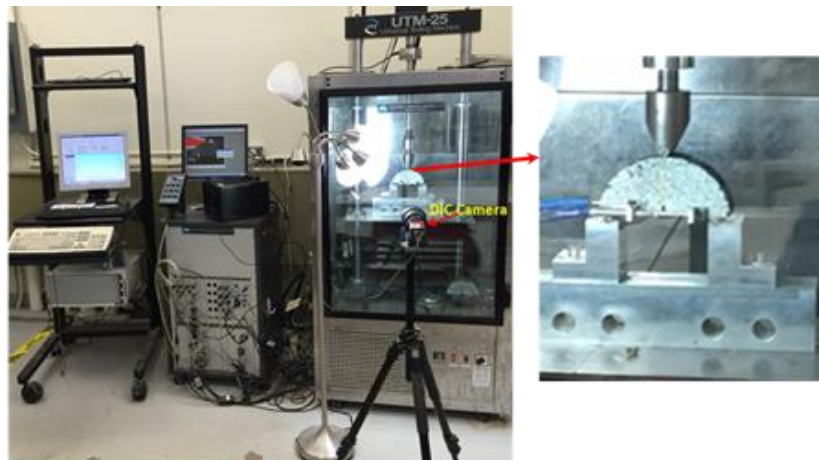
(a)
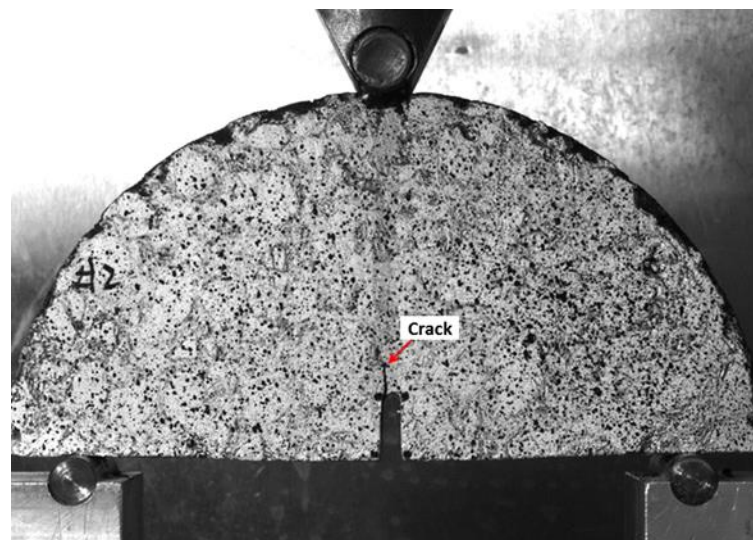
(b)

Figure 8.2 Cyclic SCB Testing: (a) Test Set-up with a DIC System, and (b) an Image of Crack Propagation Captured by the DIC System

8.3 Determination of Crack Growth Rate of SEA Mixtures

Paris's law is perhaps the most popular fatigue crack growth model to describe the relationship between cracking growth rate and stress intensity factor for various engineering materials as expressed in Equation 1 (Paris et al. 1961):

$$\frac{da}{dN} = A(\Delta K)^n \tag{8.1}$$

where,

a = crack length;

N = load cycle;

A and n = material coefficients; and

 ΔK = range of stress intensity factor.

  The important step for characterizing Paris coefficients A and n is to develop a method to determine changes in crack length corresponding to loading cycles. It is not realistic to identify each crack length corresponding to each cycle, which is tedious and time consuming. The best method is to establish a correlation between crack length and one output parameter of the test. This study is to establish a correlation between crack length and CMOD. Crack length is identified with use of the DIC, while CMOD is measured from the LVDTs. Figure 8.3 to 8.6 present the correlations established for four different SEA mixtures.

  With use of the correlations between CMOD and crack lengths, a data set of crack length (a) versus cycles (N) was obtained. And thus, the crack growth rate da/dN was calculated as well as the stress intensity factor ΔK. By fitting a linear function to the data of log (da/dN) versus log (ΔK), the Paris coefficients of A and n were determined. 8.3d, 8.4d, 8.5d and 8.6d present the fitting curves for four SEA mixtures.
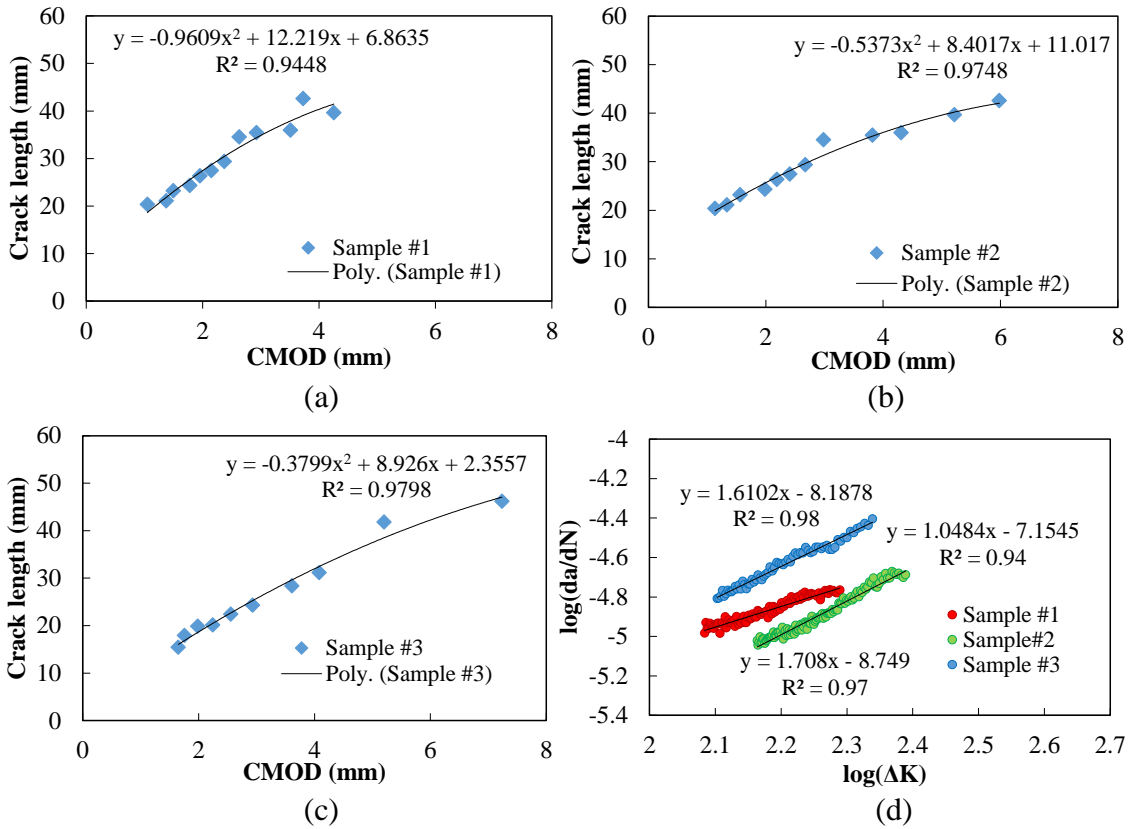
Figure 8.3 Correlations between CMOD Measured from LVDTs and Crack Length Measured by the DIC for Mixture 0S11R: (a) Sample#1, (b) Sample #2, (c) Sample #3, and (d) Crack Growth Rate versus Stress Intensity Factor
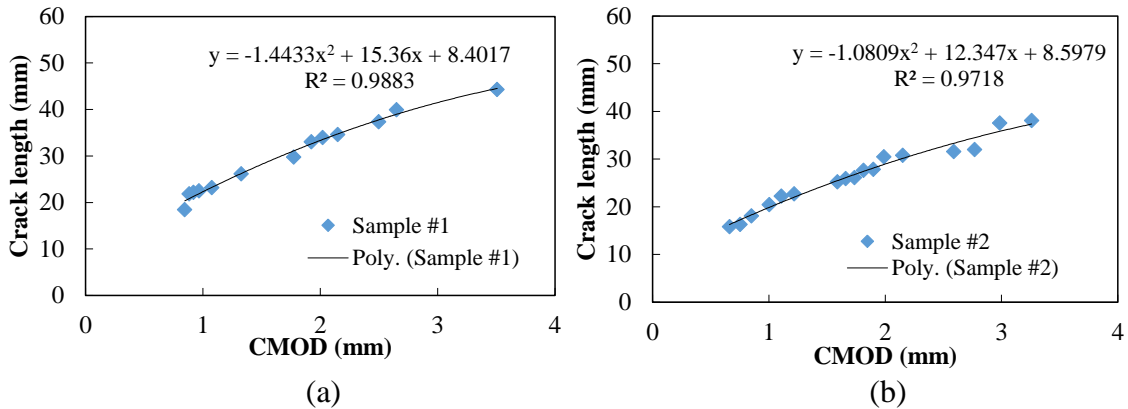
Figure 8.4 Correlations between CMOD Measured from LVDTs and Crack Length Measured by the DIC for Mixture 15S11R: (a) Sample#1, (b) Sample #2, (c) Sample #3, and (d) Crack Growth Rate versus Stress Intensity Factor

(c)

(d)
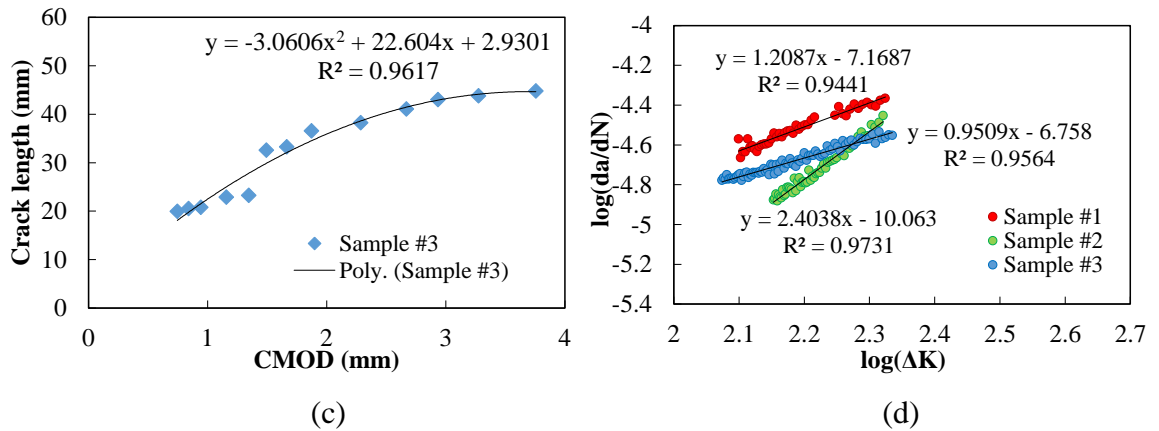
Figure 8.4 Continued

(a)

(b)

(c)

(d)
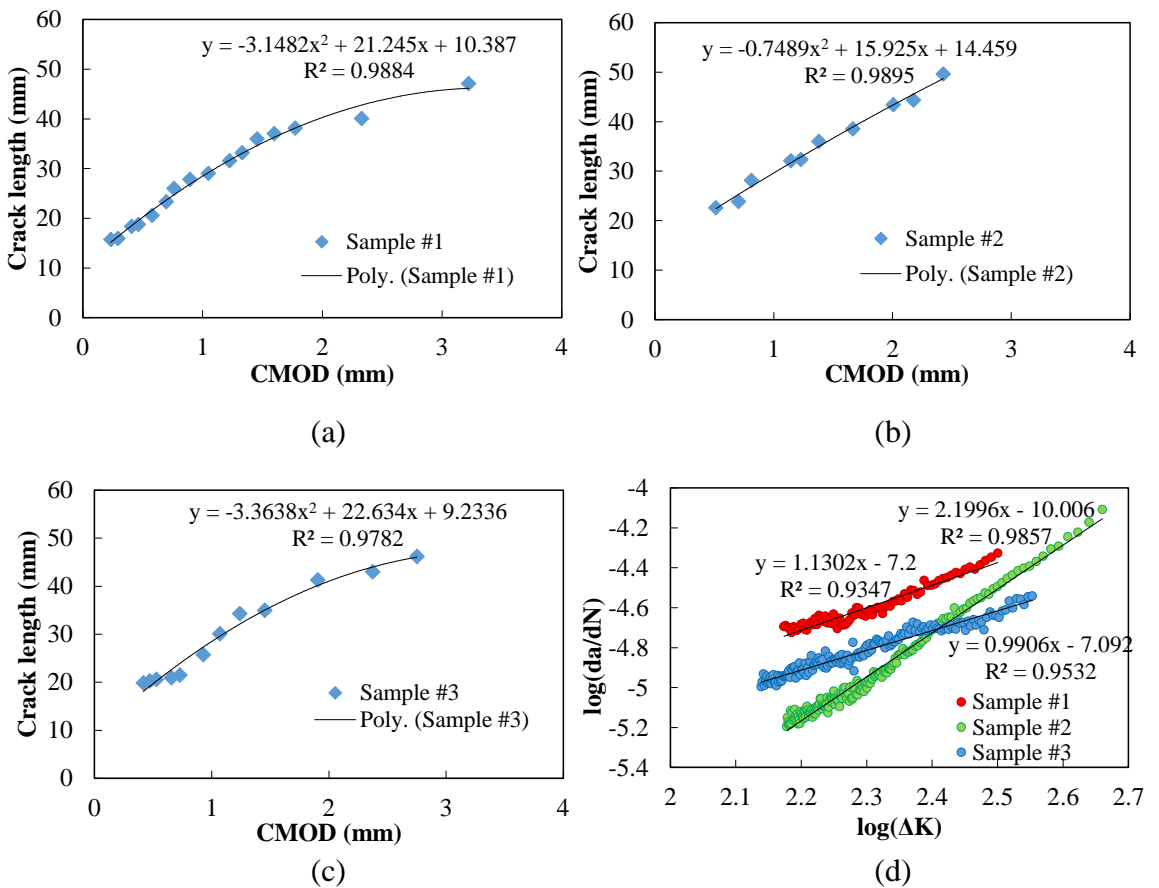
Figure 8.5 Correlations between CMOD Measured from LVDTs and Crack Length Measured by the DIC for Mixture 30S11R: (a) Sample#1, (b) Sample #2, (c) Sample #3, and (d) Crack Growth Rate versus Stress Intensity Factor
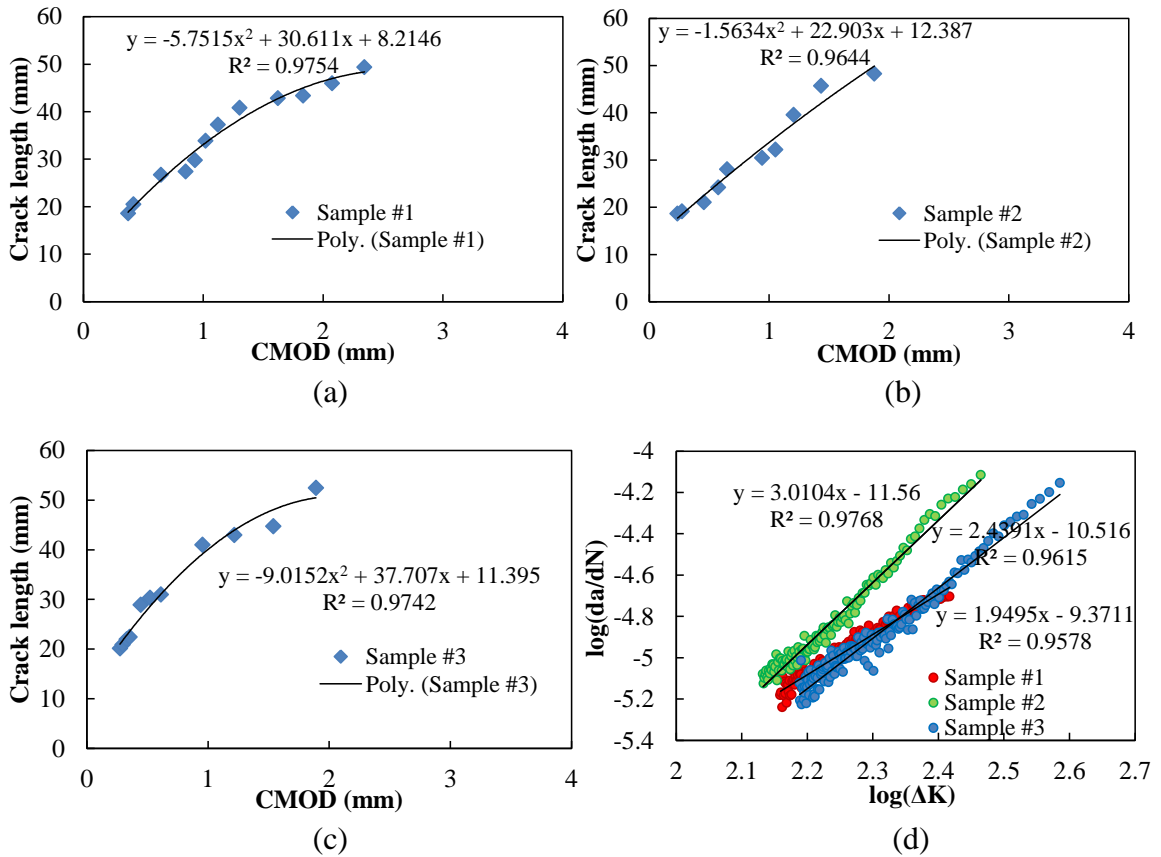
Figure 8.6 Correlations between CMOD Measured from LVDTs and Crack Length Measured by the DIC for Mixture 45S11R: (a) Sample#1, (b) Sample #2, (c) Sample #3, and (d) Crack Growth Rate versus Stress Intensity Factor

8.4 Comparisons and Discussions

The SCB fatigue test results including crack growth parameters (i.e., *A* and *n*) and failure cycles are summarized in Table 8.1. As can be seen, the mixture of 45S11R exhibits the highest number of cycles to failure while 15S11R exhibits the smallest. The 30S11R and 0S11R demonstrate comparable fatigue results.

Table 8.1 Summary of SCB Fatigue Test Results

Mixture ID		Crack Growth Parameters		Failure Cycles
		A	n	
0S11R	Sample #1	7.01E-08	1.048	2370
	Sample #2	1.78E-09	1.708	1900
	Sample #3	6.49E-09	1.61	2600
	Average	2.61E-08	1.456	2290
	COV	N/A	24.5%	15.6%
15S11R	Sample #1	6.78E-08	1.209	1311
	Sample #2	8.65E-11	2.404	2001
	Sample #3	1.75E-07	0.951	1901
	Average	8.08E-08	1.521	1738
	COV	N/A	51.0%	21.5%
30S11R	Sample #1	4.40E-08	1.203	1251
	Sample #2	9.86E-11	2.2	2861
	Sample #3	8.09E-08	0.991	2561
	Average	4.17E-08	1.464	2224
	COV	N/A	44.1%	38.5%
45S11R	Sample #1	2.75E-12	3.01	1941
	Sample #2	3.76E-11	2.415	3051
	Sample #3	5.03E-10	1.917	3521
	Average	1.81E-10	2.447	2838
	COV	N/A	12.1%	28.6%

Crack growth rate versus stress intensity factor for all four mixtures are compared in Figures 8.7 and 8.8. Mixture 15S11R exhibits the lowest fatigue resistance while the other three mixtures demonstrate comparable fatigue resistance. It should be noted that the resistance of a material to crack growth depends on both of the Paris's coefficients of *A* and *n*. In other words, both of A and n must be considered when interpreting the test results of crack growth rate. For example, although 0S11R, 15S11R and 30S11R have the similar *n* values, 15S11R have a much larger value of *A*, which results in a lower resistance to crack growth than 0S11R and 30S11R.

Figure 8.8b presents the curves of crack growth rate versus stress intensity factor based on average values of coefficients of *A* and *n*. It can be clearly seen that 0S11R, 15S11R and 30S11R have similar slopes (i.e., *n* values), whereas 0S11R has the smallest fatigue resistance to crack growth. Although 45S11R has a much larger n value, it has a comparable resistance to crack growth compared with 0S11R and 30S11R because it also has a much smaller *A* value. Overall, 15S11R has a much lower fatigue resistance while the other three mixtures have comparable resistance to fatigue crack growth rate.

A strong benefit of cyclic SCB testing is its lower coefficient of variance (COV) for the determination of cycles to failure. Among four mixtures, three mixtures had COVs less than 30%. A report indicates that flexural beam fatigue, flexural trapezoidal fatigue and diametrical fatigue tests have the COVs of 98.7%, 171.8% and 65.5%, respectively (Walubita et al. 2012). Thus, cyclic SCB testing has a much lower COVs, which shows promise to serve as a routine laboratory test for screening mixture when evaluating fatigue resistance.
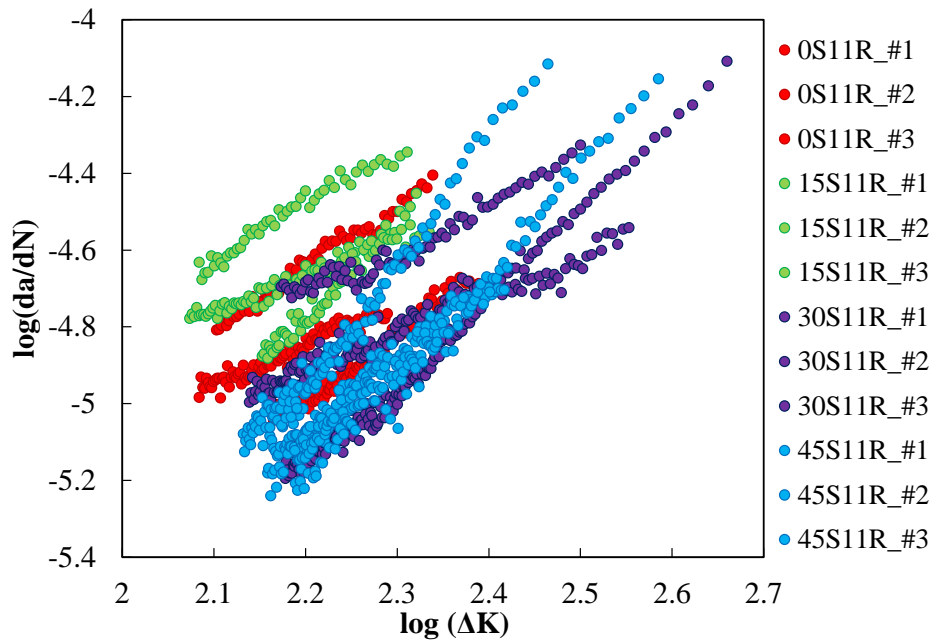
Figure 8.7 Crack Growth Rate versus Stress Intensity Factor for All the Mixtures
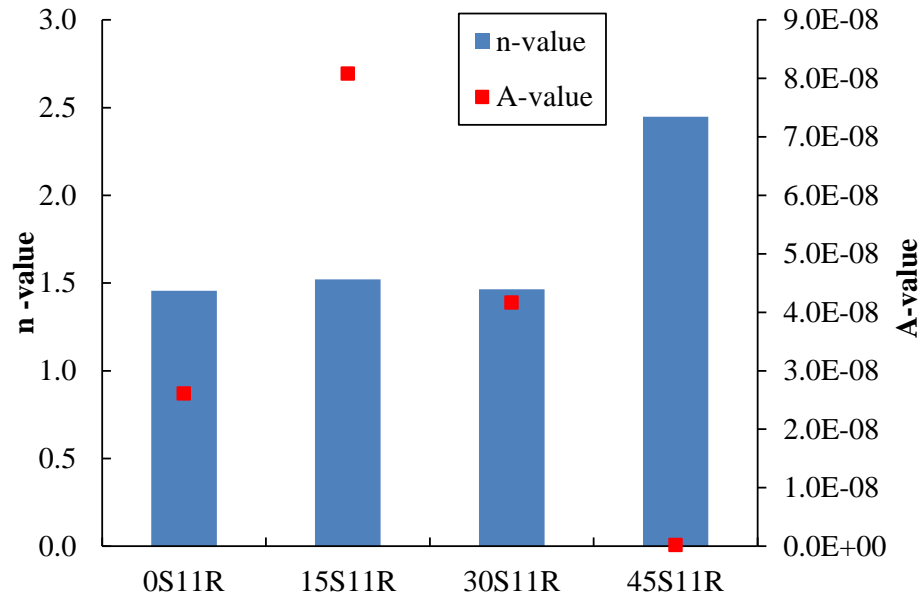
(a)

Figure 8.8 Crack Growth Characterizations: (a) Average Values of Paris's Law Coefficients, and (b) Plot of Crack Growth Rate versus Stress Intensity Factor Using Average Values of Paris's Law Coefficients
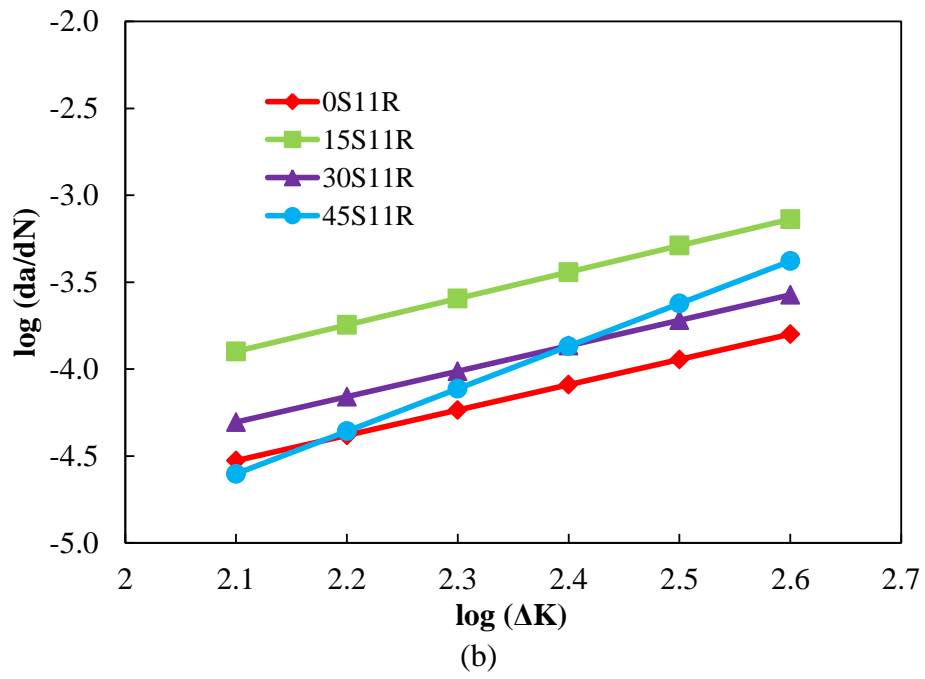
Figure 8.8 Continued

9. CONCLUSIONS AND RECOMMENDATIONS

9.1 Conclusions

The fracture resistance of a chemically stabilized base or subbase layer is important for durability and sustainability of the pavement structure. An appropriate test protocol to characterize the fracture resistance of the stabilized bases, subbases and subgrade soils is essential for design of pavement materials and structures. This research proposed a protocol based on the semi-circular bending (SCB) test to measure fracture resistance (i.e., fracture energy and fracture toughness) of the chemically stabilized material (CSM). The proposed SCB test method was successful in characterizing fracture resistance of three different CSMs. In order to more definitively address fracture properties of the CSM three-dimensional cohesive zone modeling was used and the simulations agreed very well with the experimental results. Both of the fracture properties obtained from the experiment and the cohesive zone modeling indicated that polymer-stabilized limestone exhibited a much higher fracture resistance than cement-stabilized limestone and cement-stabilized sand.

The semi-circular specimen has been used for fracture testing for a sufficient length of time to demonstrate the advantages of its simple specimen geometry and high efficiency of sample preparation. It is promising to develop a new fatigue method with use of both the compliance calibration method and the semi-circular specimen geometry. This research proposed the compliance method based on the cyclic SCB fatigue test, which was successfully used to characterize crack growth rate of cement stabilized materials. In

addition, the method is promising as it shows a much higher coefficients of correlation when fitting the data to the Paris' law equation.

Asphalt mixtures are heterogeneous composite, which have three primary phases: fine aggregate matrix (FAM), coarse aggregates and air voids. FAM phase surrounds the stiff coarse aggregates, and cracks generally occur in the FAM phase. Characterization of fracture properties of FAM is very helpful to understanding the fracture behavior of asphalt mixtures. A digital image correlation (DIC) was successfully used to measure the strain field of crack tip for FAM mixtures. It is found that the strain field of a crack tip is more localized at lower temperature and higher peak load.

Characterizing crack propagation of asphalt mixtures is helpful for optimizing mixture design and predicting cracking performance of asphalt pavements. This research proposed a new method based on the cyclic semi-circular bending test to characterize crack growth rate of asphalt mixtures. Compared with other fatigue tests, a cyclically-loaded semi-circular test has the advantages of simple specimen geometry and high efficiency of sample preparation. To accurately capture crack length for determining crack growth rate, a DIC is used, and crack mouth opening displacement is measured by linear variable differential transformers mounted on the surface of the specimen. Correlations between crack length and crack mouth opening displacement are established, which are used to determine crack lengths corresponding to loading cycles over the testing process. The proposed cyclic semi-circular bending test successfully characterizes the Paris's law coefficients of sulfur-extended asphalt mixtures. The cyclic semi-circular bending test provides substantially lower coefficients of variance in terms of cycles to

fatigue failure compared with other traditional fatigue tests such as the bending beam fatigue test and the Texas Overlay Test.

9.2 Recommendations

For the compliance method based on the cyclic SCB test, investigation of effects of loading type, frequency and geometry dimension on the test results of characterization of crack growth rate of chemically stabilized materials should be done in the future. In addition, it is promising that the proposed compliance method based on the SCB test is applied to the cement mortar and cement concrete.

Comparing with fracture test, fatigue test is time-consuming. Several researchers have made efforts to predict the coefficients of crack growth rate based on the fracture test result. More work is needed for establishing the correlation between fracture test and fatigue test results.

For the method used for characterizing crack growth of asphalt mixtures, the controlled-stress mode was used in this research. The controlled-strain mode is also widely used in fatigue test, which needs to be explored.

REFERENCES

Airy, G.B. (1863). "On the Strains in the Interior of Beams." *Philosophical Transactions of the Royal Society of London*, Vol. 153, pp. 49-79.

Al-Mehthel, M., Wahhab, H. I. A., Al-Idi S. H., and Baig, M. G. (2010). "Sulfur Extended Asphalt as a Major Outlet for Sulfur that Outperformed other Asphalt Mixes in the Gulf." Sulphur World Symposium, Doha, Qatar, April 12-15.

Aragao, F., Kim, Y., Lee, J. and Allen, D. H. (2011). "Micromechanical Model for Heterogeneous Asphalt Concrete Mixtures Subjected to Fracture Failure." *Journal of Materials in Civil Engineering*, Vol. 23, pp. 30-38.

Aragão, F. and Kim, Y. (2012). "Mode I fracture characterization of bituminous paving mixtures at intermediate service temperatures." *Experimental Mechanics*, Vol. 52, No. 9, pp. 1423-1434.

Arora, M. G., Al-Mana, A. I., Al-Tayyib, A. J., Ramadhan, R. H., and Khan, Z. A. (1994). "Long-term Pavement Performance History of Sulfur-extended Asphalt Test Roads in Eastern Province of Saudi Arabia." *Transportation Research Record: Journal of the Transportation Research Board*, Vol. 1435, pp. 77-85.

Bayomy, F. and Khedr, S. A. (1987). "Sulfur as a Partial Replacement for Asphalt in Pavement." *Transportation Research Record: Journal of the Transportation Research Board*, Vol. 1115, pp.150-160.

Bazant, Z. P. and Gettu, R. (1992). "Rate Effect and Load Relaxation in Static Fracture of Concrete." *ACI Material Journal*, Vol. 89, No. 5, pp. 456-468.

Beatty, T. L., Dunn, K., Harrigan, E. T., Stuart, K., and Weber, H. (1987). "Field Evaluation of Sulfur-Extended Asphalt Pavements." *Transportation Research Record: Journal of the Transportation Research Board*, Vol. 1115, pp. 161-170.

Birgisson, B., Montepara, A., Romeo, E., Roncella, R., Napier, J. A. L., and Tebaldi, G. (2008). "Determination and Prediction of Crack Patterns in Hot Mix Asphalt (HMA) Mixtures." *Engineering Fracture Mechanics*, Vol. 75, No. 3-4, pp. 664–673.

California Department of Transportation (2013). *2013 State of the Pavement Report Based on the 2013 Pavement Condition Survey*. Available at http://www.dot.ca.gov/hq/maint/Pavement/Pavement_Program/PDF/2013_SOP_FINAL-Dec_2013-1-24-13.pdf

Choi, Y. and Choi, J. (2013). "A Comparative Study of Concretes Containing Crushed Limestone Sand and Natural Sand." *Open Journal of Civil Engineering*, Vol. 3, No. 1, pp. 13-18.

Chong, K. P., Kuruppu, M. D., and Kuszmaul, J. S. (1987). "Fracture Toughness Determination of Layered Materials." *Engineering Fracture Mechanics*, Vol. 28, No. 1, pp. 43-54.

Cooper III, S. B., Mohammad, L. N., and Elseifi, M. A. (2011). "Laboratory Performance Characteristics of Sulfur-modified Warm-mix Asphalt." *Journal of Materials in Civil Engineering*, Vol. 23, No. 9. Pp. 1338-1345.

Crockford, W. W. and Little, D. N. (1987). "Tensile Fracture and Fatigue of Cement-Stabilized Soil." *Journal of Transportation Engineering*, Vol. 113, No. 5, pp. 520-537.

D'Angelo, J. A. (2009). "The Relationship of the MSCR Test to Rutting." *Road Material and Pavement Design*, Vol.10, pp. 61-80.

Daniel, J. S., Kim, Y. R., Brown, S., Rowe, G., Chehab, G., and Reinke, G. (2002). "Development of a Simplified Fatigue Test and Analysis Procedure Using a Viscoelastic, Continuum Damage Model." *Asphalt Paving Technology*, AAPT, Vol. 71, pp. 619-650.

Fowell, R. J. and Chen, J. F. (1990). "The Third Chevron Notch Rock Fracture Specimen -the Cracked Chevron-notched Brazilian Disk." *Proceedings of the 31st U.S. Symposium on Rock Mechanics*, pp. 295-302.

Ghuzlan, K. and Carpenter, S. (2000). "Energy-Derived, Damage-Based Failure Criterion for Fatigue Testing." *Transportation Research Record: Journal of the Transportation Research Board*, Vol. 1723, No.1, pp. 141-149.

Griffith, A. A. (1921). "The Phenomena of Rupture and Flow in Soilds." *Philosophical Transactions of the Royal Society A: Mathematical, Physical and Engineering Sciences*, Vol. 221, pp.163-198.

Hanley, H., Masad, E. A., Iyengar, S. R., Rodriguez, A. K., and Bazi, H. S. (2014). *Co-Polymer Soil Subgrade Binders*. U.S. Patent 20140169879 A1.

Harison, J. A., Hardin, B. O., and Mahboub, K. (1993). "Fracture Toughness of Compacted Cohesive Soil Using Ring Test." *Journal of Geotechnical Engineering*, Vol. 120, No. 5, pp. 872-891.

Huang B, Li, G., Pang, S. S., Eggers, J. (2004). "Investigation into Waste Tire Rubber-filled Concrete." *Journal of Materials in Civil Engineering*, Vol.16, No. 3, pp.187-194.

Huang, B., Shu, X., and Zuo, G. (2013). "Using Notched Semicircular Bending Fatigue Test to Characterize Fracture Resistance of Asphalt Mixtures." *Engineering Fracture Mechanics*, Vol. 109, pp. 78-88.

Im, S., Hoki, B., and Kim, Y. (2014). "Characterization of Mode-I and Mode-II Fracture Properties of Fine Aggregate Matrix Using a Semicircular Specimen Geometry." *Construction and Building Materials*, Vol. 52, pp. 413-421.

Inglis, C. E. (1913). "Stress in a Plate Due to the Presence of Cracks and Sharp Corners." *Transactions of the Institution of Naval Architects*, Vol. 55, pp. 219-230.

Ingraham, C. (2015). "Where America's Worst Roads Are – and How Much They're Costing Us." The Washington Post, June 25.

Iqbal, M. J. and Mohanty, B. (2007). "Experimental Calibration of ISRM Suggested Fracture Toughness Measurement Techniques in Selected Brittle Rocks." *Rock Mechanics and Rock Engineering*, Vol. 40, No. 5, pp. 453-475.

Iyengar, S. R., Masad, E., Rodriguez, A. K., Bazzi, H. S., Little, D., and Hanley, H. J. M. (2012). "Pavement Subgrade Stabilization Using Polymers: Characterization and Performance." *Journal of Materials in Civil Engineering*, Vol. 25, No. 4, pp. 472-483.

Karki, P. (2010). "Computational and Experimental Characterization of Bituminous Composites Based on Experimentally Determined Properties of Constituents." Master Thesis, University of Nebraska-Lincoln, Lincoln, Nebraska.

Khan, K. and Al-Shayea, N. A. (2000). "Effect of Specimen Geometry and Testing Method on Mixed Mode I-II Fracture Toughness of a Limestone Rock From Saudi Arabia." *Rock Mechanics and Rock Engineering*, Vol. 33, No. 3, pp. 179-206.

Kim, Y., Zhang, J., and Ban, H. (2012). Moisture Damage Characterization of Warm-mix Asphalt Mixtures Based on Laboratory-field Evaluation." *Construction and Building Materials*, Vol. 31, pp. 204-211.

Kim, Y., Allen, D. H., and Little, D. N. (2005). "Damage-induced Modeling of Asphalt Mixtures through Computational Micromechanics and Cohesive Zone Fracture." *Journal of Materials in Civil Engineering*, Vol. 17, pp. 477-484.

Lee, D. (1975). "Modification of Asphalt and Asphalt Paving Mixtures by Sulfur Additives." *Industrial & Engineering Chemistry Product Research and Development*, Vol. 14, No. 3, pp. 171-177.

Li, X. and Marasteanu, M. O. (2004). "Evaluation of the Low Temperature Fracture Resistance of Asphalt Mixtures Using the Semi Circular Bend Test." *Journal of the Association of Asphalt Paving Technologists*, Vol. 73, pp. 401-426.

Li, X. and Marasteanu, M. (2010). "The Fracture Process Zone in Asphalt Mixture at Low Temperature." *Engineering Fracture Mechanics*, Vol. 77, pp. 1175-1190.

Lim, L., Johnston, W., Choi, K. and Boland, J. N. (1994). "Fracture Testing of a Soft Rock with Semi-circular Specimens under Three-point Bending. Part1- Mode I." *International Journal of Rock Mechanics and Mining Sciences*, Vol. 31, No.3, pp. 185-197.

Little, D. N. and Nair, S. (2009). "Recommended Practice for Stabilization of Subgrade Soils and Base Materials." NCHRP Web-Only Document 144, National Cooperative Highway Research Program.

Little, D. N. (1987). "Evaluation of Structural Properties of Lime Stabilized Soils and Aggregates. Vol. 1: Summary of Finding." National Lime Association, Arlington, VA.

Lu, Z., Sun, L., and Zhou, C. (2005). "Performance and Mixture Design of High Quality Asphalt Modified by SEAM." *Acta Petrolei Sinica (Petroleum Processing Section)*, Vol. 21, No. 5, pp. 73-78.

Luo, X., Luo, R., and Lytton, R. L. (2013). "Characterization of Asphalt Mixtures Using Controlled-Strain Repeated Direct Tension Test." *Journal of Materials in Civil Engineering*, Vol. 25, No. 2, pp. 194-207.

Lytton, R. L. (1989). "Use of Geotextiles for Reinforcement and Strain Relief in Asphalt Concrete." Geotextiles and Geomembranes, Vol. 8, No.3, pp. 217-237.

Marsh, K. J., Smith, R. A., and Ritchie, R. O. (1991). "Fatigue Crack Measurement: Techniques and Applications." West Midlands: EMAS Ltd.

Molenaar, A. A. A, Scarpas, A., Liu, X., and Erkens, S. M. J. G. (2002). "Semicircular Bending Test, Simple but Useful?" *Journal of the Association of Asphalt Paving Technologists*, Vol. 71, pp. 794-815.

Mull, M. A. and STUART, K. (2002). "Fracture Resistance Characterization of Chemically Modified Crumb Rubber Asphalt Pavement." Journal of Materials Science, Vol. 37, No. 3, pp. 557-566.

Nagai, K., Shimizu, S., Iwadata, M., and Kawano, S. (1981). "The Size Effect on the Brittle Fracture Toughness under the Large Scale Yielding." Transactions of the Japan Welding Society. Vol. 12, pp. 14-18.

Nicholls, J. C. (2009). "Review of Shell Thiopave Sulfur-extended Asphalt Modifier." TRL Report 672.

Nsengiyumva, G., You, T., and Kim, Y. (2015). "Investigation of Testing Variables of a Semi-Circular Bending (SCB) Test for Asphalt Concrete Mixtures: Experimental-Statistical Approach." TRB 95th Anuual Meeting Compendium of Papers, Washington, D.C.

Paris, P. C., Gomez, M., and Anderson, W. (1961). "A Rational Analytic Theory of Fatigue." *The Trend in Engineering*, Vol. 13, pp. 9-14.

Park, S. W., Kim, Y., and Schapery, R. A. (1996). "A Viscoelastic Continuum Damage Model and Its Application to Uniaxial Behavior of Asphalt Concrete." *Mechanics of Materials*, Vol. 24, No.4, pp. 241-255.

Parvez, M. A., Al-Mehthel, M., Wahhab, H. I. A., and Hussein, I. A. (2013). "Utilization of Sulfur and Crumb Rubber in Asphalt Modification." *Journal of Applied Polymer Science*, Vol. 131, No. 7, 40046.

Paul, D. K. and Gnanendran, C. T. (2010). "Determination of Stiffness Properties of Lightly Stabilised Granular Materials from IDT Testing Using Numerical Analysis." *Proceedings of 17th Southeast Asian Geotechnical Conference*, Taipei, Taiwan. Geotechnical Society & Southeast Asian Geotechnical Society, 2010, 75–78, ISBN: 978-957-29749-3-3.

Petrossi, U., Bocca, P. L., and Pacor, P. (1972). "Reactions and Technological Properties of Sulfur-Treated Asphalt." *Industrial and Engineering Chemistry Product Research and Development*, Vol. 11, No. 2, pp. 214-219.

Piratheepan, J., Gnanendran, C. T., and Lo, S. C. R. (2010). "Characterization of Cementitiously Stabilized Granular Materials for Pavement Design Using Unconfined Compression and IDT Testings with Internal Displacement Measurements." *Journal of Materials in Civil Engineering*, Vol. 22, No. 5, pp 495-505.

Roque, R., Zhang, Z., and Sankar, B. (1999). "Determination of Crack Growth Rate Parameter of Asphalt Mixtures Using the Superpave IDT." *Journal of the Association of Asphalt Paving Technologists*, Vol. 68, pp. 404-433.

Roque, R., Birgisson, B., Sangpetngam, B., and Zhang, Z. (2002). "Hot Mix Asphalt Fracture Mechanics: A Fundamental Crack Growth Law for Asphalt Mixtures." *Journal of the Association of Asphalt Paving Technologists*, Vol. 71, pp. 816-827.

Roylance, D. (2001). "Introduction to fracture mechanics, Department of Materials Science and Engineering." Massachusetts Institute of Technology, Cambridge.

Sanford, R. J. (2003). *Principles of Fracture Mechanics*. Pearson Education, Inc.

Sanford, R. J. (1979). "A Critical Re-examination of the Westergaard Method for Solving Opening-Mode Crack Problems." *Mechanics Research Communications*, Vol.6, No. 5, pp. 289-294.

Schmidt, R. A. (1976). "Fracture-toughness Testing of Limestone." *Experimental Mechanics*, Vol. 16, No. 5, pp. 161-167.

Seo Y., Kim Y., Schapery R., Witczak M., and Bonaquist R. (2004). "A Study of Crack-tip Deformation and Crack Growth in Asphalt Concrete Using Fracture Mechanics." *Journal of the Association of Asphalt Paving Technologists*, Vol. 73, pp. 697-730.

Shu, X., Huang, B., and Vukosavljevic, D. (2008). "Laboratory Evaluation of Fatigue Characteristics of Recycled Asphalt Mixture." *Construction and Building Materials*, Vol. 22, No. 7, pp. 1323-1330.

Singh, R. N. and Sun, G. X. (1990). "A Numerical and Experimental Investigation for Determining Fracture Toughness of Welsh Limestone." *Mining Science and Technology*, Vol. 10, No. 1, pp. 61-70.

Sobhan, K. and Mashnad, M. (2002). "Tensile Strength and Toughness of Soil-Cement-Flay-Ash Composite Reinforced with Recycled High-Density Polyethylene Strips." *Journal of Materials in Civil Engineering*, Vol. 14, No. 2, pp. 177-184.

Song, S. H., Paulino, G. H., and Buttlar, W. G. (2006). "A Bilinear Cohesive Zone Model Tailored for Fracture of Asphalt Concrete Considering Viscoelastic Bulk Material." *Engineering Fracture Mechanics*, Vol. 73, No. 18, pp. 2829-2848.

Swartz S. E., Hu, K. K., and Jones, G. L. (1982). "Techniques to Monitor Crack Growth in Plain Concrete Beams." *Experimental Techniques*, Vol. 6.

Swartz S. E., Hu K. K., and Jones G. L. (1978). "Compliance Monitoring of Crack Growth in Concrete." *Journal of Engineering Mechanics*, Vol. 104, pp. 789-800.

Tayebali, A. A. (1996). "Development and Evaluation of Dynamic Flexural Beam Fatigue Test System." *Transportation Research Record: Journal of the Transportation Research Board*, Vol. 1545, pp. 89-97.

Tran, N., Taylor, A., Timm, D., Robbins, M.,Powell, B., and Dongre, R. (2010). "Evaluation of Mixture Performance and Structural Capacity of Pavements Utilizing Shell Thiopave." NCAT Report 10-05, National Center for Asphalt Technology, Auburn University, Auburn, Alabama.

Underwood, B., Baek, C., and Kim, Y. (2012). "Simplified Viscoelastic Continuum Damage Model as Platform for Asphalt Concrete Fatigue Analysis." *Transportation Research Record: Journal of the Transportation Research Board,* Vol. 2296, pp. 36-45.

Van Rooijen, R. C. and De Bondt, A. H. (2008). "Crack Propagation Performance Evaluation of Asphaltic Mixes Using a New Procedure Based on Cyclic Semi-Circular Bending Tests." Pavement Cracking: Mechanisms, Modeling, Detection, Testing, and Case Histories, CRC Press, pp. 437-446.

Velazco, G., Visalvanich, K. and Shah, S. P. (1980). "Fracture Behavior and Analysis of Fiber Reinforced Concrete beams." *Cement and Concrete Research*. Vol. 10, pp. 41-51.

Wagoner, M., Buttlar, W., and Paulino, G. (2005). "Development of a Single-Edge Notched Beam Test for Asphalt Concrete Mixtures," *Journal of Testing and Evaluation*, Vol. 33, No. 6, pp. 452-460.

Walubita, L. F., Faurk, A. N., Das, G., Tanvir, H. A., Zhang, J., and Scullion, T. (2012). "The Overlay Tester: A Sensitivity Study to Improve Repeatability and Minimize Variability in the Test Results." Report No. FHWA/TX-12/0-6607-1, Texas A&M Transportation Institute, College Station, Texas.

Wecharatana, M. and Shah, S. P. (1982). "Slow Crack Growth in Cement Composite." *Journal of the Structural Division*, Vol. 108, No. 6, pp. 1400-1413.

Westergaard, H. M. (1939). "Bearing Pressures and Cracks." *Journal of Applied Mechanics*, Vol. 6, pp. A49-A53.

Xiao, F., Zhao, W., and Amirkhanian, S. N. (2009). "Fatigue Behavior of Rubberized Asphalt Concrete Mixtures Containing Warm Asphalt Additives." *Construction and Building Materials*, Vol. 23, pp. 3144–3151.

Yu, H., Sun, L., and Zhang, Li. (2009). "Analysis of Water Stability of Sulfur Extended Asphalt Mixture." *Journal of Building Materials*, Vol. 12, No. 6, pp. 679-683.

Zhang, J. (2010). "Effects of Warm-mix Asphalt Additives on Asphalt Mixture Characteristics and Pavement Performance." Master Thesis, University of Nebraska-Lincoln, Lincoln, Nebraska.

Zhang, J., Walubita, L. F., Faruk, A. N. M., Karki, P., and Simate, G. S. (2015). "Use of the MSCR Test to Characterize the Asphalt Binder Properties Relative to HMA Rutting Performance ─ A Laboratory Study." *Construction and Building Materials*, Vol. 94, pp. 218-227.

Zhang, J., Faruk, A. N. M., Karki, P., Holleran, I., Hu, X., and Walubita, L. F. (2016). "Relating Asphalt Binder Elastic Recovery Properties to HMA Cracking and Fracture Properties." *Construction and Building Materials*, Vol. 121, pp. 236-245.

Zhang, J., Little, D. N., Grajales, J., You, T., and Kim, Y. (2017). "Use of Semicircular Bending Test and Cohesive Zone Modeling to Evaluate Fracture Resistance of Stabilized Soils." *Transportation Research Record: Journal of the Transportation Research Board*, No. 2057, pp. 67-77.

Zhou, F., Hu, S., Chen, D., and Scullion, T. (2007). "Overlay Tester: Simple Performance Test for Fatigue Cracking." *Transportation Research Record: Journal of the Transportation Research Board*, Vol. 2001, pp. 1-8.